Copyright

by

Surya Venkatesh Dhulipala

2018

The Dissertation Committee for Surya Venkatesh Dhulipala certifies that this is the approved version of the following dissertation:

Particulate matter formation from volatile chemical products including combustion and non-combustion sources

Committee:

Lea Hildebrandt Ruiz, Supervisor

David Allen

Gary Rochelle

Ying Xu

Richard Corsi

Particulate matter formation from volatile chemical products including combustion and non-combustion sources

by

Surya Venkatesh Dhulipala

Dissertation

Presented to the Faculty of the Graduate School of

The University of Texas at Austin

in Partial Fulfillment

of the Requirements

for the Degree of

Doctor of Philosophy

The University of Texas at Austin

August 2018

Dedication

This dissertation is dedicated to my grandmother, Saroja Krishnamurthy, who instilled in me a love of learning for which I am forever grateful.

Acknowledgements

I would like to thank my Ph.D. supervisor, Dr. Lea Hildebrandt Ruiz for her support and guidance. Lea is an excellent mentor and she is always there for her students. I would also like to thank my MS thesis adviser Dr. Neil Donahue and Dr. Peter Adams, both of whom inspired me to pursue research in the field of atmospheric chemistry. Neil and Peter are outstanding professors and their passion for atmospheric chemistry is infectious. I would not be here if not for their support.

My research would not have been possible without funding from The Welch Foundation, National Science Foundation, Texas Air Quality Research Program, Texas Air Research Center and the Green Fund program at The University of Texas at Austin. I appreciate their initiatives to provide funding in the field of atmospheric science and I hope they will continue to support students interested in this research area.

I would also like to thank Steve, Denzil, Terri, Susan and Jarett for facilitating my research at Center for Energy and Environmental Resources (CEER) at The University of Texas at Austin. CEER has a great workplace environment and the opportunity to interact with research staff and faculty during weekly Air Quality Seminars was an enriching experience. I had several conversations with Drs. Atila Novoselac, David Allen, David Sullivan, Joshua Apte, Neil Crain, Richard Corsi and Ying Xu where they shared their knowledge in their respective areas of expertise. This collaborative and inclusive atmosphere was highly stimulating.

During my Ph.D., I received help from a number of fellow graduate students and post-doctoral researchers in the Hildebrandt Ruiz Research Group: Puneet, Cameron, Jeff, Simon, Felipe, Sahil, Kanan and Catherine. Everyone's support, both in terms of intellectual conversations, and performing laboratory maintenance was crucial in enabling my research.

I will cherish this professional and personal network and I hope to pay it forward for future alumni.

Particulate matter formation from volatile chemical products including combustion and non-combustion sources

Surya Venkatesh Dhulipala, Ph.D.

The University of Texas at Austin, 2018

Supervisor: Lea Hildebrandt Ruiz

New evidence on the contribution of volatile chemical products from non-combustion sources to ambient particulate matter formation has renewed interest in policy-makers and atmospheric scientists to quantify these emissions which have historically been under-reported. In this dissertation, several representative compounds are chosen to provide a holistic comparison of particulate matter formation from both combustion and non-combustion sources.

For this purpose, an environmental chamber is employed with state-of-art-instruments to monitor the formation and decay of air pollutants in the gas-phase and particle-phase. The Aerosol Chemical Speciation Monitor (ACSM) is used to measure the total concentration and bulk composition of particulate matter less than 1 μm in size (PM_1). The High Resolution Time-of-Flight-Mass-Spectrometer (HR-Tof-CIMS) along with a Filter Inlet for Aerosols and Gases (FIGAERO) is used to measure the gas-phase composition in real-time and the particle-phase composition in a semi-continuous manner.

Toluene, an aromatic compound, is commonly used in solvents. Its reaction with OH radicals, the most abundant radical in the atmosphere, is well understood but its reaction with chlorine radicals is not. Chlorine is an important oxidant in both in-land and coastal areas. Here, high oxidative states of organic aerosol (component of PM) and gas-phase products formed during toluene-Cl photo-oxidation are reported. Secondary OH radical production is also observed.

Long-chain alkanes are associated with vehicular exhaust and their reactions with chlorine also remain poorly understood. Here, the Cl-initiated photo-oxidation of alkanes with 10 carbons – n-decane, 2-methyl nonane and butyl cyclohexane are reported under low NO_x environments and variable relative humidity (0% and 35-55%). Presence of gas-phase and particle-products associated with OH radical chemistry are reported in the presence of chlorine.

A class of compounds defined as Low Vapor Pressure Volatile Organic Compounds (LVP-VOCs) by policy-makers and referred to as Intermediate-Volatility Organic Compounds (IVOCs) by atmospheric scientists includes commercial grade mineral spirits, diethylene mono butyl glycol ether (DEGBE) and Texanol®, which are commonly used in solvents and coatings. Here, the Cl- and OH-radical initiated particulate matter formation from these IVOCs are discussed and compared to alkanes of similar volatility but originating from a combustion source (n-pentadecane and 2,6,10 trimethyl dodecane).

Table of Contents

List of Tables

List of Figures

Chapter 1: Introduction

The air we breathe is often taken for granted; however, exposure to ambient air pollution ranks fifth among human health risk factors in an epidemiological study published by the World Health Organization (Cohen et al., 2017). Despite environmental regulations in developed countries and growing awareness in developing countries, monitoring and reducing ambient air pollution exposure remains a work in progress. For example, while cumulative automotive emissions have decreased in the United States of America between 1990-2007 (McDonald et al., 2013), current regulations exempt many chemicals that have recently been shown to be important precursors of airborne particulate matter (PM) formation (McDonald et al., 2018), including from non-combustion sources. Humans spend a significant fraction of time in indoor environments and a lack of exposure regulations and standards has resulted in an increase in breathing-related illnesses between 1990-2015 (Cohen et al., 2017).

The United States Environmental Protection Agency (EPA) recognizes and regulates six criteria air pollutants namely ground-level ozone, PM, carbon monoxide, lead, sulfur dioxide and nitrogen dioxide (NO_2). All of these criteria pollutants are known to seriously affect human health. PM is known to increase risk of lung cancer, pulmonary infections and heart attacks, stroke, chronic inflammatory diseases, cataract, central nervous system disorders (Parkinson's, and Alzheimer's disease), age related disorders and cancer (Brook et al., 2010, 2016; Cohen et al., 2017; Kampa and Castanas,

2008; Morakinyo et al., 2016). The smaller the size of the particle, the deeper it can penetrate into the lungs, causing serious health effects. In fact, an estimated 4.2 million deaths (7.6% of total global deaths) are attributed to exposure to ambient particulate matter less than 2.5 µm in size or $PM_{2.5}$ (Cohen et al., 2017). While most EPA (and worldwide) regulations are for PM_{10} (particulate matter less than 10 µm in size) and $PM_{2.5}$; advances in research-grade instrumentation have made it possible to quantify PM_1 formation and composition.

Exposure to ozone, NO_x (NO and NO_2)and SO_2 can cause pulmonary lung infections and aggravate asthma among children and elderly (EPA, 2016). Exposure to ozone can also be fatal : 254, 000 deaths were attributed to ozone exposure in 2015 (Cohen et al., 2017). Exposure to lead can cause anemia in children and premature birth and reduced fetus growth among pregnant women (Toxic Substances Control Act, 2016). The EPA has set National Ambient Air Quality Standards (NAAQS) in place which regulate the emissions of these aforementioned criteria air pollutants. Among these criteria pollutants, ground-level ozone and particulate matter still exceed the NAAQS standards in cities and receive continued attention in the scientific community.

Particulate matter emissions can either be of biogenic or anthropogenic origin. Anthropogenic sources include industry, land traffic, residential and commercial energy use (for example, heating, cooking), biomass burning, power generation and agriculture (Lelieveld et al., 2015). Biogenic sources primarily include emissions from terrestrial ecosystems (Hallquist et al., 2009) and oceans (Kettle and Andreae, 2000). Formation of PM in the atmosphere is governed by several factors, including the reaction of volatile

organic compounds (VOCs) with atmospheric oxidants such as OH radicals, ozone, chlorine and NO_x. Some VOCs are also known to be carcinogenic in nature. Upon oxidation, these VOCs can form organic compounds with lower volatility, which can then condense on existing particles and form secondary organic aerosol (SOA) (Seinfeld and Pandis, 2006). SOA is important because it comprises 65-90% of total estimated PM_1 (Jimenez et al., 2009) in urban areas and individual contributions from a number of precursors remains poorly characterized.

Considering that there are hundreds of VOCs in the atmosphere, and they can undergo reaction with a number of oxidants, this dissertation focuses only on SOA formation from selected class of VOCs of anthropogenic origin (Table 1-1):

1) aromatics (toluene)

2) linear, branched and cyclic alkanes with 10 carbons (n-decane, 2-methyl nonane and butylcyclohexane)

3) volatile chemical products or VCPs including mineral spirits, Texanol® (2,2,4-Trimethyl-1,3-pentanediol monoisobutyrate) and diethylene glycol mono-butyl ether (DEGBE) and VOCs of similar volatility (n-pentadecane and 2,6,10-trimethyldodecane)

The following sections of Chapter 1 provide a literature review and background relevant to this dissertation. Chapter 2 provides an overview of research methods and instruments used. In Chapters 3 and 4, the SOA formation from toluene, n-decane, 2-

methyl nonane (MeNo) and butyl cyclohexane (BCH) are reported in the presence of chlorine. In Chapter 5, the SOA formation potential of selected VCPs (mineral spirits, Texanol® and DEGBE) under low NO_x and high NO_x conditions along with volatility measurements is presented. These are then compared to VOCs of similar volatility – n-pentadecane (PD) and 2, 6, 10-trimethyl dodecane (TMDD). Chapter 6 summarizes the original contributions in this dissertation and includes suggestions for future environmental chamber experiments.

1.1 COMMON METRICS FOR CHARACTERIZING SOA FORMATION AND EVOLUTION IN THE ATMOSPHERE

A common metric of reporting this SOA formation from VOCs is called SOA yield – mass of SOA formed divided by the mass of VOC reacted. In Figure 1-1, the SOA yield is plotted against number of carbons in parent hydrocarbon precursor (Lim and Ziemann, 2009c). The SOA yields follow the trend: cyclic>linear>branched under high NO_x conditions. Alkylcyclohexanes with 10 carbons were found to have yields between those of linear and cyclic alkanes.

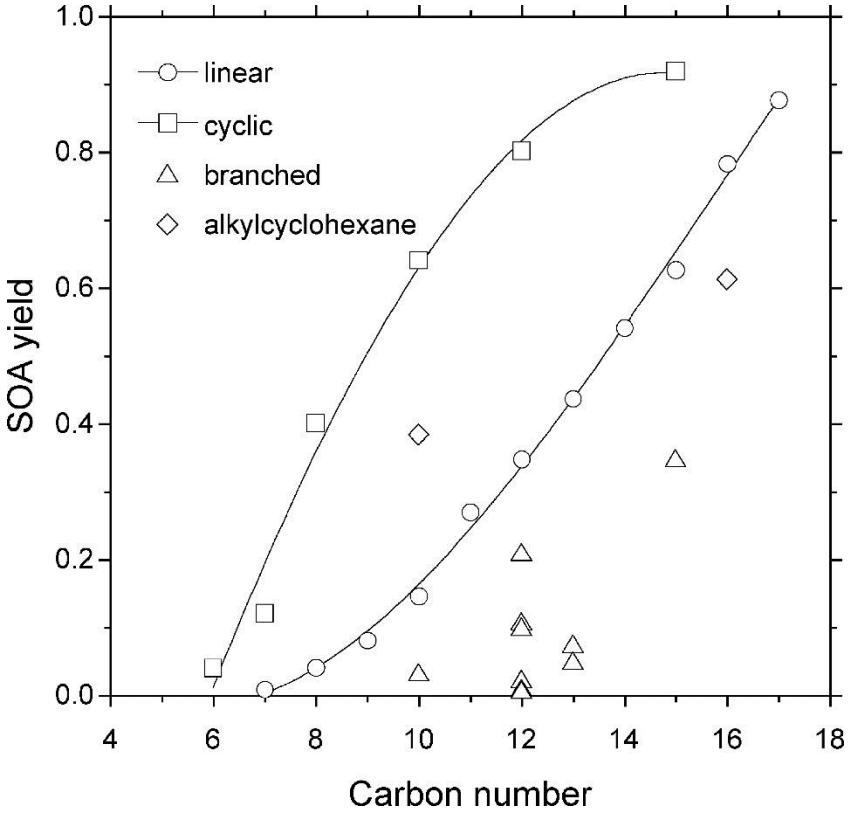

Figure 1-1. Yields of SOA formed from OH radical-initiated reactions of linear, branched, and cyclic alkanes and alkylcyclohexanes in the presence of NO_x (Lim and Ziemann, 2009c)

The volatility and composition of organic aerosol are two other parameters which have been used in different ways to describe the partitioning (amount of aerosol in gas and particle phases) and oxidative behavior of organic aerosols. Composition includes both elemental composition (O: C and H: C) and bulk composition (percentage of organics, nitrates, chlorides, sulfates, ammonium). The concept proposed by Van Krevelan, 1950 to use O:C and H:C ratios as a metric to segregate coal has also been used in the atmospheric science community to understand the oxidation states of organic aerosol in the atmosphere (Heald et al., 2010). Donahue et al. (2006) and

Robinson et al. (2007) developed a unified framework for studying the oxidation of organic aerosols by grouping sets of VOCs into "volatility bins" based on their saturation vapor concentrations (C*). This metric, C*, is basically a saturation vapor pressure with activity coefficient and converted to units of mass concentration. The collection of compounds in different volatility bins is referred to as one-dimensional "Volatility Basis Set" or 1-D VBS. An important outcome of 1-D VBS was the recognition of a class of VOCs having saturation vapor concentrations in the range of 10^3-10^6 μg m^{-3} (which were referred to as "Intermediate-Volatility Organic Compounds" or (IVOCs) which contribute significantly to ambient SOA formation.

$$C_i^* = \frac{C_i^{vap}}{C_i^{aer}} = \frac{M_i 10^6 \zeta_i' p_{L,i}^0}{760RT} \qquad \text{Equation 1-1}$$

$$C_{OA} = \sum_i C_i \xi_i \qquad \text{Equation 1-2}$$

$$\xi_i = \left(1 + \frac{C_i^*}{C_{OA}}\right)^{-1} \qquad \text{Equation 1-3}$$

Here, C_i^{aer} (μg m^{-3}) is the mass concentration of compound i in the condensed phase, C_i^{vap} (μg m^{-3}) is the concentration in the vapor phase, C_{OA} (μg m^{-3}) is the total organic aerosol concentration, R is the gas constant, T (K) is the temperature, M_i (g mol^{-1}) is the molecular weight of species i, ζ_i' is a molality-based activity coefficient, and $p_{L,i}^0$ (torr) is the saturation vapor pressure of pure compound i at temperature T and ξ_i is the partitioning coefficient. It should be noted that on a fundamental level,

Equation 1-1 is derived directly from Raoult's law and the only difference is that it uses mass fractions rather than mole fractions.

The next iteration of this framework was the plotting of elemental ratio (O: C) against the volatility (reported in the form of saturation vapor concentration C*) (Donahue et al., 2012; Jimenez et al., 2009). Kroll et al. (2011) then suggested an improved framework where elemental ratios (O: C and H: C) were used to calculate average carbon oxidation states (Equation 1-4) and those were plotted against number of carbon atoms.

$$O_{Sc} = 2O:C - H:C \qquad \text{Equation 1-4}$$

Using oxidation states along with the 1-D VBS allows one to track oxidation over an extended period of time ("photochemical aging") of any species whether non-volatile (for example, C*=0.01 μg m^{-3}) or extremely volatile (for example, C*=10^7 μg m^{-3}). Since this new method involved adding another dimension (oxidation states) to the existing 1-D VBS, it was named 2-D VBS (Chuang and Donahue, 2016; Donahue et al., 2011, 2012).

Most of the information needed for the framework described above (from different researchers) is directly available through a High Resolution Aerosol Mass Spectrometer (HR-AMS), first developed by Decarlo et al., 2006. A lower-cost version of the instrument called the Aerosol Chemical Speciation Monitor (Ng et al., 2011a) is used in this dissertation. The ACSM is unit-mass resolution unlike the HR-AMS. Ng et al. (2011) identified tracer signal ratios in the ACSM mass spectra from which, information

about elemental ratios could be extracted. The proposed co-relations for extraction of this information have been iterated and improved over the years but are still prone to errors arising from instrument limitations (Canagaratna et al., 2015). More information on the ACSM and how these approximations are made are provided in Chapter 2 of this dissertation.

These different approaches give a visual representation of progression of oxidation for different VOCs. The one common underlying principle in all frameworks is that VOCs prefer to undergo one of three oxidation processes in the atmosphere: fragmentation (cleavage of C-C bonds), functionalization (addition of polar functional groups) or oligomerization (association of two organic compounds). Given enough time for oxidation, all organic species should get converted to CO_2.

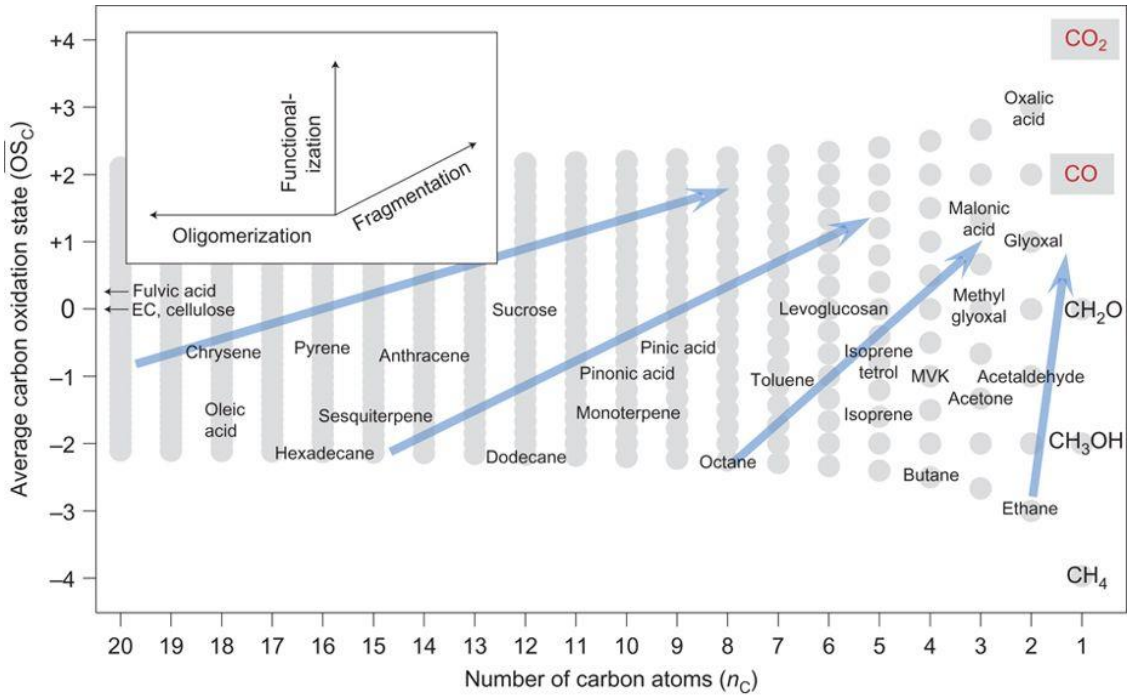

Figure 1-2. Any organic species can be placed in this two-dimensional space. Inevitably, with enough time, increase in atmospheric oxidation implies organics will generally move up and to the right (blue arrows), towards CO2 (Kroll et al., 2011).

1.2 OH AND CHLORINE RADICAL CHEMISTRY AND EFFECT OF NO_x

Historically, the focus of the atmospheric science community has been on the reactivity of VOCs with OH radicals, which are the most abundant radicals in the atmosphere. Several decades of work on OH radical reactivity with specific VOCs spanning the range of C_5-C_{16}(Atkinson, 2000, 2007; Atkinson and Arey, 2003; Ziemann and Atkinson, 2012) mean that the reaction rates (k_{OH}) and mechanisms are fairly well understood. There are a few gaps in knowledge there as well (e.g. 2, 6, 10- trimethyl dodecane and 2-methyl nonane), but it is expected that their reactivity with OH (k_{OH}) will be similar to species with similar molecular structures. In the case of some Volatile

Chemical Products (e.g. mineral spirits), exact composition is not known and thus a robust k_{OH} value is not known either.

NO_x chemistry plays an important role in the atmosphere (Seinfeld and Pandis, 2006). VOC, NO_x and ozone have a non-linear relationship which is shown in the form of an ozone isopleth plot in Figure 1-3 which plots initial VOC concentrations on the x-axis and the initial NO_x concentrations on the y-axis. Isopleths (lines of constant value) of the maximum ozone concentrations can be constructed by connecting points that correspond to various initial conditions. From the plot, it is clear that there are VOC limited regimes at which lower NO_x concentrations can actually lead to more ozone. Aside from ozone production, presence of NO_x can also lead to formation of organic nitrates, both in the gas- and –particle phases. Depending on individual VOC precursor's reaction mechanism, they can lead to formation of organic nitrates (R-ONO_2), alkyl peroxy nitrates (RO_2NO_2), or acyl peroxy nitrates (R-C(O)$OONO_2$). The chain termination reaction here is the formation of nitric acid.

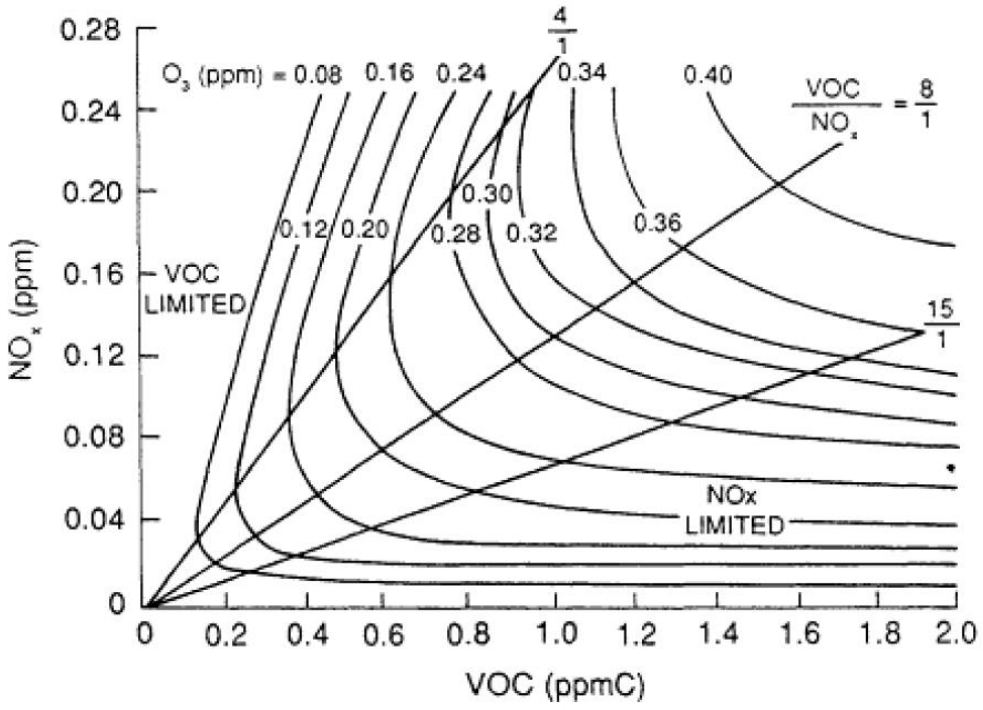

Figure 1-3. Non-linear relationship between VOC, NO_x and ozone. This image is from the National Research Council, 1991.

Ambient measurements suggest that tropospheric concentrations of chlorine atoms (Cl) are higher than previously assumed (Chang and Allen, 2006; Faxon and Allen, 2013; Graedel and Keene, 1995; Tanaka et al., 2000), and that chlorine chemistry may be important in continental as well as coastal environments (Behnke et al., 1997; Finlayson-Pitts, 1993; Finlayson-Pitts et al., 1989; Spicer et al., 1998; Tanaka et al., 2000). Chang and Allen (2006a), Chang et al. (2001) and Chang and Allen (2006b) developed an emissions inventory for chlorine-containing species in Southeast Texas and the total molecular chlorine (Cl_2) and HOCl emissions were reported to be 10^4 kg/day.

Known sources of Cl in the atmosphere include heterogeneous reactions on the surface of particles containing NaCl or NH_4Cl that form photolytic precursors of Cl (Fantechi et al., 1998; Faxon et al., 2018), the reaction of gaseous HCl with OH radicals (Fantechi et al., 1998), industrial point sources, and biocide use in cooling towers and swimming pools (Chang and Allen, 2006b; Faxon and Allen, 2013). Khalil et al. (1999) reported that CH_3CCl_3 (29% of reactive species) and CH_3Cl (43% of reactive species) are the two dominant reactive chlorine-containing species in the atmosphere. Other chlorinated species in the atmosphere include $CHClF_2$, Cl_2, HOCl, CCl_2-CCl_2, CH_2Cl_2, $COCl_2$, and $CHCl_3$. Graedel and Keene (1995); Singh and Kasting (1988) reported that the gas-phase reactions of HCl can also contribute to total Cl radical budget in the atmosphere. The photo-dissociation and oxidation processes of chloro-carbon species and HCl are low enough that it is not significant in the atmosphere (Faxon and Allen, 2013). But chlorine radical (Cl), being a strong oxidizing agent, reacts 1-2 orders of magnitude faster with most VOCs in the atmosphere as compared to OH radicals (the most abundant radicals in the atmosphere) and its reaction rates are relevant to atmospheric chemical processes (Aschmann and Atkinson, 1995; Nelson et al., 1990; Wang et al., 2005).

Table 1-1 shows the reaction rates of VOCs studied in this dissertation with OH and Cl radicals at 298 K (where available). The reaction of several of these VOCs with chlorine has not been studied.

Table 1-1. Summary of all VOCs used in this dissertation

Hydrocarbon species	Molecular Weight (gm mol^{-1})	Vapor Pressure $p^{o}_{L,i}$ (atm)	Temp (K)	Saturation Vapor Concentration C* (μg m^{-3})	Boiling Point (C)	Classification	k_{OH} (cm^3 $molecules^{-1}$ s^{-1})	k_{Cl} (cm^3 $molecules^{-1}$ s^{-1})
Toluene	92.14	2.76E-2	293	1.06E+08	111	VOC	5.63E-12	6.2E-11
n-decane	142.29	1.32E-3	290	7.88E+06	174	VOC	1.25E-11	4.87E-10
2-methyl nonane	142.29	2.49E-3	298	1.45E+07	168	VOC	Unavailable	Unavailable
Butyl cyclohexane	140.27	3.82E-3	310.7	2.10E+07	181	VOC	14.7E-12	Unavailable

Table 1-1 (continued). Summary of all VOCs used in this dissertation

Mineral Spirits	142.29	1.32E-3	290	7.88E+06	174	VOC	1.25E-11	4.87E-10
Texanol®	216.32	9.87E-5	293	8.88E+05	260	IVOC LVP-VOC	Unavailable	Unavailable
DEGBE	162.23	2.88E-5	298	1.91E+05	230	IVOC LVP-VOC	7.44E-11	Unavailable
Linear pentadecane	212.42	6.47E-6	298	5.62E+04	247	IVOC	20.7E-12	Unavailable
TMDD	212.42	4.87E-5	298	4.23E+05	252	IVOC	Unavailable	Unavailable

Table 1-1 (continued). Summary of all VOCs used in this dissertation

Physical properties of mineral spirits assumed to be similar to n-decane, its primary component (McDonald et al., 2018). Classification is based on CARB (2015) and Donahue et al. (2012). DEGBE is diethylene glycol mono-butyl ether and TMDD is 2, 6, 10- trimethyl dodecane.

1.3 LINEAR, BRANCHED, CYCLIC ALKANES AND AROMATIC VOCS

Alkanes contribute to about ~90% of anthropogenic emissions (Fraser et al., 1997; Rogge et al., 1993; Schauer et al., 1999, 2001, 2002) with a majority of them present in diesel exhaust (Miracolo et al., 2010). More recently, it has been shown that straight, branched, and cyclic alkanes account for 42 ± 4% of the SOA formation potential from Volatile Chemical Products, followed by oxidized VOCs (29 ± 12%), alkenes, terpenes (17 ± 5%), and aromatics (12 ± 3%) (McDonald et al., 2018).

Aimanant and Ziemann (2013) and Lim and Ziemann (2009a, 2009b) did some pioneering work on the effect of branching and cyclization on the SOA formation and composition from C_6-C_{17} alkanes. SOA yields were reported to be highest for cyclic alkanes, followed by linear and then branched alkanes (Figure 1-1). Presto et al. (2010) reported high SOA formation from long chain n-alkanes including n-decane, n-dodecane, n-pentadecane and n-heptadecane under high NO_x conditions. Evidence for multi-stage oxidation for IVOCs with low organic aerosol loadings (<2 μg m^{-3}) was presented. For higher loadings, a slow rise in oxidation states (a few percent over several hours) was also shown. Chacon-Madrid and Donahue (2011) reported the chemical aging mechanisms and SOA formation from n-pentadecane and n-tridecanal (saturation vapor concentration ~ 10^6 μg m^{-3}), n-nonadecane and n-heptadecanal (saturation vapor concentration ~ 10^3 μg m^{-3}), with these sets of compounds representing two extremes of IVOC classification based on vapor pressure. The presence of aldehyde group in n-heptadecanal results in more fragmentation and therefore lower SOA formation. As IVOCs products age in the atmosphere and become susceptible to fragmentation, they can still contribute to organic aerosol formation. Tkacik et al. (2012) focused their work on the effect of branching on SOA formation from selected branched and branched-

cyclic IVOCs including C_{12}-C_{19} species. It was found that the position of methyl groups in the molecular structure determined the extent of fragmentation and subsequently SOA formation.

Small aromatic VOCs (e.g. methylbenzene or toluene) are important anthropogenic SOA precursors (Seinfeld and Pandis, 2006) which lie in the volatile range (Table 1-1). These small aromatics comprise almost 44% of the total VOC abundance in urban areas with benzene, toluene, xylenes, ethylbenzene and trimethylbenzenes accounting for 60-75% of the small aromatics abundance (Jang and Kamens, 2001). Toluene is used as a model species to study the reaction mechanism of these small aromatic species. It is a known volatile component of solvents and paints (Fabri et al., 2000) and commercial gasoline fuels (Alramadan et al., 2016; Diehl and Di Sanzo, 2005). Urban toluene concentrations have been reported to vary from 1-200 ppb, depending on geography and location (Fortner et al., 2009; Wang et al., 2009).

Polycyclic Aromatic Hydrocarbons (PAHs) are present in the atmosphere as a result of incomplete combustion processes (e.g. from vehicular exhaust and power plants) and can be in the gas-phase (semi-volatile or volatile) or particle-phase (Finlayson-Pitts and Pitts, 1997). Chan et al. (2009) reported that PAHs including naphthalene, 1-methylnaphthalene, 2-methylnaphthalene and 1, 2-dimehtylnapthelene yielded more than 3-5 times more SOA than light aromatics. SOA from PAHs remained semi-volatile under high NO_x conditions and almost non-volatile under low NO_x conditions. SOA yields under high and low NO_x conditions were 25-45% and 55-75% respectively. The lower yields under high NO_x conditions were because of fragmentation, which made the resulting products more volatile. Conversely, under low NO_x conditions, several “ring-retaining” products were observed.

1.4 VOLATILE CHEMICAL PRODUCTS: AN EMERGING PROBLEM

Volatile Chemical Products (VCPs) include pesticides, coatings, printing inks, adhesives, cleaning agents, and personal care products. According to McDonald et al (2018), 39-62% of emissions from petrochemical VOCs can be attributed to VCPs , 15-43 % to mobile sources and the rest to oil and natural gas production and distribution in the USA. This suggests that VCPs have become important sources of PM formation. This is also corroborated by Warneke et al. (2012) who reported an increase in coating-related emissions along with decrease in emissions from diesel exhaust during the years 1990-2010 in the USA. McDonald et al. (2018) also reported that the total gas-phase VOC emission factors (amount emitted over unit product use) of all VCPs is 1-2 orders of magnitude higher than automobile exhaust (Figure 1-4). Because of this large difference in emission factors, it is expected that total VOC emissions from VCPs are twice as large as from mobile sources (even though VCP sales in the US are a fraction of that compared to mobile sources). This result has a significant consequence for policy-making as current regulatory standards do not include several of these VCPs which are commercially available. The composition of some of these VCPs is unknown and that adds to the challenge of quantifying their emissions individually.

Some of these are individual precursors are classified as “Intermediate-Volatility Organic Compounds” or IVOCs with saturation vapor concentration in the range of 10^3-10^6 $\mu g\ m^{-3}$(Donahue et al., 2006; Presto et al., 2009; Robinson et al., 2007). These IVOCs include long chain n-alkanes, polycyclic aromatic hydrocarbons (PAHs) or large olefins and have lower vapor pressure than most VOCs that are regulated by national and state agencies.

The California Air Resources Board (CARB) recognizes some IVOCs as Low Vapor Pressure Volatile Organic Compounds (LVP-VOCs). CARB defines a LVP-VOC as a chemical compound containing at least one carbon atom with vapor pressure less than 1.32E-4 atm at 20 °C, or having more than 12 carbon atoms (which translates to a saturation vapor concentration lesser than 9.33 E+5 μg m^{-3} assuming a molecular weight of dodecane), or having a boiling point greater than 216 °C, or as a chemical mixture being comprised solely of compounds with more than 12 carbon atoms, or as the weight percent of a chemical mixture that boils above 216 °C. CARB also regulates the use of LVP-VOCs in consumer products (CARB, 2015a) for both residential and commercial use. The CARB (2015) database provides a list of chemical compounds which are known ingredients of VCPs including straight chain alkanes, branched alkanes, cycloalkanes, aromatics, alkenes, cycloalkenes, oxygenated VOCs, halocarbons and unspeciated compounds such as those present in diesel exhaust. McDonald et al., 2018 used a shortened list of these VCPs including acetone, 2-butoxyethanol, glycol ethers, siloxanes, methyl ethyl ketone, Texanol® (2,2,4-Trimethyl-1,3-pentanediol monoisobutyrate), mineral spirits, chlorinated hydrocarbons and ethanolamines to estimate the total emissions which could be attributed to VCPs.

The VCPs listed above are also often used indoors (e.g. cleaning solutions, fragrances, air fresheners) and can have elevated concentrations as compared to outdoor environments (Nazaroff and Weschler, 2004; Weschler and Carslaw, 2018). These elevated concentrations can be harmful to human occupants, and it is important to quantify their primary and secondary emissions. Nielsen (1995) reported the health consequences of cleaning agents including increased eye irritation and sick-building syndrome. Wolkoff et al., 1998 categorized different cleaning agents and their effect on

human health. Active volatile components of cleaning agents included alkanes, alkenes, aromatics, alcohols, glycol ethers, ethers, esters, aldehydes, ketones and acids (Wolkoff et al., 1998). Several previous studies have also identified similar classes of VOCs in indoor environments in the past (Bortoli et al., 1986; Colombo et al., 1991; Knöppel and Schauenburg, 1989; Person et al., 1991; Sack et al., 1992; Steinemann, 2015; Tichenor and Mason, 1988; Vejrup, 1996; Wallace, 1991; Wolkoff, 1995; Wooley et al., 1990).

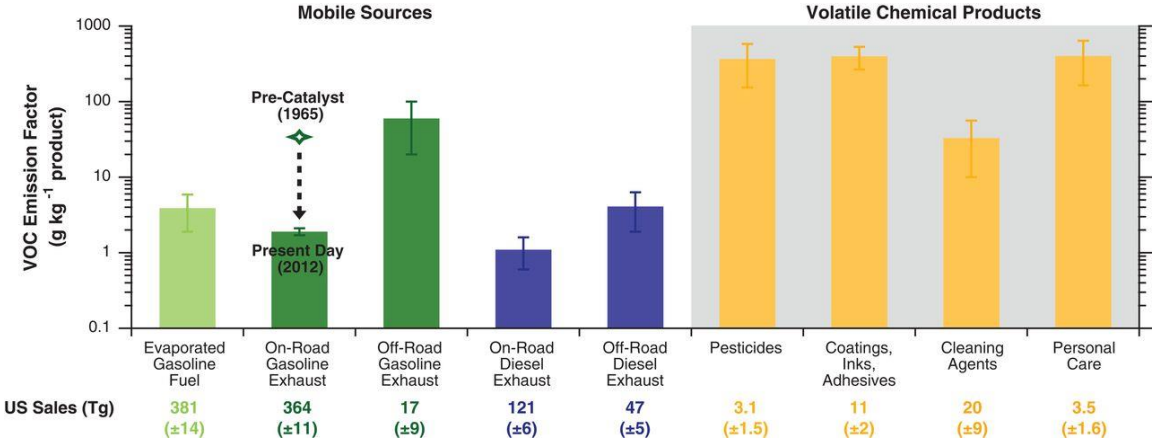

Figure 1-4. Total VOC emission factors from mobile sources and volatile chemical products (McDonald et al., 2018).

Shin et al. (2015) modeled the fate and ozone formation potential of selected VCPs in California's South Coast Air Basin (SoCAB) including Texanol® and diethylene glycol butyl ether (DEGBE), the focus of this dissertation. More than 90% of a majority of compounds are degraded in air due to OH radical reactions or advected out of control volume of their study. In an independent study, Chen and Luo (2012) reported elevated concentrations of ozone downwind of the measurement sites used in Shin et al. (2015).

Li and Cocker (2018) and Li et al. (2018) conducted environmental chamber experiments using selected VCPs and reported their evaporation rates and SOA yields. Half of the reported VCPs including glycol ethers lost more than 95% of their mass within a month and Texanol® within three months due to evaporation. Several of these compounds reported suppressed ozone formation, which suggested that they may act as radical inhibitors or removed NO_x at a faster rate than a mixture of VOCs (called surrogate reactive organic gas mixtures). About half of the VCPs studied in their work formed SOA including DEGBE which had a yield of 0.16. Texanol® was not found to form SOA.

Accounting for emissions from VCPs can also help reduce the difference between experimental measurements and modeled results. For example, the summed OH radical reactivity improved to within 25% of observed values (McDonald et al., 2018). Better closure can also be achieved between modeled and measured SOA concentrations in cities (Hayes et al., 2015; Jathar et al., 2014; Ma et al., 2017; Robinson et al., 2007). On adding SOA from VCPs to traditional transportation emissions, the inter-comparison of modeled and experimental results was also found to improve substantially (McDonald et al., 2018).

Chapter 2: Methods

2.1 Environmental Chamber Experiments

Experiments were conducted in the Atmospheric Physicochemical Processes Laboratory Experiments (APPLE) chamber at the University of Texas at Austin (Figure 2-1). The APPLE chamber is a 10 m^3 Teflon bag (Welch Fluorocarbon) suspended in a temperature controlled room lined with UVA lamps (204 GE T12 Blacklights; peak emission at 368 nm). The chamber was cleaned before each experiment by flushing it with dry clean air generated by a clean air generator (AADCO 737-11) at a flowrate exceeding 100 liters per minute (LPM) for at least 12 hours. Between experiments, "blank experiments" were conducted in which seed particles and Cl_2 (Airgas, 100 ppm in N_2) were injected into the chamber at high concentrations and 100% of UV lights were turned on to remove residual organics which could be released from the Teflon® chamber surface.

A typical environmental chamber experiment involved the following steps. Ammonium sulfate (Sigma Aldrich, 99%) seed particles were created from a 0.01 molar (M) solution using an aerosol generation system (Brechtel Manufacturing, Inc. Model 9200). These provide a surface area for condensation, thus aiding Secondary Organic Aerosol (SOA) formation. Then, the chosen oxidant is introduced into the chamber. In the case of Cl-initiated photo-oxidation, molecular chlorine (Cl_2) was introduced into the chamber using a high-pressure gas cylinder from Airgas (106 ppm in N_2). To simulate high NO_x conditions, different approaches were attempted. In selected experiments, NO and NO_2 were added separately to the chamber using high-pressure gas cylinders from

Airgas (48.73 ppm NO and 9.86 ppm NO_2 respectively). In some experiments HONO was added as a source of OH and NO_x; the HONO solution was prepared immediately before injection in a custom-made glass flask (Kimble-Chase) by adding a 0.05 M solution of sulfuric acid to a 0.1 M solution of sodium nitrite. The titrated solution was then introduced into the chamber by flushing the flask with clean air. H_2O_2 (Sigma Aldrich, 30% (w/w)) was added in some experiments as a source of OH radicals. It was introduced into the chamber by flushing clean air into a glass bottle (Kimble-Chase, 250 ml) containing the H_2O_2 solution. Next, the volatile organic compound (VOC) was introduced in the chamber via a glass sampling tube. If using a compound of lower volatility such as Intermediate- Volatility Organic Compounds (IVOCs), a custom-made heated injector was used. Microliters of the IVOC would be transferred using a glass syringe to a port on the heated injector (initially at room temperature). The injector is then immediately placed inside the environmental chamber. Using a temperature-controlled programmer, the temperature on the heated injector was increased to 150 C. A steady flow of clean air at 2 lpm is used to aid the diffusion of the volatilized IVOC into the chamber. After 30 minutes, the heated injector was removed from the chamber. After the particles and gases were injected into the chamber and allowed to mix, the UV lights were switched on, photolyzing the oxidant precursors (e.g. HONO to OH + NO, Cl_2 to 2Cl or H_2O_2 to 2OH) and starting the oxidation reactions.

A suite of instruments is used to measure the gas-phase and particle-phase species during each experiment. Figure 2-1 shows the laboratory setup and the following sections describe the operating principle of the instruments.

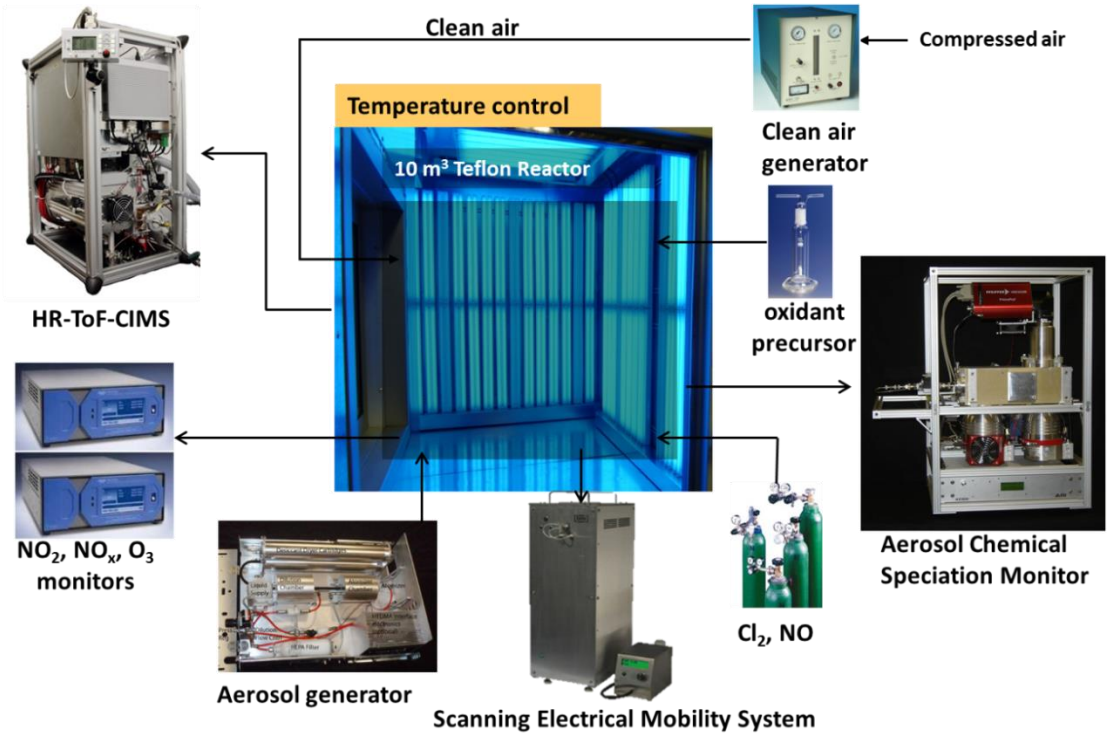

Figure 2-1. Overview of the University of Texas at Austin Atmospheric Physico-Chemical Processes Laboratory Experimental (APPLE) chamber with suite of instruments

2.2 INSTRUMENTATION

2.2.1 Scanning Electrical Mobility Spectrometer (SEMS)

2.2.1.1 Principle of operation of SEMS

The working principle behind Brechtel Manufacturing, Inc. Scanning Electrical Mobility Spectrometer (SEMS) Model 2002 was developed by Wang and Flagan (1990). SEMS measures the number and size distribution of particles. The instrument is capable of measuring particles in the size range of 10-2000 nm, but the current mode of operation is optimized to measuring particles in the size range of 10-1000 nm. SEMS consists of a Differential Mobility Analyzer (DMA) column and a Mixing Condensation Particle Counter (MCPC). The DMA column size selects particles based on their electrical mobility, which is related to size and voltage:

$$Z_p = \frac{neC_C}{3\pi\mu D_p} \qquad \text{Equation 2-1}$$

$$V = \frac{Q_{sheath} \ln(\frac{R_{outer}}{R_{inner}})}{2\pi L_{DMA} Z_p} \qquad \text{Equation 2-2}$$

The notations stand for the following terms : Z_p is electrical mobility (V/m^2s), n is the number of elementary electrical charges carried by the particle, e is the unit of electrical charge (1.6 E-19 C), C_c is the Cunningham slip correction factor (dimensionless), μ is the air dynamic viscosity (kg/m/s), D_p is particle diameter (m), V is the voltage applied to the DMA center rod (volts), Q_{sheath} is the sheath flow (m^3/s), R_{outer}

is the outer cylinder inside radius (m), R_{inner} is the center rod outside radius (m), L_{DMA} is the center rod length (m), and Z_p is the particle electrical mobility (V/m^2s).

Sheath flow (in the form of compressed air) and excess flow (in the form of vacuum) is provided to the DMA column. A programmable software controls the flow rates of sheath, excess and polydisperse inlet flows. The DMA cycles through different voltages (0-6000 V) two times – once called the "Up Scan" (when it increases from 0-6000 V) and second called the "Down Scan" (when it decreases from 6000-0 V). Each voltage is associated with a particular size range of particles. Only particles of those selected size ranges will be let through the monodisperse outlet at bottom of the DMA column, while others are scattered to the walls of the column. The time resolution of the SEMS is set to 1 minute per scan, but it can operate at a faster timescale of 30 seconds per scan.

The MCPC (McMurry, 2002) counts the number of particles in each range or "bin" which are let through the DMA column. The size of these particles is increased by condensing a super-saturated vapor onto the surface of the particles. The MCPC used here utilizes high purity 1-butanol (Sigma Aldrich, ≥99.4%). Other versions of the MCPC have also been developed which use water as the condensing vapor. The monodisperse sample stream of aerosols is exposed to 1-butanol at a high temperature, and then bought in contact with a cooled condenser, where the super-saturated vapor condenses onto the particles, which can then be optically counted. The MCPC's maximum detection limit is 2 μm. Both the CPC and the DMA column can also be used separately, for example, when calibrating other instruments.

Figure 2-2 shows the schematic diagram of the SEMS while in operation, Figure 2-3 shows the schematic diagram of the DMA column and Figure 2-4 shows the schematic diagram of the MCPC. The polydisperse (containing different sized particles) sample passes through a pre-impactor which removes particles larger than the selected size range of the instrument. The in-line Nafion dryer then removes water (up to 30% relative humidity). The neutralizer then exposes particles to a bipolar charged ion and imparts a Boltzmann equilibrium distribution. It does so using two radioactive Polonium-210 strips (0.5mCi each) that emit alpha particles that ionize the air molecules passing through the neutralizer. The charged particles then pass through the DMA column (Figure 2-2) where they are size selected based on their electrical mobility. The monodisperse outlet (containing one size range of particles) is then sent to the MCPC which counts the number of particles in the sample.

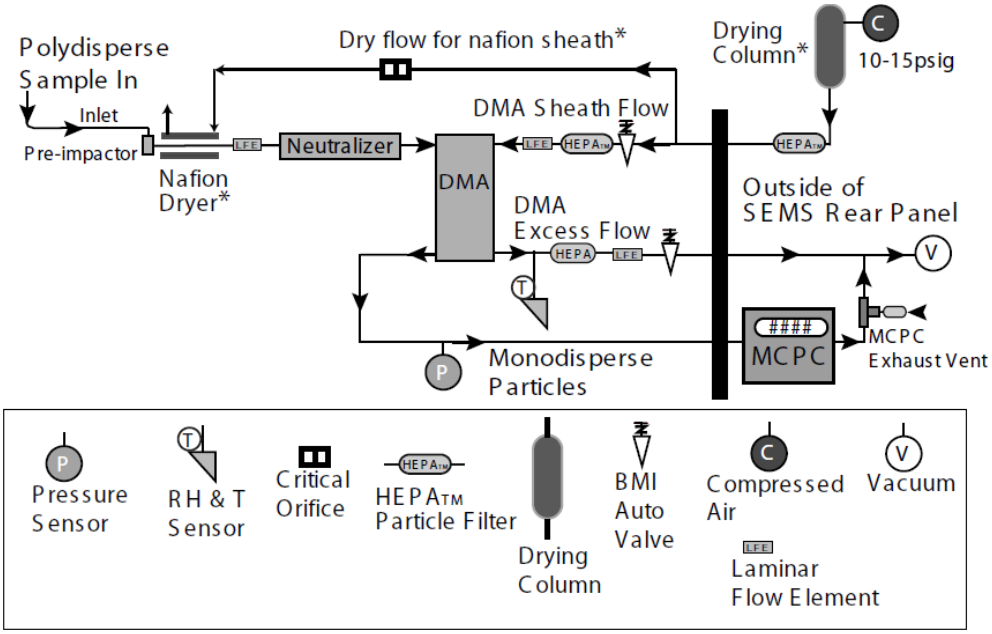

Figure 2-2. Schematic of Brechtel Scanning Electrical Mobility Spectrometer (SEMS) Model 2002 from Brechtel Operating Manual.

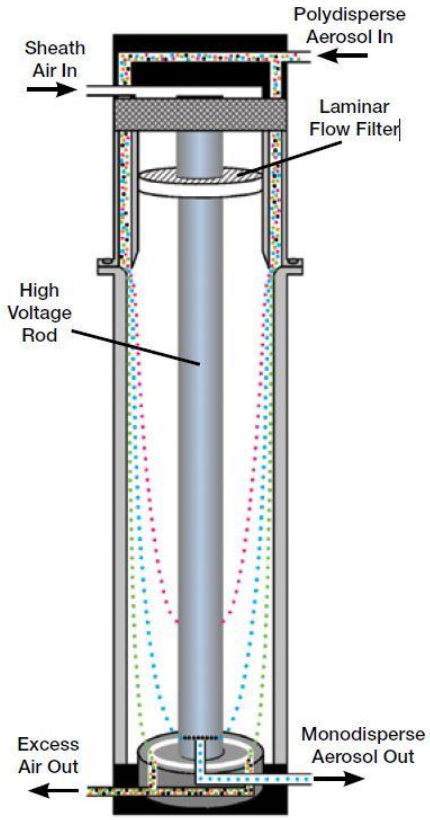

Figure 2-3. Schematic of a Differential Mobility Analyzer (DMA) column (Emanuelsson, 2013).

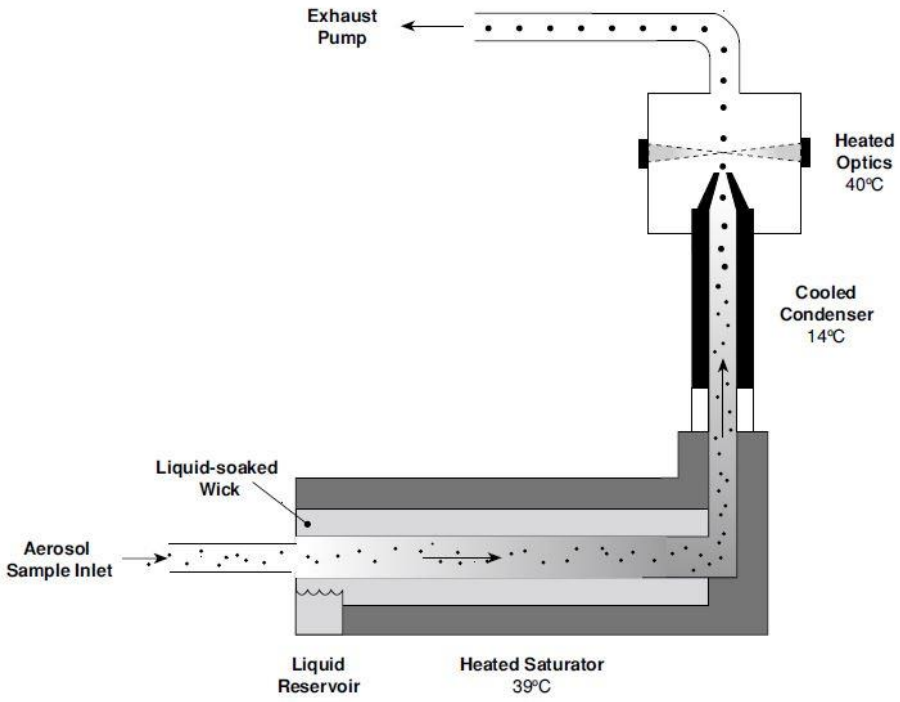

Figure 2-4 Schematic of a Mixing Condensation Particle Counter (Emanuelsson, 2013).

2.2.1.2 Calibration and Data Analysis

Periodic flow rate calibrations of laminar flow elements inside the DMA column, including sheath, excess and inlet flow rates are carried out to ensure the instrument flow rates are correct. The size distribution function of the DMA column is also periodically verified using Polystyrene Latex (PSL) particles with a specified size (for example: 300 nm, 600nm and 900 nm). A “plumbing delay” exists between when the time that particles are size selected in the DMA and when the CPC measures the count. This is characterized periodically and manually entered into the system software which incorporates these before reporting final concentrations.

The output form SEMS is in the form of number of particle per "bin" (or size range). Here, the measured size ranges are optimized for 10-1000 nm and the SEMS divides these into 60 bins or 60 different size ranges. This initial number count of particles per bin can be converted into total particle surface area and total particle volume. The accompanying SEMS software automatically does this and also corrects for multiple charging, CPC size dependent collection efficiency, Cunningham factor and plumbing delay.

Volume from the SEMS can be converted to mass using density. The density for organic and inorganic particulates was reported by Ng et al., 2007: 1.77 g/cc for ammonium sulfate, 1.72 g/cc for ammonium nitrate and 1.4 g/cc for organics and organic nitrates.

2.2.2 Aerosol Chemical Speciation Monitor (ACSM)

The Aerosol Chemical Speciation Monitor (ACSM) (Ng et al., 2011a) measures the total concentration of particles less than 1 um in size (PM_1) along with its bulk composition (percentage of organics, sulfates, ammonium, chlorides, nitrates). A unit-mass resolution mass spectrum can also be obtained from the ACSM. A higher end version of the instrument is the High Resolution Aerosol Mass spectrometer (HR-AMS) (Decarlo et al., 2006) which reports the total PM_1 concentration, high resolution mass spectrum, elemental composition (H:C, O:C), oxidation states (O_{Sc}) and particle size distributions using a vacuum aerodynamic diameter measurement (different from SEMS). Some correlations have been developed over the years to extrapolate similar HR-AMS information from the ACSM (within the instrument limitations). In this section,

the working of the ACSM, its calibration techniques, data analysis routines and extrapolation of information about oxidation states of organic aerosols from ACSM will be discussed.

2.2.2.1 Principle of operation of the ACSM

Figure 2-5 illustrates the operating principle of the ACSM. Particles are sampled and focused through an aerodynamic lens (Liu et al., 1995a, 1995b) and then flash-vaporized on a heater at 600 °C; the resulting gas molecules are ionized using electron-impact ionization. This harsh ionization method results in fragmentation of most molecules. The molecular fragments, which are measured by a quadrupole mass spectrometer, are attributed to six categories—organics, nitrate, sulfate, ammonium, chloride, and water. These categories are determined using a fragmentation table (Allan et al., 2004), which uses a combination of calculations and empirically measured relationships to determine the source of signal at each mass to charge ratio. An internal source of naphthalene is used to calibrate the mass to charge of measured ions. The instrument alternates between normal sampling and sampling through a particle filter, enabling subtraction of a gas-phase background. Here, the ACSM was typically operated at a time resolution (filter/sample cycle length) of approximately 90 seconds, and additional averaging is performed in post analysis of the data.

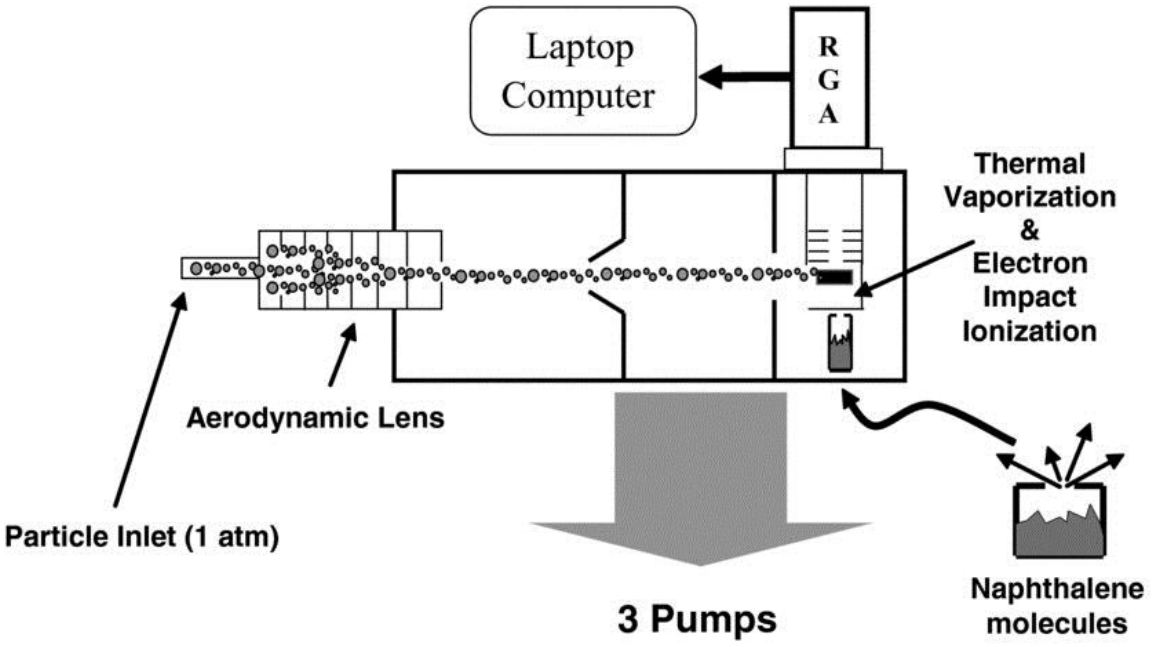

Figure 2-5. Schematic of the Aerosol Chemical Speciation Monitor (ACSM) (Ng et al., 2011a).

2.2.2.2 Calibration Techniques

The nitrate ionization efficiency (IE) of the ACSM (response of instrument – the portion of fragments which are ionized and measured by the instrument), as well as the relative ionization efficiencies (RIEs) of sulfate and ammonium (e.g. the IE of sulfate relative to the IE of nitrate) are measured using dried ammonium nitrate and ammonium sulfate particles with a diameter of 300 nm. Calibration particles are generated using an aerosol generation system. The 300 nm particles are separated from a polydisperse particle distribution using the DMA column (see Section 2.2.1). After being separated, these 300 nm particles are sampled by the ACSM and the condensation particle counter, where their number concentration is measured and converted to mass

using a shape factor. This measurement is used to obtain the IE and RIE values. Periodic calibration is carried out to make sure no major changes in instrument measurements appear over time. More details relating to new and improved ACSM calibration techniques can be found in a Ph.D. dissertation by Wang, D.S. (2018).

2.2.2.3 Data Analysis

Data from the ACSM are analyzed in Igor Pro using the software package "ACSM Local," which corrects for IE/RIE and changes to the air beam and flow rate throughout a measurement period. It applies a relative ion transmission efficiency correction – which accounts for less efficient measurement of larger ions. The software also applies the fragmentation table (Allan et al., 2004) to determine the composition of particles. The ACSM does not detect all sampled particles, primarily due to particle bounce at the vaporizer, resulting in a collection efficiency (CE) smaller than 1. In some cases, this is corrected with data from the SEMS (after the density correction described in Section 2.2.1.1), which samples all particles.

2.2.2.4 Extraction of oxidation state information from ACSM

The ACSM provides unit-mass resolution data which means that we have to rely on certain correlations to derive elemental ratios (H: C, O: C) and oxidation states (O_{sc}). Chapter 1 provided a brief introduction to different graphic descriptions of oxidized organic aerosols. The one relevant to this dissertation is the framework proposed by Ng et al. (2011). The tracer ratio – m/z 44 or f_{44} (relative to total signal in component mass spectrum) was found to be representative of CO_2^+, forming likely from acid groups and

m/z 43 or f_{43} (also relative to total signal in component mass spectrum) was found to be representative of $C_2H_3O^+$. Ambient Organic Aerosol tended to lie inside a triangular region and on "photochemical aging" (extended periods of oxidation); the ambient organic aerosol approached the apex of the triangle (which represents CO_2^+). This means that f_{44} signal increases with oxidation and can be used theoretically to derive O: C elemental ratios (and subsequently oxidation states). The movement of f_{43} signal in this plot is representative of fragmentation (cleavage of C-C bonds). Temporal movement (with extended period of oxidation) to the left would indicate the organic aerosol contains ring-retaining products (less fragmentation) and temporal movement to the right would indicate the organic aerosol contains ring-opened products (more fragmentation). This means that f_{43} signal can be used to derive H: C elemental ratios (and subsequently as a proxy for fragmentation behavior (C-C cleavage). The movement along this triangle can be unique to individual precursor VOCs, but ambient organic aerosol, almost exclusively lie inside the triangle.

This "triangle plot" framework was extended to laboratory chamber experiments, but it has been found difficult to replicate the high oxidation levels found in ambient environments. The reasons for this could be low oxidation levels inside environmental chambers resulting from inability to reach high concentrations of OH radicals in several previous studies. Figure 2-6 shows the graphic representing ambient organic aerosol from Chhabra et al. (2011). The left panel parameterization was developed by Ng et al. (2011) and the right parametrization was developed by Van Krevelan (1950). Data points are from chamber experiments conducted in Caltech environmental chamber using a High Resolution Aerosol Mass Spectrometer (HR-AMS).

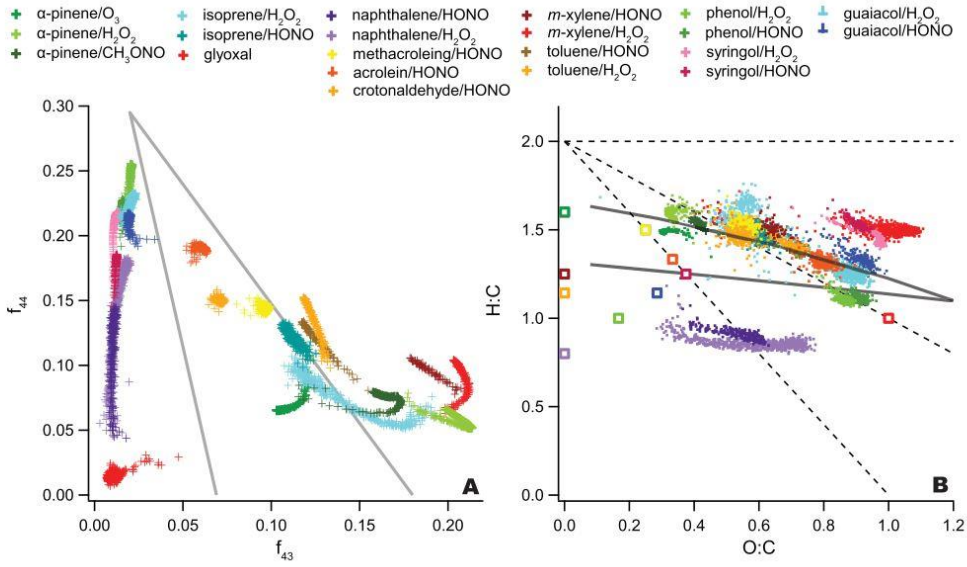

Figure 2-6. f_{44} vs f_{43} signals from a collection of precursor VOCs is shown on the left panel and the H: C vs O: C parameterization is shown on the right (Chhabra et al., 2011).

The most recent update on calculating the O: C and H: C from f_{44} and f_{43} is the Improved-Ambient (IA) method developed by Canagaratna et al., 2015 which improved on the previous parameterization by Aiken et al., 2008; Ng et al., 2011b :

$$O:C_{I-A} = 0.079 + 4.31 * f_{CO2^+} \qquad \text{Equation 2-3}$$

$$H:C_{I-A} = 1.12 + 6.74 * f_{43} - 17.77 * f_{C_2H_3O^+}^2 \qquad \text{Equation 2-4}$$

Equations 2-3 and 2-4 only hold when f_{44} > 0.05 *and* f_{43} > 0.04 but are further used calculate oxidation state using Equation 1-1.

HR-AMS reports the elemental ratios directly and the high resolution mass spectrum can be used to distinguish between individual hydrocarbon species at same m/z (analogous to molecular weight). A caveat of employing this method for an ACSM is that it cannot distinguish between individual hydrocarbon species.

2.2.2.5 Thermo-denuder

A custom-built thermo-denuder (Huffman et al., 2008) is used in the APPLE chamber to experimentally measure the mass fraction of organics remaining by heating (increased step-wise from 25 C to 150 C) the sampling line to the ACSM and SEMS. This gives us the ability to measure the volatility as a function of temperature. Upon using this information in conjunction with an evaporation kinetics modeled developed by Karnezi et al. (2014), and updated in a Ph.D. dissertation by Wang, D.S (2018), we can get an estimate the fraction of products that partition into the particle-phase and the fraction that remain in the gas-phase.

Theoretically, the change in C_i^* (saturation vapor concentration) with temperature (T_D) is described by the Clausius-Clapeyron equation,

$$C_i^*(T_D) = C_i^*(298K)\exp\left[\frac{dH_{vap,i}}{R}\left(\frac{1}{298}-\frac{1}{T_D}\right)\right]\frac{298}{T_D} \qquad \text{Equation 2-6}$$

where T_D is in Kelvin, and $dH_{vap,i}$ (or $\Delta H_{vap,i}$) is the enthalpy of vaporization in kJ mol^{-1}. A further correction for the kinetic and transition regime effects $\beta_{m,}$ is then applied:

$$\beta_{m,i} = \frac{1+Kn_i}{1+\left(\frac{4}{3\alpha_{m,i}}+0.377\right)Kn_i+\frac{4}{3\alpha_{m,i}}Kn_i^2} \quad \text{Equation 2-7}$$

where $\alpha_{m,i}$ is the mass accommodation coefficient (proportion of colliding molecules which will be incorporated into the surface) included to account for mass-transfer resistance and K_{ni} is the Knudsen number.

The aerosol evaporation rate is then calculated as the summed mass flux from the particle-phase, which is equal to the increase in the gas-phase concentration (based on equilibrium partitioning behavior).

The input to the model includes the fraction of organics remaining in the environmental chamber at specific temperatures, user-defined number of "C* bins" (Section 1), user-defined sensitivity and the average diameter (D_p) of organic aerosol formed. In this dissertation, in addition to above parameters, the mass accommodation coefficient and enthalpy of vaporization are also fixed (after conducting several runs of the model without these constraints). The mass accommodation coefficient theoretically can vary from 0-1 but here it is fixed at 1 while the enthalpy of vaporization is fixed at values unique to individual VOC species.

2.2.3 High Resolution Chemical Ionization Mass Spectrometer (HR-Tof-CIMS)

2.2.3.1 Principle of operation of HR-Tof-CIMS

Gas and particle phase compounds can be monitored using the High-Resolution Time-of-Flight Chemical Ionization Mass Spectrometer (HR-ToF-CIMS, Aljawhary et al.,

2013) coupled with a Filter Inlet for Gases and Aerosols (FIGAERO; Lopez-Hilfiker et al., 2014) from Aerodyne Research, Inc. The HR-ToF-CIMS uses softer chemical ionization which results in minimal fragmentation of parent molecules. Ionization occurs as the sample encounters reagent ions in the Ion-Molecular Reaction Chamber (IMR, Figure 2-7). Ions are then focused through chambers with progressively decreasing pressure in the Atmospheric Pressure Interface (API) until they reach the Time of Flight (ToF) region. Mass spectra are derived from measurements of the ions' time-of-flight as they are pulsed through the low-pressure ToF chamber in a "V" shape. Several reagents can be used to ionize the sample. The most common are acetate clusters, water clusters, iodide-water clusters, and nitrate ions. Two chemical reagent ions are used here – positively-charged water clusters ($H_3O^+ \cdot (H_2O)_n$) and negatively-charged iodide-water clusters ($I^- \cdot (H_2O)_n$). Water cluster ionization is most sensitive towards detection of moderately oxidized hydrocarbons; the ability to ionize and thus sensitivity is based on the relative proton affinity between the water cluster and the parent molecule. Iodide-water cluster ionization is most sensitive towards detection of more highly oxidized hydrocarbons and acids.

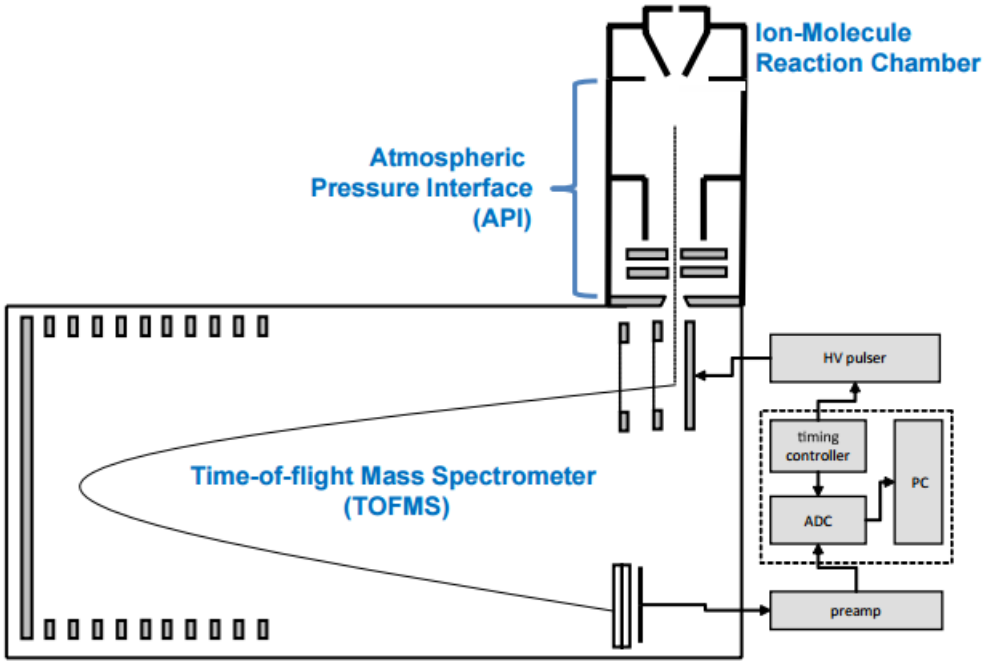

Figure 2-7. Schematic of a Chemical Ionization Mass Spectrometer as shown on manufacturer's website: Aerodyne Research Inc. (www.aerodyne.com).

2.2.3.2 Data Analysis

Data from the HR-ToF-CIMS are analyzed in Igor Pro (Wavemetrics) using Tofware, the software provided with the instrument. The data are first mass calibrated based on HR-ToF-CIMS reagent ions and other known ions. The baseline is subtracted and the average peak shape is found as a function of *m/z* so it can be used for high-resolution analysis. Because of the high resolution in mass spectra, multiple ions can be identified at any given integer *m/z* as shown in Figure 2-8. Overlapping peaks at close m/z have previously been shown to introduce errors in quantification (Cubison and Jimenez, 2015).

Based on the peak shape each integer *m/z* of the mass spectrum is fit by adding multiple peaks to minimize error. Isotopes from lower *m/z* peaks are included in the fit. After ions are identified in the high-resolution spectrum, the peaks are integrated to yield a time series of ions. Analyte ion concentrations are then normalized by the reagent ion concentrations – the sum of H_3O^+, $H_3O^+ \cdot(H2O)$ and $H_3O^+ \cdot(H_2O)_2$ for water cluster ionization and the sum of I^- and $I^- \cdot(H2O)$ for iodide-cluster ionization. This correction accounts for changes in reagent ion concentrations and instrument sensitivity during and between experiments. The HR-Tof-CIMS is very sensitive to certain species and it is important to account for these changes either during the course of an experiment or for inter-comparison with experiments. Sensitivity curves can be measured using known concentrations of observed compounds –by injecting known amounts to environmental chambers. However, three reasons prevented us from reporting quantitative values – 1) many of the VOCs used in this dissertation are not detected by the water-cluster or iodide-water cluster CIMS (n-alkanes) 2) some VOCs have overlapping peaks at their m/z (toluene as shown in Figure 2-8) 3) CIMS is highly sensitive to IVOCs such as glycol ethers and mineral spirits (sometimes overwhelming the dominant reagent signal itself).

That being said, the advantage of the HR-ToF-CIMS is the ability to detect a large variety of volatile organic compounds (VOCs) and its oxidized products. Because of this the HR-ToF-CIMS is mainly used qualitatively as a means to identify important compounds in the gas and particle phase.

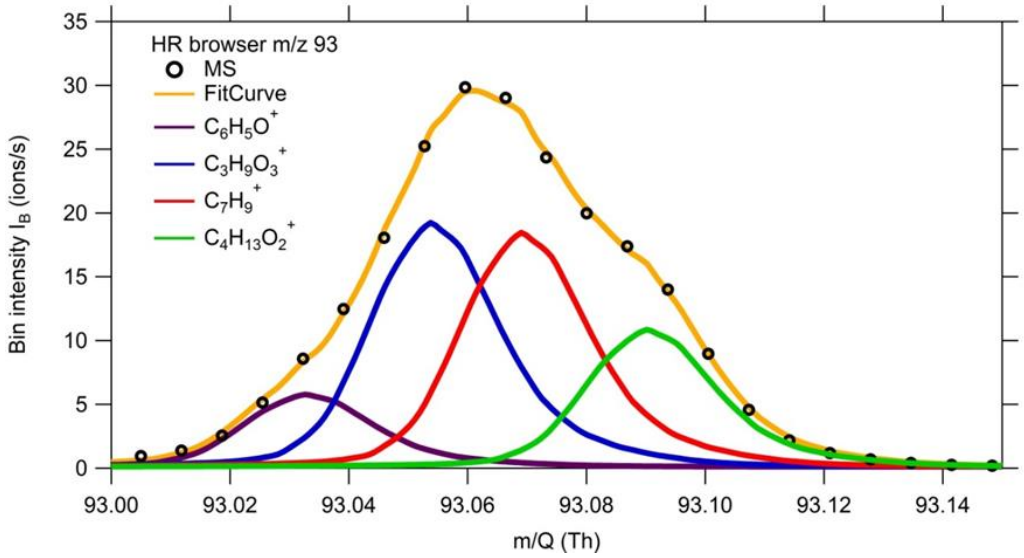

Figure 2-8. HR-Tof-CIMS mass spectrum from an environmental chamber experiment with Toluene (m/z 93; $C_7H_9^+$).

2.2.4 Filter Inlet for Gases and Aerosols (FIGAERO)

The Filter Inlet for Gases and Aerosols (FIGAERO, Figure 2-9) is an inlet manifold that operates in two modes: (1) air sampling and analysis of gas-phase composition while particles are collected on a PTFE filter and (2) temperature-programmed thermal desorption of the collected particles and composition analysis of desorbed vapors. Coupling the FIGAERO to a HR-ToF-CIMS allows for the identification and quantification of gas and particle-phase species at high mass and time resolution. The FIGAERO-CIMS also provides information on the vapor pressure of particle-phase components as higher-volatility species will desorb earlier from the filter than lower-volatility species.

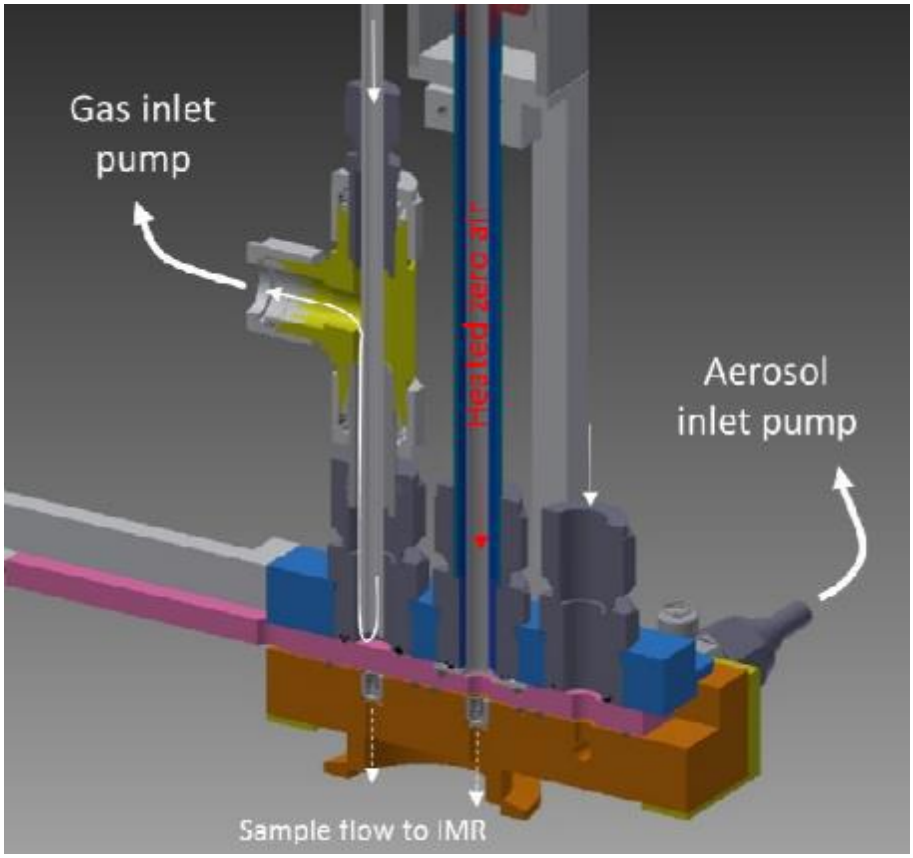

Figure 2-9. Schematic of the FIGAERO inlet as shown on manufacturer's website: Aerodyne Research Inc. (www.aerodyne.com).

The calibration techniques of FIGAERO are presently debated in the atmospheric science community. This dissertation follows the routine described in Wang and Hildebrandt Ruiz (2018). Particles are deposited onto a PTFE filter (Zefluor®, 2.0 µm 24mm, Pall Corp.) by drawing the sample at 3 SLPM through the filter during filter collection mode. During filter desorption mode, the carrier gas temperature (N_2) is ramped from 25 ^{o}C to ~200 ^{o}C resulting in compounds desorbing from the filter at different temperatures. Based on thermodynamics and kinetics, we know that less

volatile compounds desorb at higher temperature than more volatile compounds. It should be noted that volatility is not just a function of a physical property (temperature) – it is also a function of chemical composition of organic aerosol (such as oxidation states, functional groups, elemental ratios). So there needs to be further fine-tuning of this framework, both with respect to calibration methods, and incorporating this information in existing evaporation kinetics models.

2.2.5 Gas-phase monitors

Ozone is measured using a Teledyne absorption O_3 monitor (Model 400E). This instrument uses the Beer-Lambert law to calculate the concentration of O_3 based on the amount of UV light that is absorbed in a sample cell. The instrument alternates in 3 second intervals between the sample stream and a stream that has been scrubbed of ozone for reference. This instrument is calibrated using known concentrations of ozone. Clean air is used as a reference point for zero concentration before each experiment.

Concentrations of NO and NO_x are measured using a Teledyne NO_x monitor (Model 200E). NO is measured through its chemiluminescent reaction with O_3 and NO_2 is catalytically converted to NO and then the total NO_x concentration is reported. NO_2 concentration as reported by this instrument is simply the total NO_x concentration minus the NO concentration. The NO_x monitor is subject to certain interferences which could lead to errors in its NO_2 concentrations – most notably other oxidized nitrogen compounds such as HONO and organic nitrates which can also be converted to NO in the instrument (Winer, 1994; Winer et al., 1974). The NOx monitor is calibrated with

fixed concentrations of NO gas. Clean air is used as a reference point for zero concentration before each experiment.

Concentrations of NO_2 are measured via an NO_2 monitor from Environnement (Model AS32M), which uses a Cavity Attenuated Phase Shift (CAPS) method to directly measure NO_2 (Kebabian et al., 2005, 2008). This instrument measures the phase shift in square-wave modulated light that passes through a sample cell. The degree of phase shift correlates to fixed instrument properties as well as the concentration of NO_2. The advantage of this direct NO_2 measurement is that it does not rely on NO_2 conversion to NO and is therefore not subject to interference from other nitro-containing compounds. The NO_2 monitor is calibrated with fixed concentrations of NO_2 gas. Clean air is used as a reference point for zero concentration before each experiment.

Chapter 3: Formation of oxidized organic compounds from Cl-initiated photo-oxidation of toluene

The formation of secondary organic aerosol (SOA) from toluene can impact urban air quality and therefore human health. Most SOA studies have focused on OH chemistry; however recent work suggests that chlorine atoms (Cl) may affect tropospheric chemistry more than previously assumed. This chapter focuses on SOA formation from Cl-initiated oxidation of toluene under different conditions. The fast reaction between Cl and toluene enabled complete consumption of toluene in most experiments and aging of the toluene SOA. A high resolution time-of-flight chemical ionization mass spectrometer was used to observe several generations of gas-phase products. The presence of nitric oxides (NO_x) appears to slow down the chemistry, presumably due to the formation of $ClNO_2$ which serves as temporary sink of Cl and NO_x. Data from an aerosol chemical speciation monitor (ACSM) suggest that all SOA formed had high oxidation state, and that the bulk organic composition was different for SOA from Cl-dominated reactions than for SOA from OH-dominated reactions. Addition of oxidant after all toluene had been consumed did not result in significant change in the organic aerosol (OA) oxidation state, suggesting that the system may have reached an oxidative end-point in the particle phase.

3.1 BACKGROUND

Hydroxyl is the most abundant tropospheric free radical, and previous work on the formation and aging of SOA from toluene has focused on OH chemistry (Hildebrandt Ruiz et al., 2015; Jang and Kamens, 2001; Ng et al., 2007; Qiu et al., 2012). However, ambient measurements suggest that tropospheric concentrations of chlorine atoms (Cl) are higher than previously assumed (Chang and Allen, 2006; Faxon and Allen, 2013; Graedel and Keene, 1995; Tanaka et al., 2000), and that chlorine chemistry may be important in continental as well as coastal environments (Behnke et al., 1997; Finlayson-Pitts, 1993; Finlayson-Pitts et al., 1989; Tanaka et al., 2000). Known sources of Cl in the atmosphere include heterogeneous reactions on the surface of particles containing NaCl or NH_4Cl that form photolytic precursors of Cl (Fantechi et al., 1998; Faxon et al., 2018), the reaction of gaseous HCl with OH radicals (Fantechi et al., 1998), industrial point sources, and biocide use in cooling towers and swimming pools (Chang and Allen, 2006b; Faxon and Allen, 2013). Chlorine atoms are very reactive towards most VOCs, with some reaction rate constants one to two orders of magnitude larger than the corresponding rate constants with OH. For example, the toluene-Cl reaction rate constant is 6.2×10^{-11} cm^3 molecule $^{-1}s^{-1}$ (Wang et al., 2005), a factor of 10 larger than the toluene-OH reaction rate constant of 5.63×10^{-12} cm^3 molecule $^{-1}s^{-1}$ (Calvert et al., 2002). This difference in reaction rate constants implies that even when tropospheric Cl concentrations are relatively low, reaction rates of Cl with VOCs can be competitive with or even exceed the reaction rates of OH with the same VOCs.

Toluene is a small aromatic compound and is an important volatile component of solvents, paints (Fabri et al., 2000) and commercial gasoline fuels (Alramadan et al., 2016; Diehl and Di Sanzo, 2005). Urban toluene concentrations have been reported to vary from 1-200 ppb, depending on geography and location (Fortner et al., 2009; Wang et al., 2009). The toluene-OH reaction mechanism in the atmosphere has been studied extensively (Birdsall et al., 2010; Birdsall and Elrod, 2011; Calvert et al., 2002; Molina et al., 1999; Noda et al., 2009; Suh et al., 2002, 2003; Zhang et al., 2012), as well as SOA formation from toluene-OH-initiated reactions (Angove et al., 2008; Hildebrandt et al., 2009; Li et al., 2016; Ng et al., 2007; Odum et al., 1997). The OH-initiated oxidation of toluene proceeds via OH-addition to the aromatic ring (approximately 90%) or H-atom abstraction from C-H bonds (Molina et al., 1999); major products formed include phenol, cresol, epoxide, methylbutanedial, methylhexanedial, benzaldehyde and butanedial (Birdsall et al., 2010). The Cl-initiated oxidation of toluene proceeds primarily (if not exclusively) via H-atom abstraction to form benzyl peroxy radicals (Wang et al., 2005), which continue reacting to form major gas phase products including benzaldehyde, benzyl hydro peroxide and benzyl alcohol, benzyl methyl nitrate and peroxybenzoyl nitrate (Fantechi et al., 1998; Huang et al., 2012, 2014; Karlsson et al., 2001a; Wang et al., 2005). In the absence of NO_x, peroxy radicals are expected to mostly undergo self-reaction leading to radical termination (Young et al., 2014). The presence of NO_x in the toluene + Cl system enhances radical propagation and formation of secondary radicals including OH. These OH radicals can further react with other intermediate products (for example, carbonyls), to increase radical propagation. A competing pathway is reaction of chlorine atoms with the intermediate products. In this

reaction, formation of an alcohol or carboxylic acid leads to chain termination, while formation of another carbonyl leads to further radical propagation. Figure 3- 1 depicts first steps in the toluene-Cl reaction mechanism and Figure 3-2 shows the continued oxidation of the benzyl criegee intermediate.

Even with significant effort in the scientific community, a detailed understanding of SOA formation and aging from toluene photochemistry remains uncertain (Hildebrandt Ruiz et al., 2015; Zhang et al., 2014). SOA yields (Y, the mass of organic aerosol formed divided by the mass of precursor reacted) from Cl-initiated oxidation of toluene were measured in one previous study and ranged from 3-8% at OA concentrations up to 12 μg m^{-3}(Cai et al., 2008). SOA yields from toluene-OH photo-oxidation reported in the literature vary widely. Previous work on the aging of toluene-OH SOA was complicated by the slow reaction between toluene and OH, which makes complete toluene consumption infeasible during a typical environmental chamber experiment (Hildebrandt Ruiz et al., 2015).

This chapter describes results from environmental chamber experiments (Table 3-1) focused on Cl-initiated oxidation of toluene leading to the formation of SOA. The fast reaction between toluene and Cl enables complete precursor consumption and evaluation of SOA aging using different oxidants. Several generations of gas-phase products are observed and their qualitative trends evaluated. SOA yields are quantified and bulk SOA composition is evaluated.

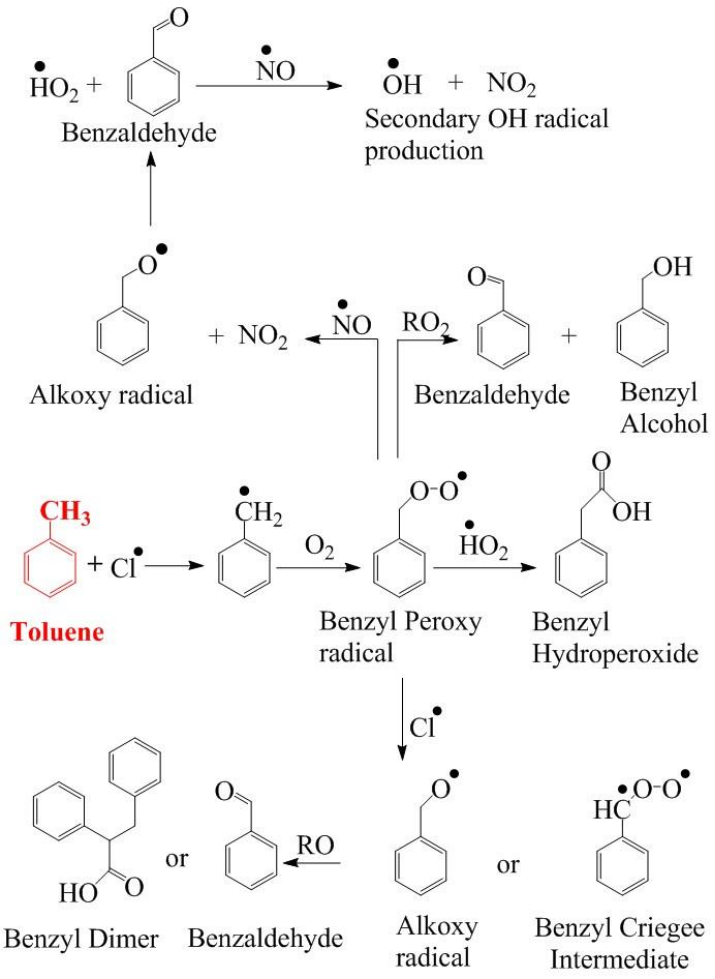

Figure 3-1.Outline of H-atom abstraction pathway for Cl-initiated oxidation of toluene, modified from several sources (Cai et al., 2008; Fantechi et al., 1998; Huang et al., 2012, 2014; Karlsson et al., 2001a; Wang et al., 2005; Young et al., 2014).

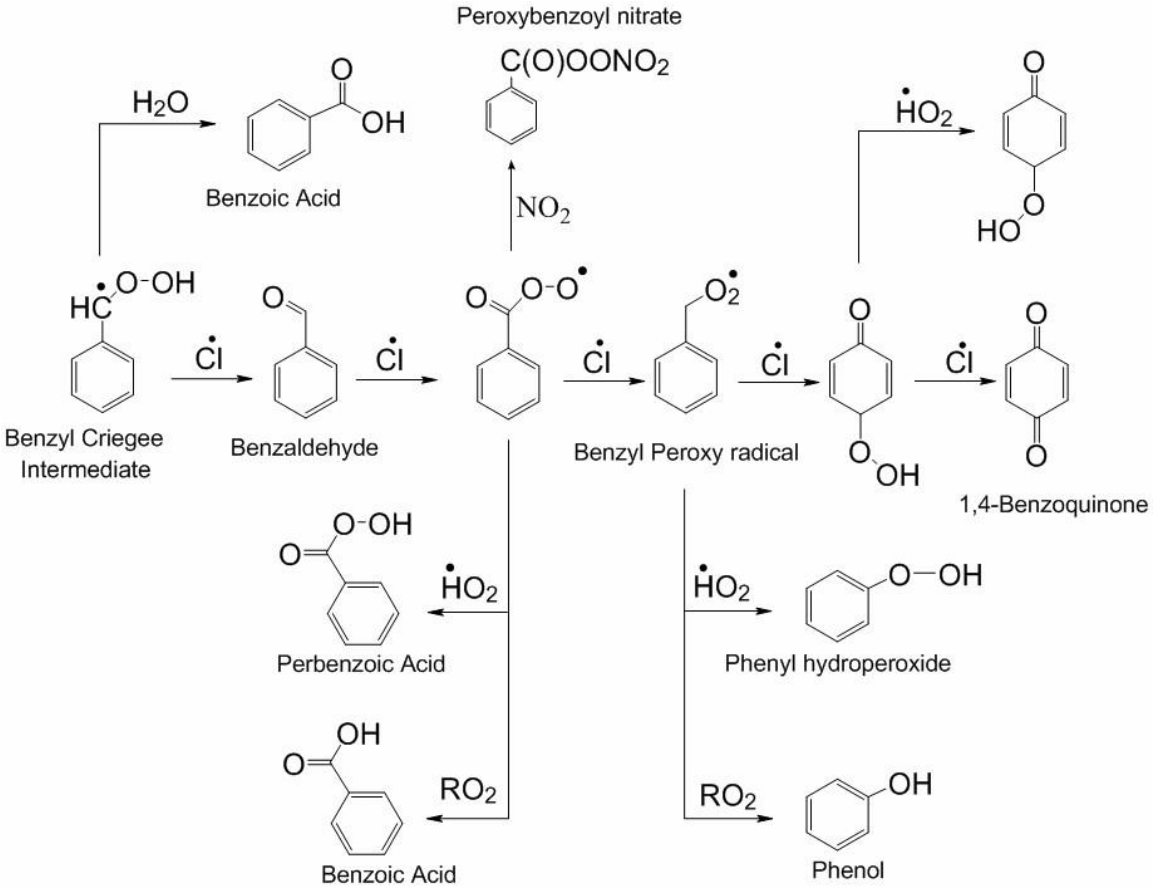

Figure 3-2. Continued oxidation of Benzyl Criegee intermediate modified from several sources (Cai et al., 2008; Fantechi et al., 1998; Huang et al., 2012, 2014; Karlsson et al., 2001a; Wang et al., 2005; Young et al., 2014).

Table 3-1. Experimental conditions and summary of results for toluene-Cl

Exp.	$[VOC]_0$ (ppb)	$[Cl_2/VOC]_0$ (ppb/ppb)	$[NO]_0$ (ppb)	f_{44}	f_{43}	C_{OA}[d]	SOA Yield[d]	f_{HCl}^+	% VOC[e] reacted with Cl
1	51	0.78	<2	17%	3%	49	0.25	0.05	100%
2	54	2.1	<2	16%	3%	95	0.47	0.06	100%
3	37	2.2	19	18%	3%	73	0.53	0.07	91%
4	39	1.04	21	18%	5%	22	0.15	0.05	84%
5	53	1.5	<2	17%	4%	75	0.38	0.05	100%
6	43	0.94	<2	19%	3%	35	0.22	0.07	100%
7	22	2.0	18	25%	3%	9	0.10	0.01	88%
8[abc]	430	HOOH	<2	16%	9%	11	N/A	0.006	0%
9[abc]	300	HONO	369	14%	10%	250	N/A	0.004	0%
10[bc]	490	0.08	490	15%	10%	227	N/A	0.007	21%
11[b]	230	0.17	433	16%	8%	70	N/A	0.008	55%

Table 3-1 (continued). Experimental conditions and summary of results for toluene-Cl

[a] No chlorine was added in these experiments. [b] Toluene was not completely consumed in these experiments. [c] 100% UV lights at beginning of experiment; all other experiments conducted at 40% UV lights. [d] C_{OA} (μg m^{-3}) and SOA yields reported at time t=60 minutes. SOA yields were only calculated for experiments where modeling results suggested complete consumption of toluene. [e] VOC reacted with Cl divided by total VOC reacted (with OH or Cl) based on model results.

3.2 METHODS

The principle of operation of instruments and setup of environmental chamber experiments, the results of which are described below, can be found in Chapter 2. As a short summary, the Aerosol Chemical Speciation Monitor (ACSM) is used to measure the total concentration and bulk composition of particulate matter less than 1 μm in size (PM_1). The High Resolution Time-of-Flight-Mass-Spectrometer (HR-Tof-CIMS) along with a Filter Inlet for Aerosols and Gases (FIGAERO) is used to measure the gas-phase composition of organic aerosols in real-time and the particle-phase composition in a semi-continuous manner. The Scanning Electrical Mobility System (SEMS) is used to measure the number and size distributions of particles. The setup of the environmental chamber is shown in Figure 2-1.

A typical environmental chamber experiment involved the following steps. Ammonium sulfate (Sigma Aldrich, 99%) seed particles were created from a 0.01 molar

(M) solution using an aerosol generation system (Brechtel Manufacturing, Inc. Model 9200). These provide a surface area for condensation, thus aiding Secondary Organic Aerosol (SOA) formation. Then, molecular chlorine (Cl_2) was introduced into the chamber using a high-pressure gas cylinder from Airgas (106 ppm in N_2). To simulate high NO_x conditions, different approaches were attempted. In selected experiments, NO and NO_2 were added separately to the chamber using high-pressure gas cylinders from Airgas (48.73 ppm NO and 9.86 ppm NO_2 respectively). In some experiments HONO was added as a source of OH and NO_x; the HONO solution was prepared immediately before injection in a custom-made glass flask (Kimble-Chase) by adding a 0.05 M solution of sulfuric acid to a 0.1 M solution of sodium nitrite. The titrated solution was then introduced into the chamber by flushing the flask with clean air. H_2O_2 (Sigma Aldrich, 30% (w/w)) was added in some experiments as a source of OH radicals. It was introduced into the chamber by flushing clean air into a glass bottle (Kimble-Chase, 250 ml) containing the H_2O_2 solution. Next, toluene was introduced in the chamber via a glass sampling tube. After the particles and gases were injected into the chamber and allowed to mix, the UV lights were switched on, photolyzing the oxidant precursors (e.g. HONO to OH + NO, Cl_2 to 2Cl or H_2O_2 to 2OH) and starting the oxidation reactions.

3.3 BOX MODELING AND ANALYSIS

Box-modeling was conducted in the SAPRC framework (Carter and Heo, 2013) using the condensed carbon bond mechanism CB6 (Yarwood et al., 2010) with an updated gas-phase chlorine mechanism (Sarwar et al., 2012). Results from chamber characterization experiments were utilized to account for light intensity, dilution and

chamber radical sources (Carter et al., 2005). Initial measured reactant concentrations of toluene, nitrogen oxides (NO, NO_2), and chlorine gas (Cl_2) were used as inputs to the model. Two "dummy species" and corresponding reactions were added to the model to track the reaction of toluene with chlorine atoms (CLVTOL) and with OH (OHVTOL). HONO was not measured directly, but initial concentrations were estimated from the difference of NO_2 concentrations reported by the chemiluminescence NO_x monitor (where HONO is measured as NO_2) and CAPS NO_2 monitor (which does not detect HONO). The sensitivity of the chemiluminescent NO_x monitor to HONO has not been measured and was assumed to be equal to the sensitivity of NO. Initial HONO concentration in the model was varied within 10% to evaluate model sensitivity to this input, which was found to be low. Experimental and modeled results for experiments 10 and 11 are shown in Figures 3-3 and 3-4.

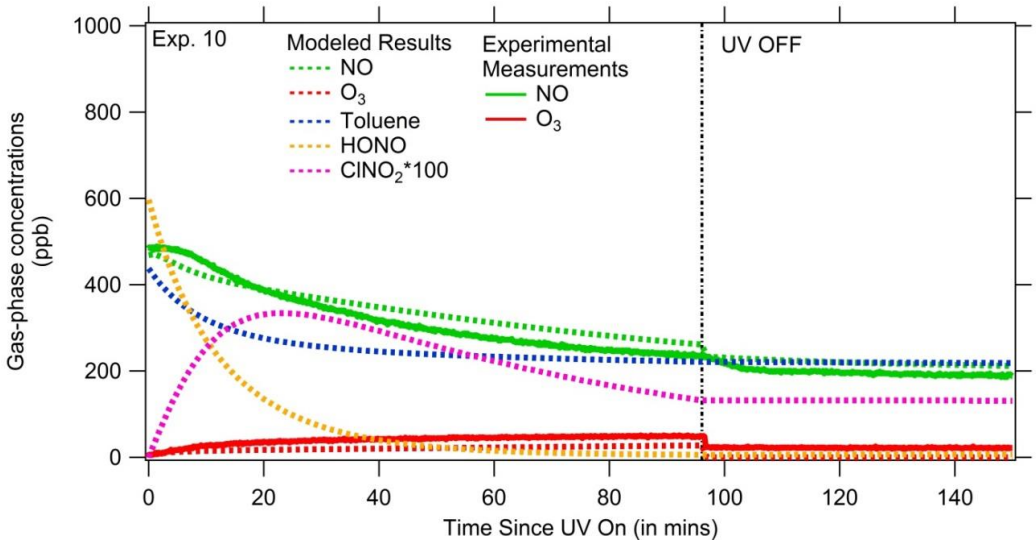

Figure 3-3. Time series of experimental measurements and modeled results for gas-phase species formed under toluene-Cl-high NO_x environment (experiment 10).

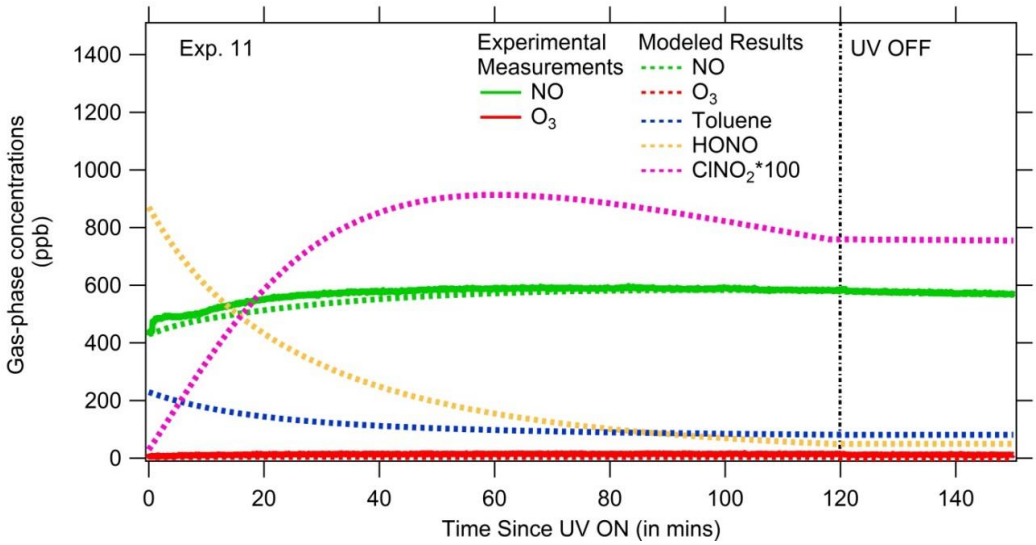

Figure 3-4. Time series of experimental measurements and modeled results for gas-phase species formed under toluene-Cl-high NO_x environment (experiment 10).

3.4 Results and Discussion

All experiments formed SOA. The first few generations of gas-phase chemistry were observed with the CIMS, and the evolution of organic aerosol was observed with the ACSM. Figure 3-5 (top panel) shows time series of gas and particle-phase species from Expt. 1, a typical low NO_x experiment (toluene+Cl) and time series from Expt. 4 (bottom panel), a typical high NO_x (toluene+Cl+NO+NO_2) experiment. Gas-phase species shown in Figure 3-5 are expected to form from toluene + Cl chemistry as shown in Figure 3-1. The SOA yields from Cl-initiated oxidation of toluene are in the range of SOA yields from OH-initiated oxidation of toluene reported by Hildebrandt et al., 2009 (Table 3-1; Figure 3-6).

According to results from the chamber model, for experiments in which Cl was the dominant oxidant, nearly all toluene reacted away in less 30 min of photo-oxidation. This is quite different from experiments in which OH is the dominant oxidant, where less than half of the toluene reacts after several hours of photo-oxidation in this chapter and previous studies (Hildebrandt et al., 2009; Hildebrandt Ruiz et al., 2015; Karlsson et al., 2001b; Ng et al., 2007). The inability to react all or most of the toluene in the toluene + OH system poses challenges in investigating the aging of SOA formed from the oxidation of toluene (Hildebrandt et al., 2009; Hildebrandt Ruiz et al., 2015; Ng et al., 2007). Chlorine atoms thus enable studying toluene SOA aging, as explored in more detail in Section 3.4.3.

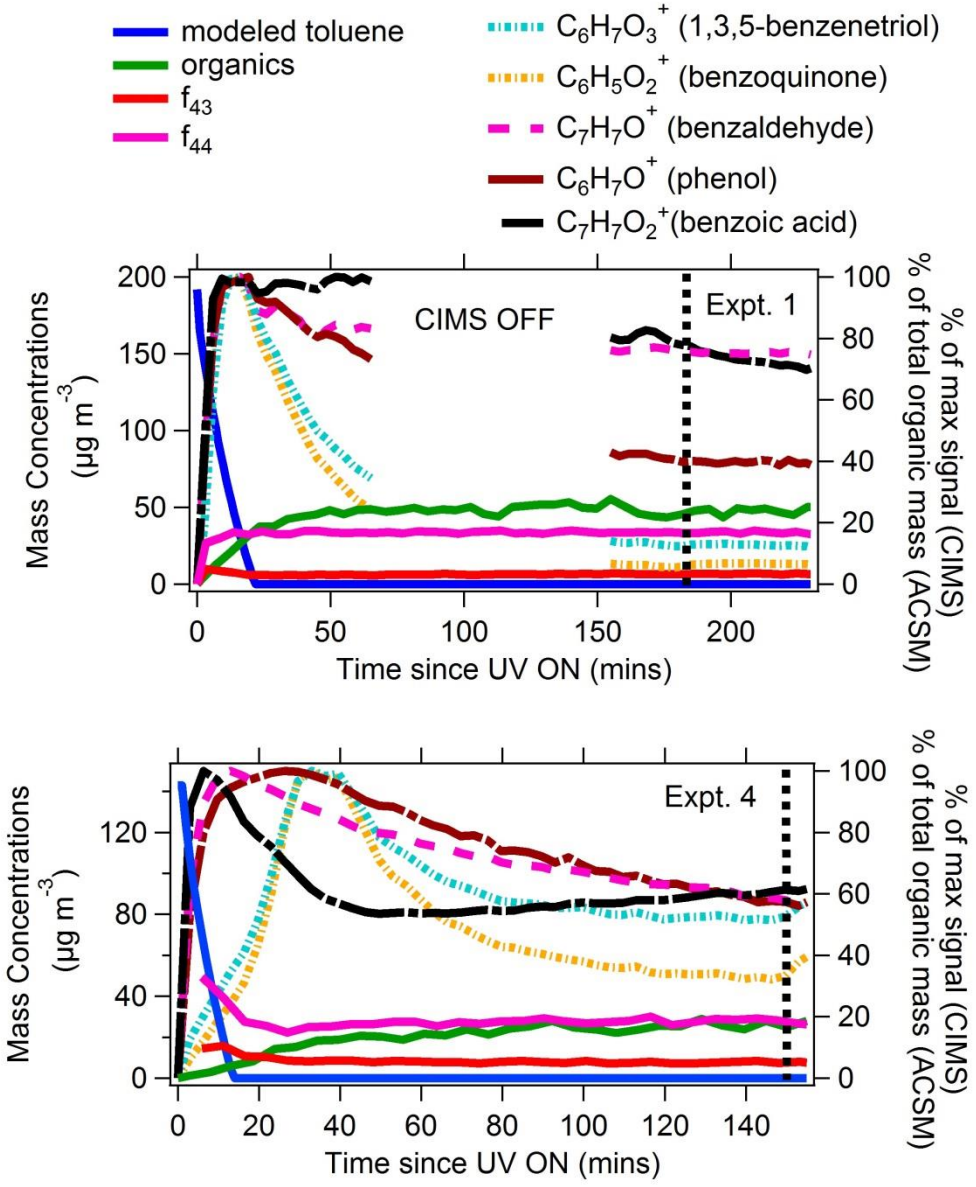

Figure 3-5. Time series of wall-loss corrected OA concentration and modeled toluene decay (left vertical axis) and gas-phase products and f_{43}, f_{44} time series (right vertical axis) during experiment 1 (toluene+Cl; top panel) and experiment 4 (toluene+Cl+NO+NO_2; bottom panel). The dotted black vertical line indicates the time when UV lights were switched off.

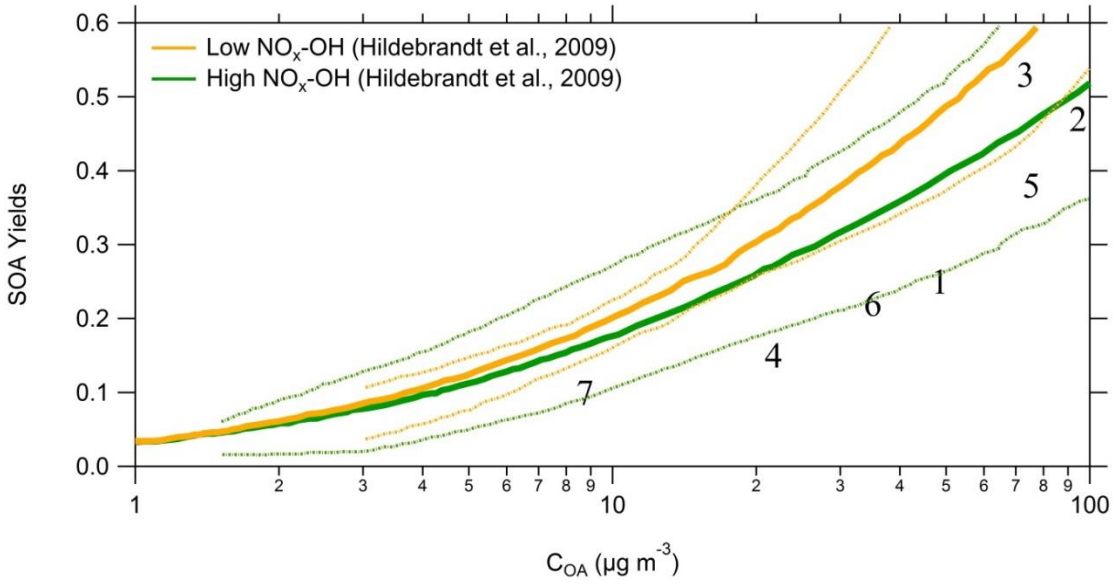

Figure 3-6. SOA yields as a function of total organic mass concentration in the environmental chamber for experiments 1 through 7. SOA yields were only calculated for experiments where modeling results suggested complete consumption of toluene. Dotted lines represent upper and lower bounds for low NO_x-OH (orange) and high NO_x-OH (green) from Hildebrandt et al., 2009.

3.4.1 Gas-phase products

Multi-generational products are formed within minutes of the start of photo-oxidation (Figure 3-5). The vapor pressure of gas-phase products shown in Figure 3-5 are in the intermediate volatility range (Donahue et al., 2011; Tkacik et al., 2012): benzaldehyde (6.4E+06 µg m^{-3}), benzyl alcohol (4.7E+05 µg m^{-3}), phenol (2.1E+06 µg m^{-3}), benzoic acid (4.6E+03 µg m^{-3}), 1,3,5 benzenetriol (1.1E+03 µg m^{-3}), and benzoquinone (5.8E+05 µg m^{-3}) (Linstrom and Mallard, 2001), evaluated at 298K. These species are thus not expected to partition to the aerosol phase under the conditions of these experiments – additional oxidation is required for the formation of secondary organic

aerosol. Higher-generation (lower-volatility) gas phase species were not observed due to the choice of reagent ion - the water cluster CIMS is only sensitive to moderately oxygenated species.

While the presence of NO_x and OH affect the reaction pathway and can result in the formation of different reaction products, here we focus on products that are observed in all experiments. The formation of later generation products is consistently delayed in high NO_x experiments relative to low NO_x experiments (e.g. Figure 3-5). A main difference between high NO_x and low NO_x experiments specific to chlorine-initiated chemistry is the formation of $ClNO_2$ in the high NO_x environment. $ClNO_2$ formation results in decreased concentrations of Cl atoms at the beginning of the experiment and a sustained source of Cl throughout the experiment. In contrast, in low NO_x experiments most of the Cl forms HCl, which is relatively stable to photolysis and does not result in significant recycling of Cl. A further main difference in the oxidative conditions between low and high NO_x experiments is the generation of secondary OH: in high NO_x experiments, a significant fraction of the toluene reacts with OH instead of with Cl (Table 3-1). The delay in formation of later generation products could thus be because the formation of $ClNO_2$ in the high NO_x experiments slows down the chemistry, and/or the presence of NO_x initially inhibits the formation of the higher-generation products formed through the low NO_x pathway.

3.4.2 Organic aerosol bulk composition and oxidation state

Chlorine-initiated oxidation of toluene is thought to proceed primarily, if not exclusively, via hydrogen abstraction at the methyl group (Wang et al., 2005). However,

later-generation chemistry could include chlorine-addition to double bonds, for example, those in benzoquinone. Thus, formation of organochlorides in later-generation chemistry is possible. Wang and Hildebrandt Ruiz (2017) recently evaluated the ability of the ACSM to quantify organochlorides and pointed out that, under normal operating conditions and using standard ACSM analysis techniques, the ACSM generally under predicts concentrations of organochlorides. However, the ion signal at *m/z* 36 (HCl^+) seems to be a good proxy for particulate chloride, and an average mass ratio of HCl to total organics of 7% for SOA formed from Cl-initiated oxidation of isoprene. (Uptake of HCl onto particulate matter was not found to occur unless the relative humidity of the system was very high, which is not the case here.) In the experiments evaluated in this chapter, when Cl was the only oxidant added to the system, the HCl: organic mass ratio or f_{HCl}^+ ranged from 5-10% (Table 3-1, Figure 3-7). This ratio was less than 1% for experiments in which an OH source (HONO or HOOH) was added at the beginning of the experiment, likely due to lower formation of unsaturated products through OH chemistry and/or because a majority of the later-generation products reacted with OH instead of Cl. Overall, the ACSM data suggest that organochlorides form from Cl-initiated oxidation of toluene. The molecular identity or abundance of gas or particle-phase organochlorides cannot be evaluated with the available data – future experiments utilizing iodide as reagent ion in the CIMS can be used to evaluate the molecular identity of gas and particle-phase organochlorides.

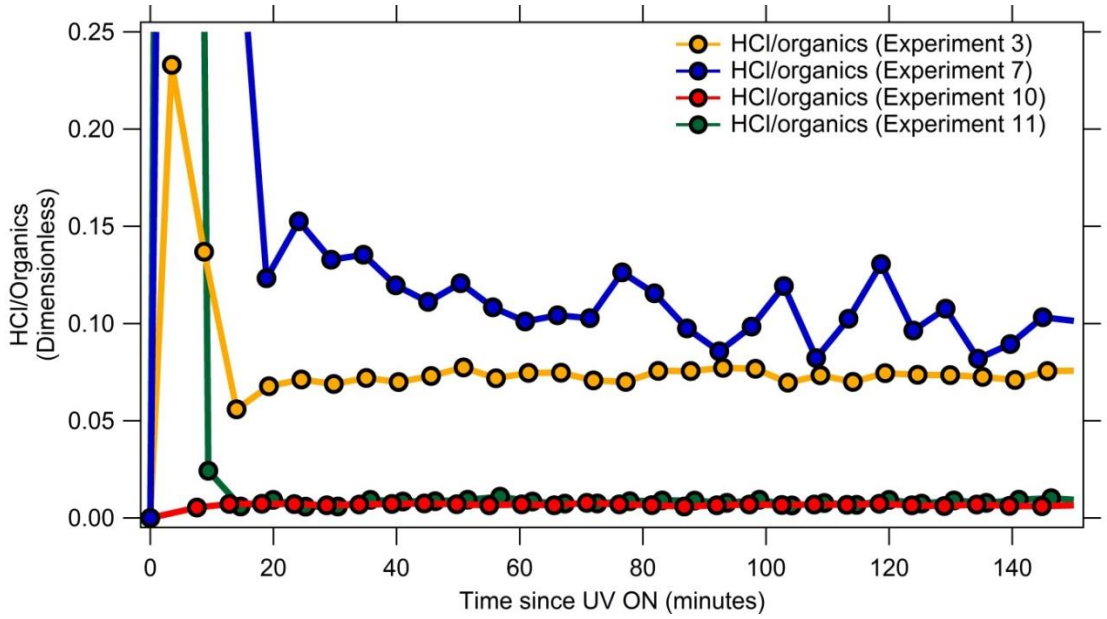

Figure 3-7. Time series of particulate HCl over organics over duration of experiment for toluene-Cl (experiments 3, 7, 10 and 11).

SOA formed from Cl-initiated oxidation of toluene was more oxidized than SOA from OH-initiated oxidation of toluene (Figure 3-8). Furthermore, while f_{43} of SOA from toluene + OH was relatively high (generally lying to the right hand side (RHS) of the Ng triangle), f_{43} of SOA from toluene + Cl was relatively low (generally lying to the left hand side (LHS) of the triangle) (Ng et al., 2010). OH-initiated oxidation of toluene proceeds primarily via OH-addition to the aromatic ring and is known to form ring-opened products such as butenedial, methyl glyoxal and epoxides. On the other hand, Cl-initiated oxidation of toluene mainly forms ring-retaining products. Previous work has analyzed the SOA from different precursors and also found that SOA from OH-oxidation of toluene and xylene fall to the RHS of the triangle (Chhabra et al., 2011). On the other hand, SOA from OH-oxidation of naphthalene, phenol and methoxyphenol which

primarily forms ring-retaining products, falls to the LHS of the triangle (Chhabra et al., 2011). The data presented here are thus consistent with SOA dominated by ring-retaining products (such as SOA from Cl-initiated oxidation of toluene) located on the LHS of the Ng triangle while SOA dominated by ring-opened products (such as SOA from OH-initiated oxidation of toluene) located on the RHS of the Ng triangle.

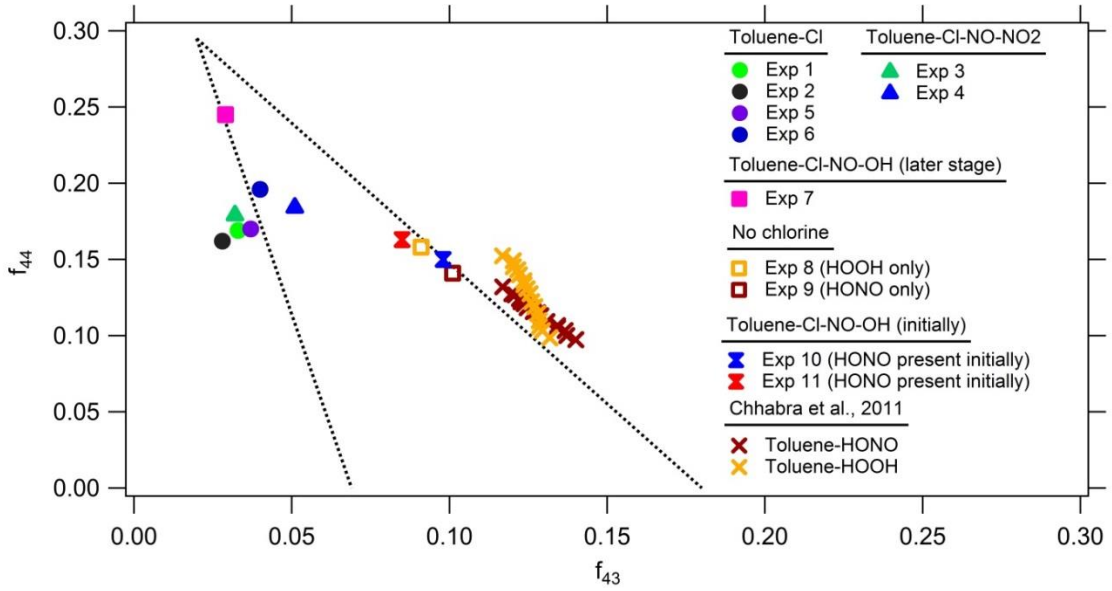

Figure 3-8. f_{44} and f_{43} signals as measured by the ACSM in all experiments for toluene under different conditions. The dotted black lines show typical ambient data (Ng et al., 2011b).

Results from the SAPRC model were used to estimate the fraction of toluene reacting with Cl versus with OH as summarized in Table 3-1. The fraction of toluene reacting with Cl ranged from 0% for experiments in which no source of reactive Cl was added (e.g. Experiments 8 and 9) to 100% for experiments in which no source of OH or NO was added (e.g. Expts. 1, 2 and 5) and included intermediate values of 21% (Expt.10)

and 55% (Expt. 11). In general, f_{43} decreases with the fraction of toluene reacting with Cl consistent with the analysis of the extreme cases (0 and 100%) described above. For SOA from experiments in which at least half of the toluene reacts with OH, f_{43} is similar to experiments in which all toluene reacts with OH. This could suggest that the presence of OH results in a higher abundance of ring-opened higher generation products, regardless of whether the initial oxidation of toluene is by Cl or OH. First and later generation products of toluene oxidation generally react more quickly with OH than toluene itself. Reaction rates of toluene photo-oxidation products with Cl are unknown; however, this would be consistent with OH oxidation being more important for later-generation chemistry than for the first-generation chemistry. It is also possible that the SAPRC model, which uses a condensed mechanism, underestimates the formation of secondary OH. Reaction mechanisms (Cl vs OH-initiated reactions and ring-opened vs ring-retained products) appear to play an important role in determining the oxidation states of SOA from the photo-oxidation of toluene.

3.4.3 Organic aerosol aging

The complete consumption of toluene observed in these experiments makes it possible to evaluate the aging of organic aerosol upon continued oxidation. In several experiments, additional oxidant was added after all toluene had reacted with Cl in order to study aging: in Expt. 5, HOOH was added as a low NO_x source of OH (Figure 3), in Expt. 6 additional Cl_2 was added as a source of Cl (Figure 3-10) and in Expt. 3 (Figure 3-11), HONO was added as a source of OH and NO_x. The addition of HOOH (low NO_x-OH) in Expt. 5 resulted in a noticeable increase in higher generation gas-phase products but

no noticeable change in OA concentrations or bulk composition (f_{43}, f_{44}). The addition of Cl_2 in Expt. 6 resulted in a significant increase in OA, a large decrease in all detected gas-phase products but only a small decrease in f_{43} and no noticeable change in f_{44}. The addition of HONO in Expt. 7 resulted in a small increase in OA concentration but no noticeable change in f_{43} or f_{44}. (CIMS data were not available after HONO injection in Expt. 7). Thus, overall, continued oxidation of the system changes the gas-phase composition but not the bulk particle-phase composition. This may indicate that the system has reached an oxidative end point in the particle phase. Upon further oxidation, more highly oxidized species fragment and partition to the gas-phase while less oxidized species become more oxygenated and partition to (or stay in) the particle phase. The first effect (fragmentation of highly oxidized species) is expected to decrease OA loading and could increase or decrease f_{44}; the second effect (functionalization of less oxidized species) is expected to increase f_{44} and OA loading. In this system, once a high f_{44} has been reached (after the initial toluene + Cl reactions resulting in OA), these two effects appear to approximately cancel resulting in a stable f_{44}.

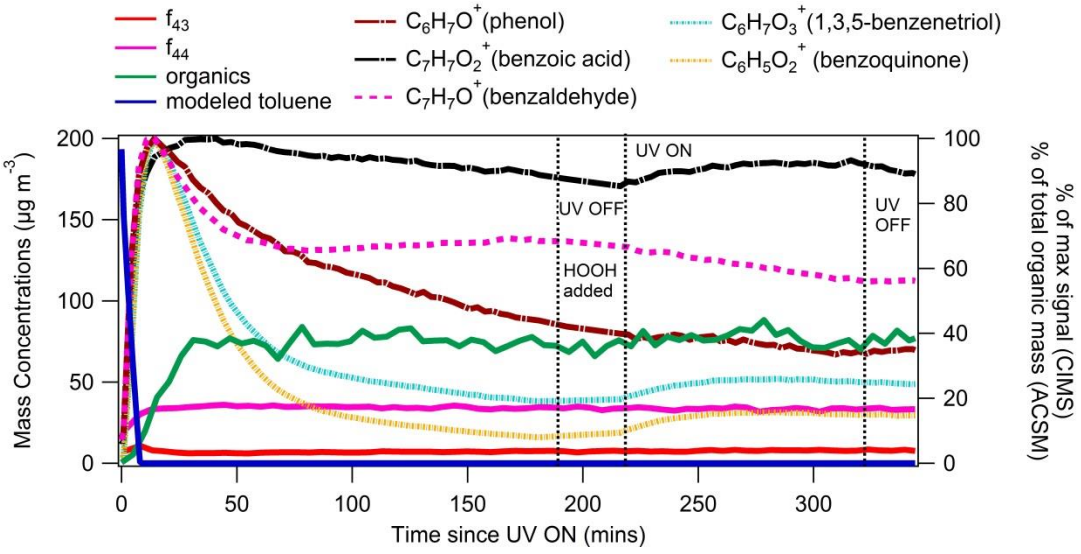

Figure 3-9. Time series of wall-loss corrected OA concentration and modeled toluene decay (left vertical axis) and gas-phase products and f_{43}, f_{44} time series (right vertical axis) during experiment 5 (Low NO_x-Cl-HOOH).

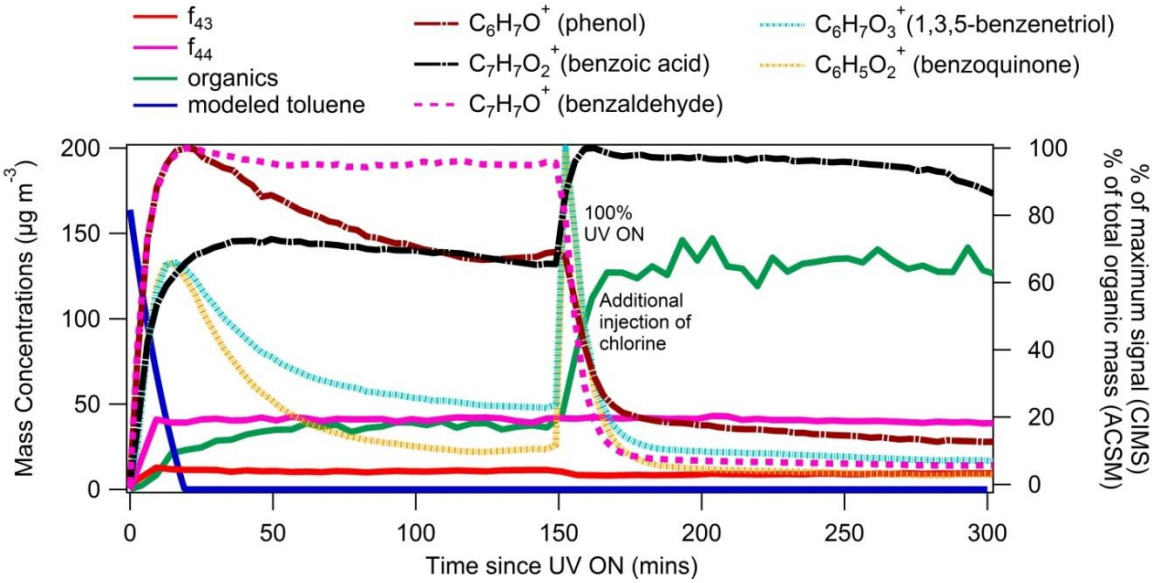

Figure 3-10. Time series of wall-loss corrected OA concentration and modeled toluene decay (left vertical axis) and gas-phase products and f_{43}, f_{44} time series (right vertical axis) during experiment 6 (Low NO_x-Cl).

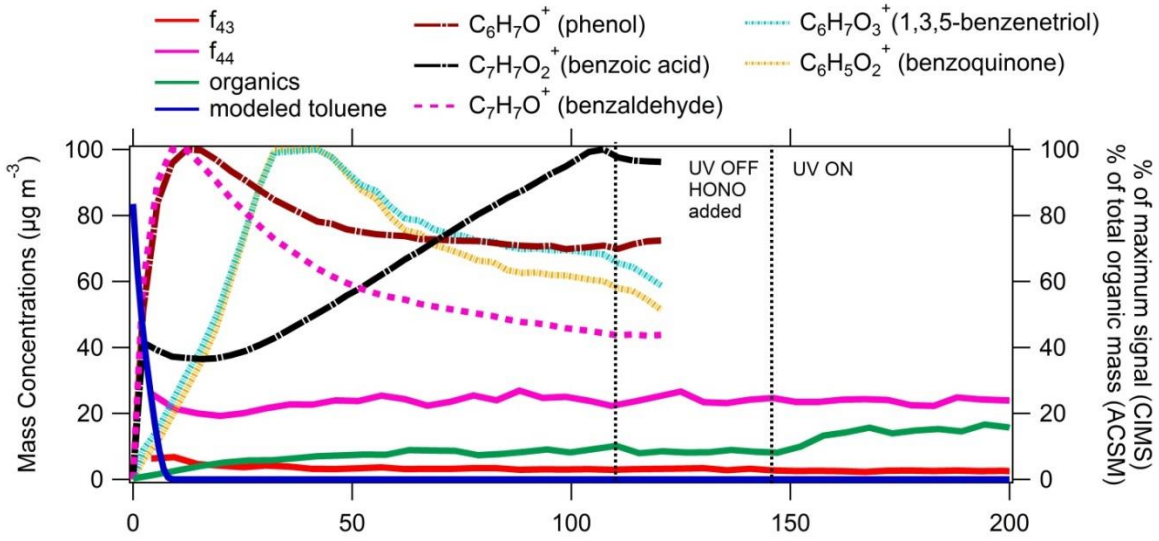

Figure 3-11. Time series of wall-loss corrected OA concentration and modeled toluene decay (left vertical axis) and gas-phase products and f_{43}, f_{44} time series (right vertical axis) during experiment 7 (Cl-High NO_x-OH). CIMS was offline after 120 minutes.

3.5 CONCLUSIONS

Chlorine-initiated oxidation of toluene was investigated inside an environmental chamber. Several generations of gas-phase products were observed which followed different qualitative trends in low NO_x and high NO_x environments and responded to the addition of oxidants. SOA formed quickly, and when no source of OH was added to the system initially, all toluene was consumed within less than 30 min of oxidation, enabling the investigation of organic aerosol aging. SOA concentrations remained stable upon continued exposure to UV suggesting that semi-volatile products are not photo-labile. The mass yields of SOA formed from toluene + Cl chemistry are similar to yields formed from toluene + OH reactions; however, the bulk OA composition is different: Cl-initiated

oxidation of toluene forms SOA with an overall higher oxidation state and lower fraction of organic signal due to ions at *m/z* 43 (f_{43}). These differences are probably due to the approximately 10-fold faster reaction timescales of toluene with Cl than with OH, and the predominance of ring-retaining products in the toluene + Cl system and ring-opened products in the toluene + OH system. Addition of oxidant (Cl_2, HOOH or HONO) after all toluene was consumed did not change the organic aerosol oxidation state, suggesting a potential oxidation end-point in the particle phase.

SOA formation from Cl-initiated oxidation of hydrocarbons including toluene may significantly impact tropospheric composition considering that concentrations of reactive chlorine species are higher than previously assumed, and that Cl reacts more quickly than OH with most hydrocarbons. This faster reaction rate also enables complete precursor consumption and investigation of aging reactions on normal experimental timescales. In addition to its relevance to tropospheric composition, chlorine chemistry could thus be important as an experimental tool.

Chapter 4: Secondary Organic Aerosol Formation (SOA) from Cl-initiated photo-oxidation of C_{10} alkanes

Alkanes contribute to about ~90% of anthropogenic hydrocarbon emissions and 12% (140 Tg yr^{-1}) of annual non-methane hydrocarbon emissions (Fraser et al., 1997; Rogge et al., 1993; Schauer et al., 1999, 2001, 2002) with a majority of them present in diesel exhaust (Miracolo et al., 2010). Consequently, alkanes can have significant contributions to SOA production in urban environments (Dunmore et al., 2015).

Several decades of work on OH radical reactivity with VOCs spanning the range of C_8-C_{16} mean that the reaction rates (k_{OH}) and mechanisms are fairly well understood (Aschmann, 1998; Aschmann et al., 1997; Aschmann and Atkinson, 1995; Atkinson, 2000, 2007; Atkinson et al., 2001; Atkinson and Arey, 2003; Jordan et al., 2008; Ziemann and Atkinson, 2012). But recent ambient measurements suggest that tropospheric concentrations of chlorine atoms (Cl) are higher than previously assumed (Chang and Allen, 2006; Faxon and Allen, 2013; Graedel and Keene, 1995; Tanaka et al., 2000), and that chlorine chemistry may be important in continental as well as coastal environments (Behnke et al., 1997; Finlayson-Pitts, 1993; Finlayson-Pitts et al., 1989; Spicer et al., 1998; Tanaka et al., 2000).

Very few studies have reported the Cl-chemistry of n-alkanes (Alwe et al., 2013, 2014, Aschmann and Atkinson, 1976, 1995). Chlorine-initiated SOA formation under high NO_x conditions has recently been reported for n-alkanes (Wang and Hildebrandt Ruiz, 2018). Here, the focus is on SOA formation from low NO_x-Cl-initiated photo-

oxidation of linear, branched and branched-cyclic alkanes with 10 carbon atoms: n-decane, 2-methyl nonane (henceforth MeNo) and butyl cyclohexane (henceforth BCH).

4.1 BACKGROUND

Formation of particulate matter (PM) in the atmosphere is governed by several factors, including the reaction of volatile organic compounds (VOCs) with atmospheric oxidants such as OH radicals, ozone, chlorine and NO_x. Upon oxidation, these VOCs can form organic compounds with lower volatility, which can then condense on existing particles and form secondary organic aerosol (SOA) (Seinfeld and Pandis, 2006). SOA is important because it comprises 65-90% of total estimated PM_1 (Jimenez et al., 2009) in urban areas and individual contributions from a number of precursors remains poorly characterized.

In general, reaction of OH radicals with VOCs involve H-atom abstraction from C–H bond, OH radical addition to the carbon atoms of unsaturated C=C bonds, and OH radical addition to the carbon atoms of aromatic rings. In the case of alkanes-OH chemistry, the reaction mechanism proceeds via H-atom abstraction from primary, secondary or tertiary C-H bonds (Ziemann and Atkinson, 2012). The preference for breaking the secondary and tertiary C-H bonds are marginally higher than the primary –CH_3 bond. Some common intermediates in this reaction include organic peroxy (RO_2) and alkoxy (RO·) radicals; product species include hydroperoxides (ROOH), carboxylic acids (RC(O)OH), peroxyacids (RC(O)OOH), peroxynitrates ($ROONO_2$), nitrates ($RONO_2$), alcohols (ROH), carbonyls (RC(O)R'), where R may be H, and 1,4-hydroxycarbonyls. The NO_2 containing product species formed under high NO_x environments.

Previous work (Aimanant and Ziemann, 2013b; Lim and Ziemann, 2009a, 2009c) reported the effect of branching and cyclization on SOA formation and composition from OH-initiated photo-oxidation of C_6-C_{17} alkanes, in the presence of NO_x. SOA yields for alkanes were highest for cyclic alkanes, followed by linear and then branched alkanes under high NO_x-OH conditions (Figure 1-1). Alkoxy radical decomposition in linear and branched alkanes leads to fragmentation whereas for cyclic alkanes, it leads to ring-opened alkyl radicals that have an intact carbon chain with an additional aldehyde group, thus forming low-volatility products with a higher tendency to form SOA. Varying the concentrations of NO_x (with respect to VOC concentrations) and ozone, and the acidity of inorganic seed particles resulted in minor changes in reaction mechanisms; the branching ratios remained the same for alkoxy radical isomerization and decomposition (under high NO_x conditions).

Chlorine-initiated oxidation of volatile organic compounds such as isoprene, monoterpenes, toluene, and polycyclic aromatic hydrocarbons have also been shown to rapidly form SOA with high yields (Cai et al., 2008; Huang et al., 2014; Karlsson et al., 2001b; Ofner et al., 2012; Wang and Hildebrandt Ruiz, 2017, 2018). The gas-phase reaction rate constants of linear alkanes with hydroxyl radicals and chlorine radicals has been shown to increase with the alkane chain length (Lim and Ziemann, 2009a, 2009c). The reaction rate constant of decane with chlorine is 4.87×10^{-10} cm^{-3} $molecules^{-1}$ s^{-1} at 298 K and 1 atm (Aschmann and Atkinson, 1995) which is over an order of magnitude higher than the rate constant of decane with hydroxyl radicals, 1.25×10^{-11} cm^{-3} $molecules^{-1}$ s^{-1} (Atkinson and Arey, 2003). The reaction rate constant for hydroxyl radicals and butyl cyclohexane is 14.7×10^{-12} cm^{-3} molecules-1 s^{-1}(Aschmann et al., 2001). Table 1-1 shows the k_{OH} and k_{Cl} values for all VOCs used in this dissertation, where information is available.

Alkanes with 5 or more linear carbons produce 1, 4-hydroxycarbonyl which can undergo a rate-limiting, acid-catalyzed heterogenous reaction to produce dihydrofuran (DHF) compounds (Lim and Ziemann, 2009c). DHF is highly reactive: for 2, 5-dihydrofuran, the bimolecular reaction rate constants with O_3, OH and Cl are $1.65 \pm 0.31 \times 10^{-17}$, $6.45 \pm 1.69 \times 10^{-11}$, and $4.48 \pm 0.59 \times 10^{-10}$ cm^3 $molecule^{-1}$ s^{-1}, respectively (Alwe et al., 2013, 2014). Similar to hydroxyl radicals, chlorine radicals can react with DHF via both H-abstraction and Cl-addition, producing chlorinated (e.g. dichlorotetrahydrofurans) and non-chlorinated compounds (e.g. furanones) under low NOx conditions (Alwe et al., 2013).

Wang and Hildebrandt Ruiz (2018) reported SOA formation from n-alkanes of different chain lengths from C_8-C_{12} under high NO_x-Cl conditions. Alkane-Cl SOA was shown to exhibit more hydrocarbon-like characteristics as the alkane precursor length increased. Organonitrates dominated the gas-and –particle phase SOA composition. Small concentrations or organochlorides were formed, presumably from Cl-addition to DHF. Organochloride and total SOA formation was reported to be suppressed under high relative humidity conditions.

In this chapter, the focus is on the photo-oxidation of linear, branched and cyclic C_{10} alkanes under low NO_x conditions. A summary of experimental conditions and type of VOCs is provided in Table 6-1.

Table 4-1. Experimental conditions and summary of results for alkanes-Cl

Exp No.	VOC	$[RH]_0$ (%)	$[VOC]_0$ (ppb)	Cl_2 (ppb)	SOA ($\mu g\ m^{-3}$)	Y_{SOA}	f_{43}	f_{44}	f_{HCl+}
1	Decane	<2	13	40	N/A	N/A	0.08	0.11	0.01
2	Decane	<2	13	40	80	1.1	0.09	0.07	0.01
3	Decane	55	13	40	96	1.4	0.09	0.07	0.01
4	Decane	40	13	40	74	1.0	0.09	0.07	0.01
5	BCH	50	14	40	123	1.5	0.06	0.10	0.02
6	BCH	55	14	100	126	1.6	0.07	0.13	0.03
7	BCH	<2	14	40	151	N/A	0.08	0.10	0.01
8	BCH	<2	14	40	N/A	N/A	0.08	0.10	0.01
9	MeNo	44	13	40	61	0.8	0.10	0.09	0.02
10	MeNo	34	13	40	N/A	N/A	0.10	0.07	0.01

4.2 METHODS

The principle of operation of instruments and setup of environmental chamber experiments, the results of which are described below, can be found in Chapter 2. As a short summary, the Aerosol Chemical Speciation Monitor (ACSM) is used to measure the total concentration and bulk composition of particulate matter less than 1 µm in size

(PM_1). The High Resolution Time-of-Flight-Mass-Spectrometer (HR-Tof-CIMS) along with a Filter Inlet for Aerosols and Gases (FIGAERO) is used to measure the molecular gas-phase composition in real-time and the molecular particle-phase composition in a semi-continuous manner. The Scanning Electrical Mobility System (SEMS) is used to measure the number and size distributions of particles. A thermo-denuder is used in-line with the ACSM and SEMS to increase the temperature of sampling lines in a step-wise controlled manner to measure the organic mass fraction remaining. The setup of the environmental chamber is shown in Figure 2-1.

A typical environmental chamber experiment involved the following steps. Ammonium sulfate (Sigma Aldrich, 99%) seed particles were created from a 0.01 molar (M) solution using an aerosol generation system (Brechtel Manufacturing, Inc. Model 9200). These provide a surface area for condensation, thus aiding secondary organic aerosol (SOA) formation. Then, molecular chlorine (Cl_2) was introduced into the chamber using a high-pressure gas cylinder from Airgas (106 ppm in N_2). Next, the VOC (n-decane, 2-methyl nonane (MeNo) or butyl cyclohexane) was introduced in the chamber via a glass sampling tube. After the particles and gases were injected into the chamber and allowed to mix, the UV lights were switched on, photolyzing the oxidant precursors (Cl_2 to 2Cl·) and starting the oxidation reactions.

The ACSM provides unit-mass resolution data which means that we have to rely on certain correlations to derive elemental ratios (H: C, O: C) and oxidation states (O_{sc}). Chapter 1 provided a brief introduction to different graphic descriptions of oxidized organic aerosols. The tracer ratio – m/z 44 or f_{44} (relative to total signal in component

mass spectrum) is representative of CO_2^+, forming likely from acid groups and m/z 43 and f_{43} (also relative to total signal in component mass spectrum) is representative of $C_2H_3O^+$ (Ng et al., 2011b). Ambient Organic Aerosol lie inside a triangular region and on "photochemical aging" (extended periods of oxidation); the ambient organic aerosol approached the apex of the triangle (which represents CO_2^+) (Figure 2-6). This means that f_{44} signal increases with oxidation and can be used theoretically to derive O: C elemental ratios (and subsequently oxidation states). The movement of f_{43} signal in this plot is representative of fragmentation (cleavage of C-C bonds). Temporal movement (with extended period of oxidation) to the left would indicate the organic aerosol contains ring-retaining products (less fragmentation) and temporal movement to the right would indicate the organic aerosol contains ring-opened products (more fragmentation). This means that f_{43} signal can be used to derive H: C elemental ratios (and subsequently as a proxy for fragmentation behavior (C-C cleavage). The movement along this triangle can be unique to individual precursor VOCs, but ambient organic aerosol, almost exclusively lie inside the triangle.

This "triangle plot" framework was extended to laboratory chamber experiments, but it has been found difficult to replicate the high oxidation levels found in ambient environments. The reasons for this could be low oxidation levels inside environmental chambers resulting from inability to reach high concentrations of OH radicals in several previous studies.

4.3 RESULTS AND DISCUSSION

All experiments formed SOA (Table 4-1). The amount of VOC and chlorine injected in all experiments was ~75 μg m^{-3} while the relative humidity (low RH (<2%) or high RH (34%-55%)) was varied. BCH was found to form the most SOA. In Expts. 5 and 6, the RH was 50% and 55% respectively and the resulting maximum SOA concentration was 123 μg m^{-3} and 126 μg m^{-3} respectively. In Expt. 6, the estimated chlorine concentration (~100 ppb) is higher than all other experiments (~40 ppb) but the amount of organic aerosol was found to be similar to Expt. 5. It is thus possible that all of the VOC has been exhausted in Expt. 6. Complete consumption of all alkanes was assumed for the calculation of SOA yields reported in Table 4-1. The SOA yields for n-alkanes under low NO_x-Cl conditions range from 0.8-1.6. Such high yields have previously been reported under high NO_x-Cl conditions (Y=0.84-1.65) for C_{10} and C_{12} alkanes (Wang and Hildebrandt Ruiz, 2018).

4.3.1 Organic Aerosol bulk composition

Cl-initiated SOA from C_{10} alkanes formed low levels of organochlorides (< 2%). These measurements are based on the tracer signal ratios from the ACSM (f_{HCl}^{+})(Wang and Hildebrandt Ruiz, 2017). f_{HCl}^{+} denotes the fraction of organics attributed to HCl in the ACSM and has been shown to be a proxy for measuring organochlorides. It is also noted that organo-chloride formation is slower than organic aerosol formation under low RH conditions (Figure 4-1), similar to that reported under high NO_x-Cl conditions (Wang and Hildebrandt Ruiz, 2018). Under high RH conditions, the rate of formation of organo-chlorides is similar to that for organics (Figure 4-1). Figure 4-1 plots the time

series of organic aerosol formation and organic chloride formation for two linear decane experiments: Experiment 2 (Low RH) and Experiment 3 (High RH). A carbon-carbon double bond is required to enable chlorine addition reactions and organo-chlorine formation. This could point towards dihydrofuran (DHF) production under low NO_x- Cl conditions. DHF is a known product of alkane-OH chemistry and it can undergo dehydration reactions (Jordan et al., 2008; Lim and Ziemann, 2009b, 2009c) followed by Cl addition to the DHF double bond, which could explain the organic chloride formation.

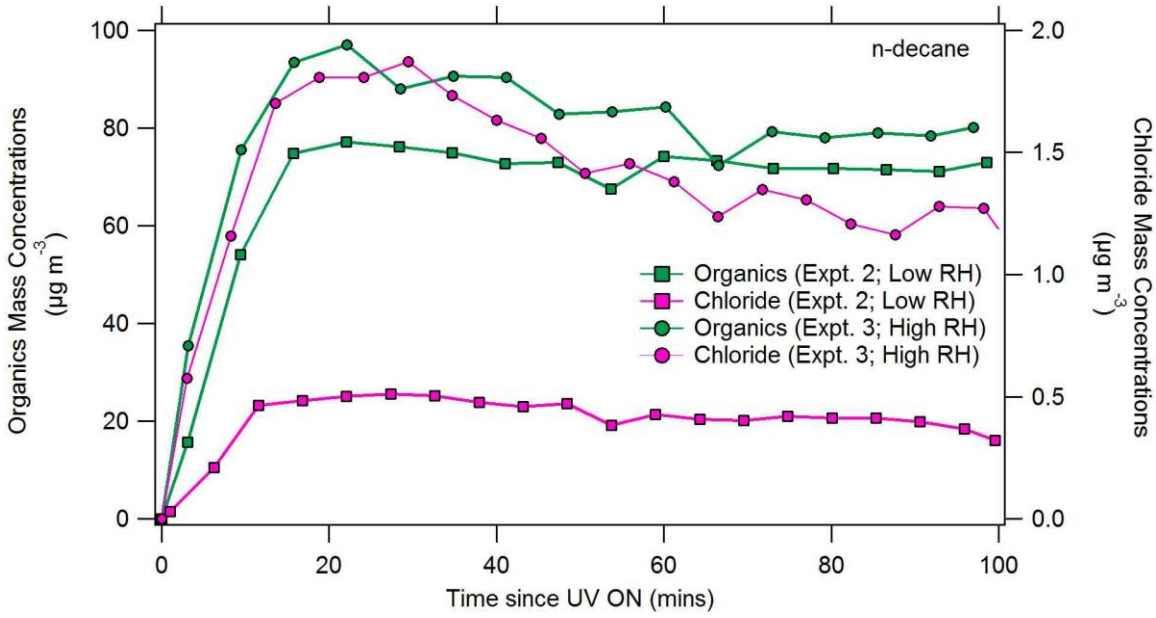

Figure 4-1. Organic Aerosol (left) and particulate chloride formation (right) with n-decane during experiment 2 (low RH) and experiment 3 (high RH) as measured from ACSM.

4.3.2 Oxidative states and experimental volatility of SOA

The f_{44} and f_{43} signals for all experiments are reported in Table 6-1. The range of f_{44} and f_{43} for n-decane remains same across experiment 2 through experiment 4, under low and high RH conditions. The highest f_{44} (0.13) across set of experiments is observed for BCH under very high chlorine (~100 ppb) conditions in Expt. 6. Addition of chlorine can facilitate oxidation of VOCs, as previously reported in Dhulipala et al. (2018) *(in review)*. Using Equations 1-4, 2-3 and 2-4, elemental ratios (H: C and O: C) can be estimated from f_{43} and f_{44}. Figure 4-2 plots the f_{44} and f_{43} (top panel) and the elemental ratios (H: C and O: C) (bottom panel) for experiments conducted in this dissertation compared to alkane-OH-NO_x chemistry reported previously (Presto et al., 2010; Tkacik et al., 2012; Wang and Hildebrandt Ruiz, 2018). It should be noted that the experimental conditions in this dissertation (low NO_x-Cl) are different from other studies – high NO_x-Cl (Wang and Hildebrandt Ruiz, 2018) and high NO_x-OH (Presto et al., 2010; Tkacik et al., 2012).

Under all conditions, the oxidized organic aerosol lies within the ambient range, as shown in Figure 4-2.

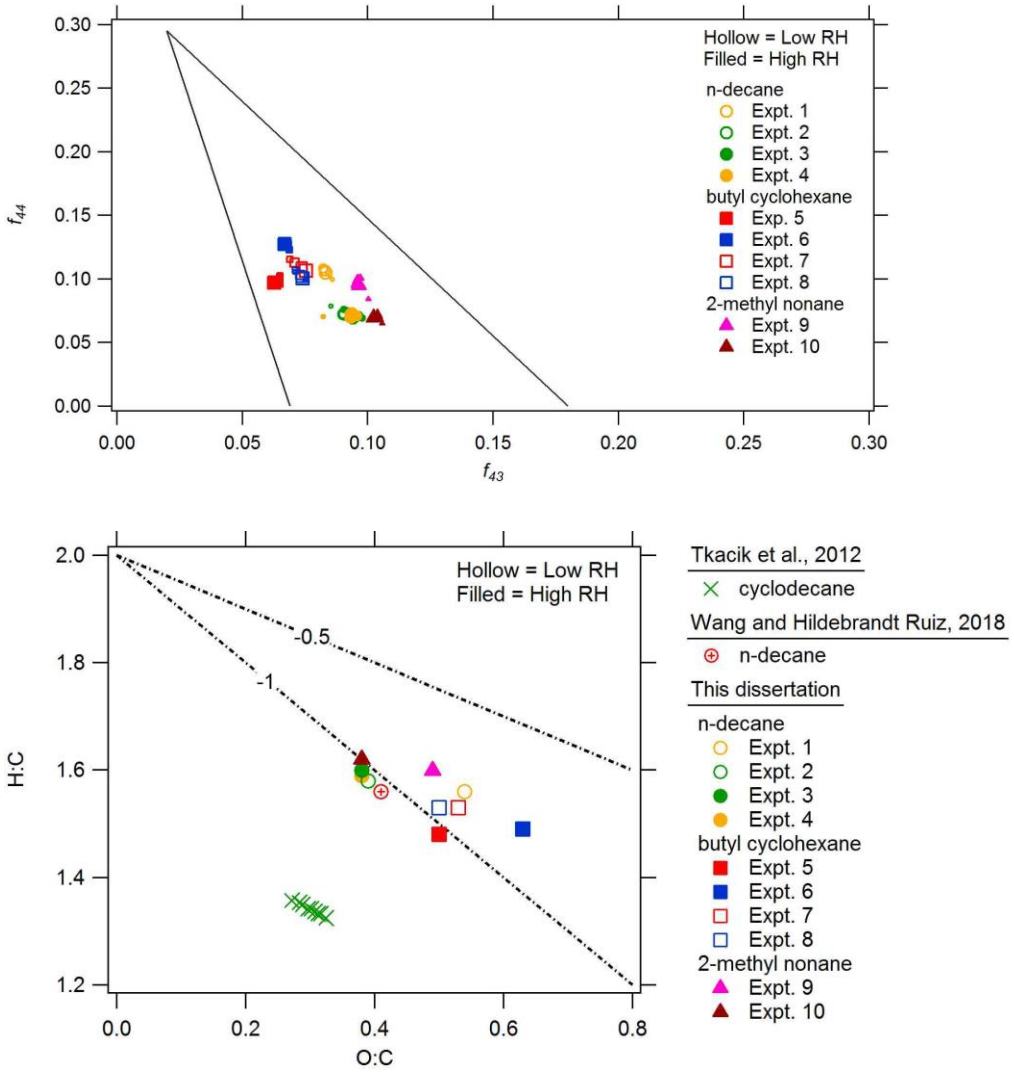

Figure 4-2. f_{43} and f_{44} signals for all experiments shown in the top panel and elemental ratios (H:C and O:C) shown in the bottom panel. f_{43} is used as a tracer for $C_2H_3O^+$ (or fragmentation) and f_{44} for CO_2^+ (or oxidation states) of organic aerosol respectively. Black solid lines (top panel) show typical ambient measurements (Ng et al., 2011b). Marker size (top panel) is a function of UV exposure time with maximum size corresponding to 100 minutes of exposure. Hollow markers represent low RH experiments and filled markers represent high RH experiments. Dotted lines (bottom panel) are drawn to represent slopes of -1 and -0.5.

4.3.3 Experimental volatility of SOA from C_{10} alkanes

An example of thermo-denuder temperature ramping method is shown in Figure 4-3. At 100 minutes, the periodic temperature ramp is started. After a period of sampling, it is switched to "bypass" mode and the temperature inside sections of the thermo-denuder is increased. The step wise increase in temperature and the decrease in SOA mass (as it evaporates) can be seen clearly. This can be also plotted in the form of a 1-D thermogram, depicting the mass fraction remaining and the temperature in the thermo-denuder (Figure 4-4). Note that this is different from filter desorption temperature as plotted in Figure 4-5.

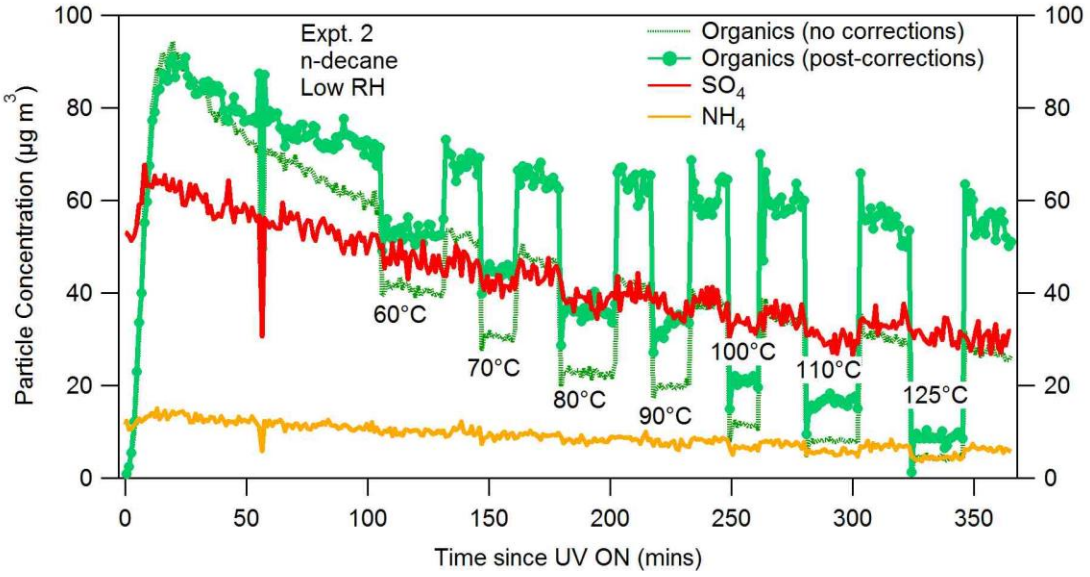

Figure 4-3. Time series of organic aerosol formation measured from the ACSM during Expt. 2 (n-decane, low RH) depicting temperature ramping method using the thermo-denuder. Dashed green trace shows pre-corrected organic aerosol from ACSM and solid green trace shows organic aerosol concentrations corrected for depositional particle wall losses (Pathak et al., 2007).

Under low RH conditions, the organic mass fraction remaining appears to be higher than under high RH conditions (Figure 4-5). The temperature at which half of the organics evaporates or the T_{50} gives preliminary information about the volatility of the SOA. It appears that the T_{50} for C_{10} alkanes lies in the region 80-100° C. Among the C_{10} alkanes, butyl cyclohexane has the highest T_{50}, suggesting that it is the least volatile organic aerosol among the three C_{10} alkanes part of this work. T_{50} as a metric for comparing evaporation was previously also used by Tkacik et al. (2012) for alkanes in the intermediate-volatility range. The caveat of using experimental volatility measurements for inter-comparison is that SOA mass can alter the organic mass fraction remaining at T_{50}. The SOA mass concentrations for all experiments are shown in Table 6-1 and range from 74-96 µg m^{-3} for n-decane and 123-151 µg m^{-3} for butyl cyclohexane.

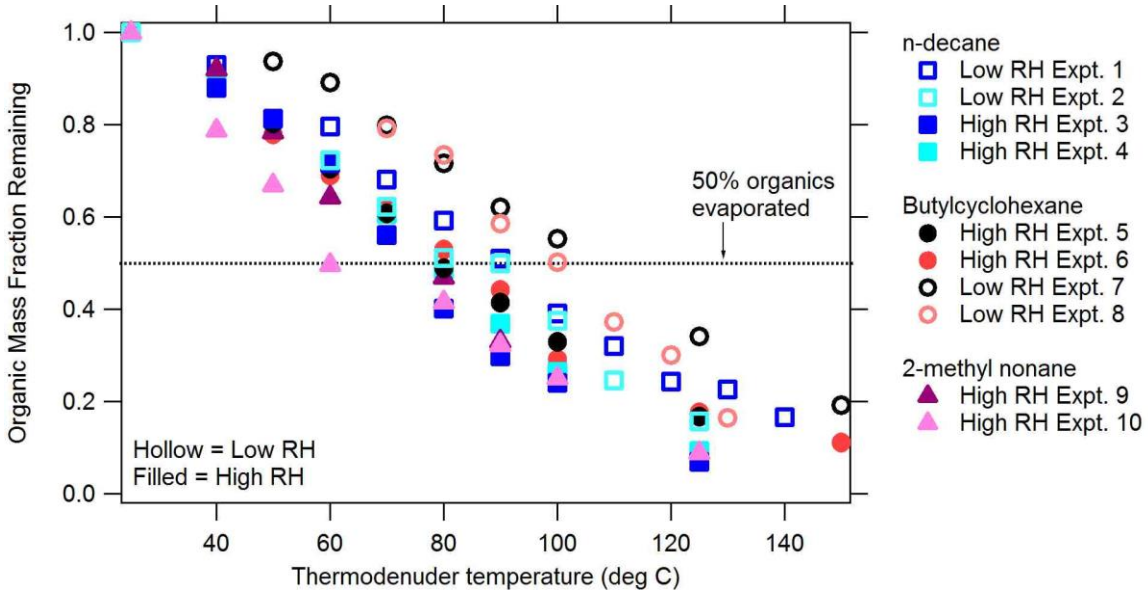

Figure 4-4. Experimental volatility measurements from all experiments as measured by increasing temperature step-wise in a thermo-denuder.

4.3.4 Composition of SOA

4.3.4.1 Particle-phase composition

The particle-phase composition of SOA from butyl cyclohexane includes bi-modal peaks with different desorption temperature ranges: 80-100 °C and 110-120 °C (Figure 4-5). The two ranges include ring-opened carboxylic acids such as adipic acid, chlorinated organics such as nonanedioyl dichloride and ring-retaining products such as 3,4-dihydroxyphenylglycol. The FIGAERO-CIMS cannot distinguish between different molecular structures and as such, these represent suggested products based on predicted reaction mechanisms. The filter desorption temperatures (T_{max}) are also dependent on filter loadings and thus, caution needs to be exercised before using it to infer volatility (Wang and Hildebrandt Ruiz, 2018). The presence of hydrofuran groups is

also seen in Experiments 5 through 8 which were conducted using butyl cyclohexane under both low and high RH conditions.

The particle-phase composition of SOA from n-decane contains more ring-opened products and a similar bi-modal peak is also observed (Figure 4-6). Chlorinated organics included $C_5ClH_9I^-$ and $C_5ClH_9O_4I^-$. Furan-containing products were again observed, similar to butyl cyclohexane.

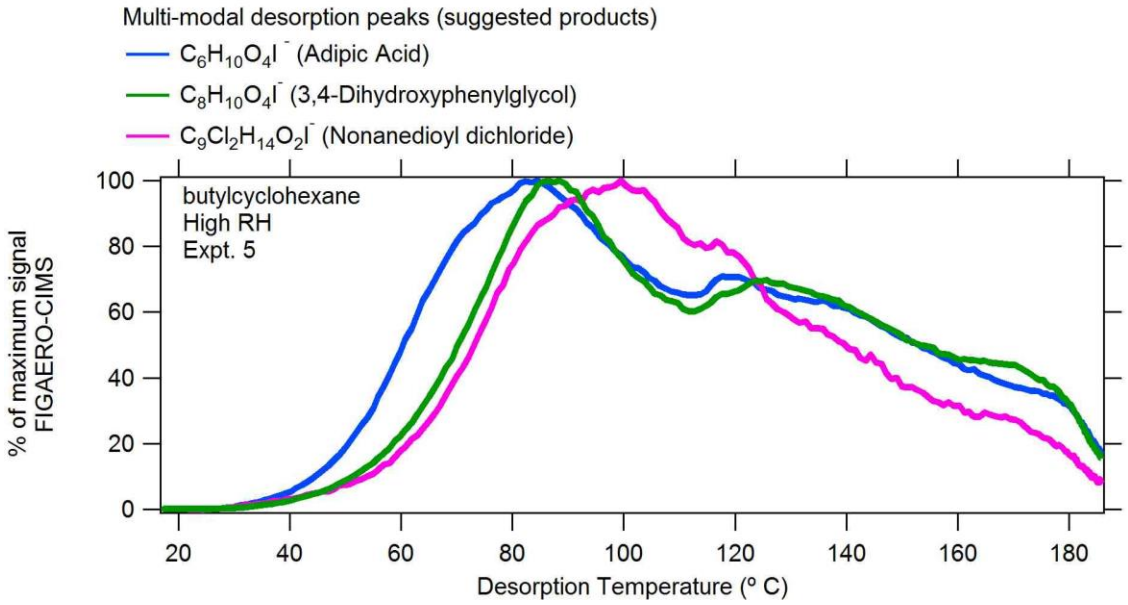

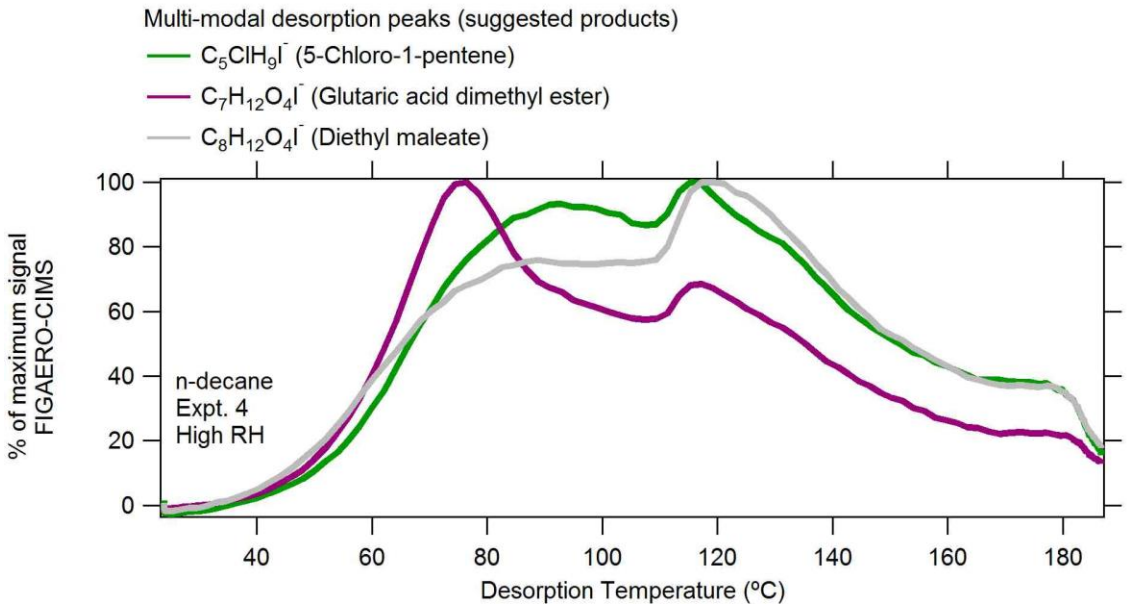

Figure 4-5. 1-D thermogram of particle-phase products formed during Experiments 4 and 5 as measured by the FIGAERO-CIMS. Species shown were first normalized against I^- reagent ion signal and then normalized against their respective maxima.

4.3.4.2 Gas-phase composition

Here, a number of organic acids are observed under low and high RH conditions on oxidation of n-decane (Figure 4-6) and butyl cyclohexane (Figure 4-7). Selected products for n-decane oxidation reaction are shown in Figure 4-6. It should be noted the HR-Tof-CIMS cannot distinguish between molecular structures and thus, these products represent molecular formula consistent with those expected from alkane-OH chemistry. Observed acids included formic acid, pyruvic acid, glyceric acid, glutaric acid, adipic acid and camphoric acid. Adipic acid, glutaric acid and glyceric acid form at a faster rate than the other species during Expt. 6. The reason for this difference is as yet unclear but it is

possible that the slower forming represent later generation products (higher O: C). Other gas-phase products included 2, 5-Bis(hydroxymethyl) furan and acetic anhydride.

Butyl-cyclohexane results in formation of similar acids as n-decane, but a few chlorinated organic species are also observed here (Figure 4-7). Two gas-phase chlorinated products: chloro-cyclopentane and 1-chloro-2-butene form at a faster rate than other chlorinated products. Benzofuran (fused benzene and furan rings) is observed here instead of an open chain furan containing structure as is the case for n-decane. The hydroxycinnamate group ($C_9H_7O_3$) has the structure R(OH)-R'-O_2 and decays faster than the products with carboxylic acid groups.

For 2-methyl nonane, the gas-phase products are similar to those of n-decane owing to similar ring structure. For example, benzofuran products are not observed as in the case of butyl cyclohexane. Relative humidity did not change the reaction pathway, as no drastic change in relative signal intensities of gas-phase products in CIMS was observed.

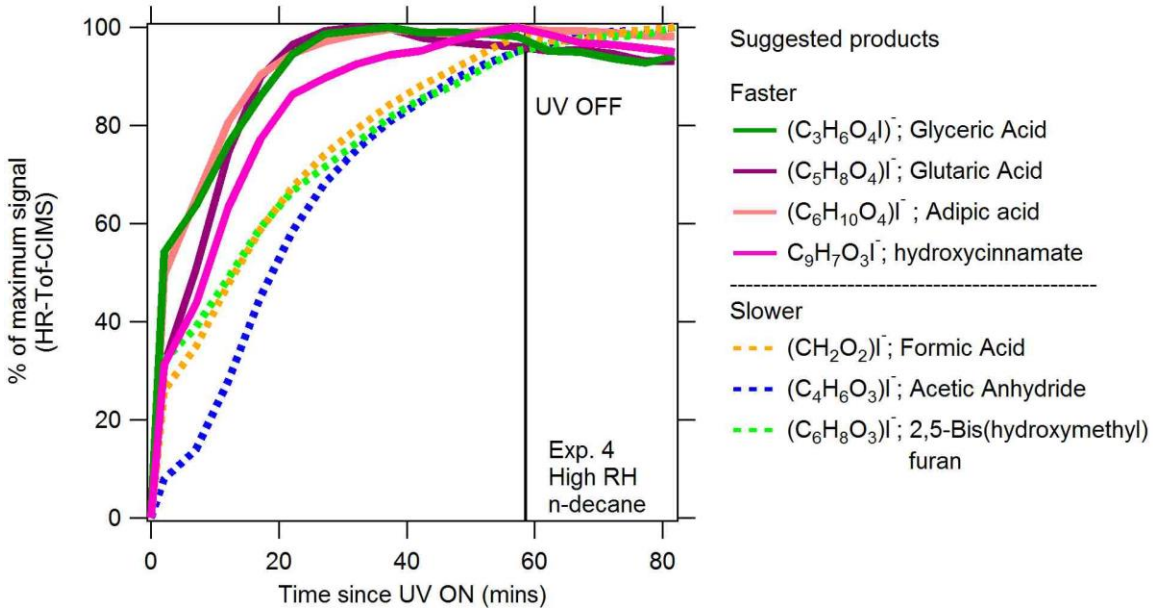

Figure 4-6.Time series of gas-phase products observed from n-decane in Expt. 4 (high RH). Species shown were first normalized against I^- reagent ion signal and then normalized against their respective maxima.

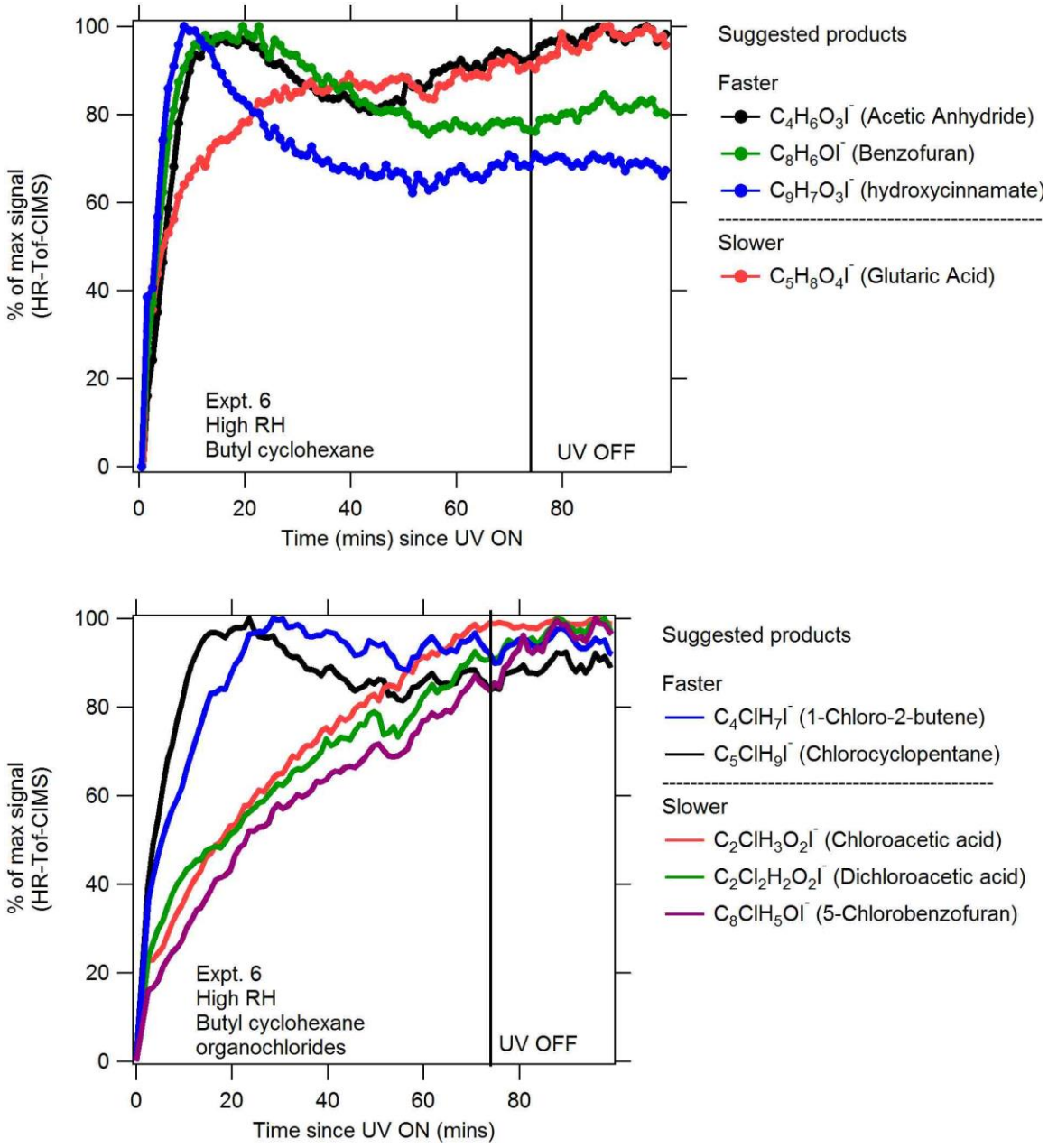

Figure 4-7.Time series of gas-phase products measured from HR-Tof-CIMS during butyl cyclohexane experiment (Expt. 6; high RH). Top panel shows $C_xH_yO_z$ species and bottom panel shows chlorinated organics. Species shown were first normalized against I^- reagent ion signal and then normalized against their respective maxima.

4.4 CONCLUSIONS

SOA formation from n-decane, butyl cyclohexane and 2-methyl nonane is reported for the first time under low NO_x-chlorine conditions. A clear dependency of relative humidity (RH) is not established. An excess injection of chlorine (for butyl cyclohexane) results in a higher f_{44} suggesting that excess chlorine results in higher oxidation states of SOA. SOA yields for butyl cyclohexane are the highest, which is expected based on previous work on linear, branched and cyclic alkanes (Lim and Ziemann, 2009a). The experimental thermogram measured from the thermo-denuder shows that RH affects the fraction of organic aerosol evaporating. Under low RH conditions, a higher organic fraction remains in the particle-phase. The gas-phase and particle-phase products are also reported using the HR-Tof-CIMS and the FIGAERO inlet. Chlorinated organics as well as furan-containing products are observed both in the gas- and –particle phases.

Chapter 5: Secondary Organic Aerosol formation from combustion and non-combustion Intermediate Volatility Organic Compounds (IVOCs)

Intermediate volatility organic compounds (IVOCs) are a subset of VOCs with saturation vapor concentrations (C_i^*) between 10^3-10^6 μg m^{-3} (Donahue et al., 2006; Robinson et al., 2007) ; a summary (and background theory) of VOC categorization and properties is provided in Table 1-1 and Chapter 1. Due to their low vapor pressure, IVOCs can form secondary organic aerosol (SOA) at high yield and affect ozone formation in the atmosphere. This chapter reports results on the formation of SOA from different IVOCs which encompass combustion and non-combustion sources. Most of the previous work on IVOCs has focused on the former. However, recent studies (McDonald et al., 2018) have shown that non-combustion IVOCs constitute an increasing fraction of total IVOC emissions, and they can therefore significantly contribute to the SOA budget of the atmosphere. In this chapter, the SOA formation from linear pentadecane and 2, 6, 10- trimethyl dodecane (TMDD) are reported, both of which are associated with combustion emissions. SOA formation from other non-combustion IVOCs reported in this chapter includes diethylene glycol monobutyl ether (DEGBE), Texanol® and commercial grade mineral spirits.

5.1 Background

Formation of particulate matter (PM) in the atmosphere is governed by several factors, including the reaction of intermediate volatility organic compounds (IVOCs) with

atmospheric oxidants such as OH radicals, ozone, chlorine and NO_x. Upon oxidation, these IVOCs can form organic compounds with lower volatility, which can then condense on existing particles and form secondary organic aerosol (SOA) (Seinfeld and Pandis, 2006). SOA is important because it comprises 65-90% of total estimated PM_1 (Jimenez et al., 2009) in urban areas and individual contributions from a number of precursors remains poorly characterized.

The majority of previous work on IVOCs (Jathar et al., 2012; Presto et al., 2009, 2010; Tkacik et al., 2012; Zhao et al., 2014) focused on quantifying SOA formation (yields) and chemical mechanisms of alkanes, which are associated with gasoline and diesel exhaust emissions. More recently, it has been shown that use of volatile chemical products (VCPs) including pesticides, coatings, printing inks, adhesives, cleaning agents, and personal care products constitutes half of fossil fuel VOC emissions in industrialized cities (McDonald et al., 2018). In 2015, the California Air Resources Board (CARB) mandated the regulation for reducing emissions from consumer products including glycol ethers and mineral spirits (CARB, 2015a, 2015b). This serves as motivation to explore SOA formation from ingredients of consumer products, which are not emitted from combustion sources.

Here, diethylene glycol monobutyl ether (DEGBE) was chosen as a model compound to study organic aerosol formation from glycol ethers, which are used in industrial solvents, pesticides, coatings and household cleaning solutions (EPA, 2000). The total emissions of known glycol ethers are estimated to be 13.44 tons per day by 2020 (Li et al., 2018). DEGBE has previously been reported to have a SOA yield of 0.16 in

the presence of NO_x (Li et al., 2018) which means it could have a significant impact on the SOA budget in the atmosphere.

Glycol ethers have received attention before in the scientific community (Aschmann et al., 2001; Li and Cocker, 2018). The chemical mechanism of glycol ethers with OH radicals and the rate constant for DEGBE : k_{OH}= 7.44 E-11 cm^3 $molecule^{-1}$ s^{-1} have been previously reported (Aschmann et al., 2001). Some reaction products included formaldehyde (HCHO), propanal (CH_3CH_2CHO), butanal ($CH_3CH_2CH_2CHO$), 2-hydroxyethylformate ($HOCH_2CH_2OCHO$), small amounts of organic nitrates ($RONO_2$) and some unidentified products with molecular weights 118, 134, 146 and 176 gm mol^{-1}. The four -CH_2- groups adjacent to the two ether -O- atoms, and the -CH_2OH group, accounted for more than 90% of the overall reactivity (with respect to H-abstraction pathway).

DEGBE's chemical mechanism under three conditions: NO only, HOOH only and NO and HOOH has been reported before (Li and Cocker, 2018). The presence of an –OH functional group facilitates a cyclisation mechanism pathway which is critical to SOA formation from glycol ethers. Cyclization reduces fragmentation thereby yielding higher molecular weight products, which will likely partition into the particle-phase, on account of their low volatility. But organic nitrate formation in the presence of NO_x promotes a fragmentation pathway thereby competing with the cyclization mechanism. Any further oxidation of glycol ethers lowers SOA yields. Large fragments of $C_3H_5O_2^+$ (m/z 73) and $C_nH_{2n+1}O_2^+$ (m/z 47, 61, 89) in the particle phase as measured by the High Resolution-

Time-of-Flight-Aerosol Mass Spectrometer (Aerodyne Research Inc. HR-ToF-AMS) (Decarlo et al., 2006) have previously also been reported (Li and Cocker, 2018).

Linear pentadecane is an important SOA precursor which has recently been reported in ambient measurements (Borbon et al., 2014) with mean concentrations of 23 ppt in summer time. It is associated primarily with emissions from combustion sources (Schauer et al., 2001). SOA formation from linear pentadecane has been reported before under high NO_x-OH conditions (Aimanant and Ziemann, 2013a; Chacon-Madrid and Donahue, 2011; Presto et al., 2009, 2010). The reaction rate of linear pentadecane with OH radicals has previously been reported to be 20.7 E+12 cm^3 $molecule^{-1}$ s^{-1} (Atkinson and Arey, 2003). The reaction mechanism of linear pentadecane and 2, 6, 10- trimethyl dodecane in the presence of NO_x is also well understood (Aimanant and Ziemann, 2013b). Major first generation gas-phase reaction products include alkyl nitrates (yield =0.3), 1, 4-hydroxynitrates (yield=0.1) and 1, 4-hydroxycarbonyls (yield =0.6). Second generation products include cyclic hemiacetals, cyclic hemiacetal nitrates, carbonyl esters, dinitrates, hydroxydinitrates and hydroxycarbonyl nitrates. Third generation products reported included acylperoxynitrate esters. The mass spectra from linear, branched and cyclic alkanes remain similar with similar peaks observed across experiments(Aimanant and Ziemann, 2013b).

The “photochemical aging” or progressive oxidation processes of linear pentadecane and how molecular structure (presence of alkanes, aldehydes and ketone groups) affects SOA formation has been studied before (Chacon-Madrid and Donahue,

2011). SOA formation from branched alkanes ranging from carbon numbers C_{10}-C_{15} (Lim and Ziemann, 2009c; Tkacik et al., 2012) has also been reported before. SOA yields from linear alkanes were found to be higher than the yields from branched alkanes (Figure 1-1).

SOA formation from mineral spirits has not been reported before. Previously, the lack of SOA formation from Texanol® under low NO_x-OH and high NO_x-OH conditions has been reported (Li et al., 2018). In this dissertation, the study of Texanol® was extended by photo-oxidizing Texanol® using Cl radicals. Ambient reactive chlorine concentrations have been shown to be higher than previously reported and more recently, chlorine chemistry has also been shown to be important in indoor environments (Gligorovski and Abbatt, 2018). Addition of chlorine is also relevant to this dissertation as glycol ethers and Texanol® are ingredients of commercial cleaning solutions and their ability to form SOA could be a health hazard both in outdoor (as part of their manufacturing processes) and indoor environments (end-use).

The oxidation states and experimental thermo-grams of SOA formed from glycol ethers and mineral spirits has previously not been reported. Experimental volatility measurements using a thermo-denuder (Huffman et al., 2008) can be used in evaporation kinetic models (Karnezi et al., 2014) to give information about the gas-particle partitioning behavior of these organic aerosols.

To summarize, this chapter focuses on SOA formation from IVOCs including DEGBE, linear pentadecane, 2,6,10 – trimethyl dodecane (TMDD), Texanol® and mineral spirits under different oxidation conditions. Original contributions include:

1) SOA formation from DEGBE oxidation under non-combustion related IVOCs

2) Reporting ozone formation from non-combustion related IVOCs

3) Experimental volatility of SOA formed from several IVOCs using thermo-denuder measurements

4) Identifying gas-phase and particle-phase reaction products (depending on instrument availability)

5.2 METHODS

The principle of operation of instruments and setup of environmental chamber experiments, the results of which are described below, can be found in Chapter 2. As a short summary, the Aerosol Chemical Speciation Monitor (ACSM) is used to measure the total concentration and bulk composition of particulate matter less than 1 μm in size (PM_1). The High Resolution Time-of-Flight-Mass-Spectrometer (HR-Tof-CIMS) along with a Filter Inlet for Aerosols and Gases (FIGAERO) is used to measure the gas-phase composition of organic aerosols in real-time and the particle-phase composition in a semi-continuous manner. The Scanning Electrical Mobility System (SEMS) is used to

measure the number and size distributions of particles. The setup of the environmental chamber is shown in Figure 2-1.

A typical environmental chamber experiment involved the following steps. Ammonium sulfate (Sigma Aldrich, 99%) seed particles were created from a 0.01 molar (M) solution using an aerosol generation system (Brechtel Manufacturing, Inc. Model 9200). These provide a surface area for condensation, thus aiding Secondary Organic Aerosol (SOA) formation. Then, molecular chlorine (Cl_2) was introduced into the chamber using a high-pressure gas cylinder from Airgas (106 ppm in N_2). To simulate high NO_x conditions, HONO was added as a source of OH and NO_x; the HONO solution was prepared immediately before injection in a custom-made glass flask (Kimble-Chase) by adding a 0.05 M solution of sulfuric acid to a 0.1 M solution of sodium nitrite. The titrated solution was then introduced into the chamber by flushing the flask with clean air. H_2O_2 (Sigma Aldrich, 30% (w/w)) was added in some experiments as a source of OH radicals. It was introduced into the chamber by flushing clean air into a glass bottle (Kimble-Chase, 250 ml) containing the H_2O_2 solution. Next, the intermediate-volatility organic compound (IVOC) was introduced in the chamber via a custom-made heated injector. Microliters of the IVOC were transferred using a glass syringe on to a port on the heated injector (initially at room temperature). The injector is then immediately placed inside the environmental chamber. Using a temperature-controlled programmer, the temperature on the heated injector was increased to 150 C. A steady flow of clean air at 2 lpm is used to aid the diffusion of the volatilized IVOC into the chamber. After 30 minutes, the heated injector was removed from the chamber. After the particles and gases were injected into the chamber and allowed to mix, the UV lights were switched

on, photolyzing the oxidant precursors (e.g. HONO to OH + NO, or H_2O_2 to 2OH) and starting the oxidation reactions.

The ACSM provides unit-mass resolution data which means that we have to rely on certain correlations to derive elemental ratios (H: C, O: C) and oxidation states (O_{sc}). Chapter 1 provided a brief introduction to different graphic descriptions of oxidized organic aerosols. The tracer ratio – m/z 44 or f_{44} (relative to total signal in component mass spectrum) is representative of CO_2^+, forming likely from acid groups and m/z 43 and f_{43} (also relative to total signal in component mass spectrum) is representative of $C_2H_3O^+$ (Ng et al., 2011b). Ambient Organic Aerosol lie inside a triangular region and on "photochemical aging" (extended periods of oxidation); the ambient organic aerosol approached the apex of the triangle (which represents CO_2^+) (Figure 2-6). This means that f_{44} signal increases with oxidation and can be used theoretically to derive O: C elemental ratios (and subsequently oxidation states). The movement of f_{43} signal in this plot is representative of fragmentation (cleavage of C-C bonds). Temporal movement (with extended period of oxidation) to the left would indicate the organic aerosol contains ring-retaining products (less fragmentation) and temporal movement to the right would indicate the organic aerosol contains ring-opened products (more fragmentation). This means that f_{43} signal can be used to derive H: C elemental ratios (and subsequently as a proxy for fragmentation behavior (C-C cleavage). The movement along this triangle can be unique to individual precursor VOCs, but ambient organic aerosol, almost exclusively lie inside the triangle.

This “triangle plot” framework was extended to laboratory chamber experiments, but it has been found difficult to replicate the high oxidation levels found in ambient environments. The reasons for this could be low oxidation levels inside environmental chambers resulting from inability to reach high concentrations of OH radicals in several previous studies.

5.3 RESULTS AND DISCUSSION

A summary of all experiments conducted is listed in Table 5-1. SOA formation was observed in all experiments using DEGBE, mineral spirits, 2, 6, 10-trimethyl dodecane (TMDD) or pentadecane; no SOA formation was observed from Texanol®. Figure 5-1 shows times series of SOA formed from all experiments. The non-combustion products that were tested included Texanol® and commercial grade mineral spirits. Texanol® did not form SOA under ozone, low NO_x-OH and high NO_x-OH-Cl conditions. Mineral spirits was found to form significant SOA. The initial concentration of mineral spirits needs to be estimated as the exact composition is unknown. Initial concentrations listed in Table 5-1 are hence estimated using the injected volume and assuming the molecular weight of decane. This assumption is based on the fact that mineral spirits contains a mixture of C_9-C_{11} compounds (McDonald et al., 2018).

Loss of vapor to the Teflon® walls is a concern in all environment chamber experiments (Ye et al., 2016; Zhang et al., 2014). These losses can be greater in magnitude for IVOCs (Li et al., 2018) and thus characterizing these losses are important before reporting SOA yields. The HR-Tof-CIMS, with water-clusters as reagent, was found to give unreliable calibration results for DEGBE, Texanol and mineral spirits and it

could not detect alkanes altogether. Thus, this loss could not be quantified. Complete consumption of IVOCs could not be assumed as an additional injection of oxidants (e.g. Expt. 2; Figure 5-5) resulted in an increase in organic aerosol formation. Considering these limitations, SOA yields are not reported in Table 5-1.

In two DEGBE experiments (Expts. 6 and 7), propene was used as a tracer to track the consumption of IVOC. Propene-OH reaction rate constant is 2.6 E-11 cm^3 $molecules^{-1}$ s^{-1} (at 298K) and it does not form SOA. Perfect DEGBE injection is assumed and the propene-OH decay is used to model the decay of DEGBE during the photo-oxidation reaction. The SOA yields based on these two experiments were found to be 0.10 in Expt. 6 and 0.14 in Expt. 7 (at organic aerosol mass concentrations of 25 μg m^{-3}). This is consistent with previously reported yield of 0.16 (at organic aerosol mass concentrations of 47 μg m^{-3}) for DEGBE under high NO conditions (Li et al., 2018).

Table 5-1. Experimental conditions and summary of results for Intermediate-Volatility Organic Compounds (IVOCs) under different conditions

Expt No.	VOC (ppb)	Oxidant	SOA in µg m^{-3} (time in minutes)	f_{44}	f_{43}	$[NO_x]_0$ (ppb)	Ozone (ppb)	Nitrate /Org	HCl^+ /Org
				DEGBE					
1	240	Cl	144 (14)	0.10	0.06	<2	N/A	N/A	0.003
2	120	Cl+Cl	211(55)	0.11	0.06	<2	N/A	N/A	0.002
3	24	Cl	77(10)	0.14	0.06	<2	N/A	N/A	0.004
4	30	HONO	221(70)	0.13	0.06	>500	>500	0.16	N/A
5	120	HONO	107(17)	0.09	0.07	>1000	>500	0.11	N/A
6	24	HONO	31(155)	0.15	0.06	700	>500	0.15	N/A
7	288	HONO	61(80)	0.10	0.06	600	>500	0.12	N/A
8	120	H_2O_2	247(261)	0.11	0.07	<2	N/A	N/A	N/A
9	60	H_2O_2	226(108)	0.11	0.07	<2	30	N/A	N/A
				Texanol					
10	340	HONO +Cl	N/A	N/A	N/A	>500	45	N/A	N/A
11	310	H_2O_2 + ozone	N/A	N/A	N/A	<2	N/A	N/A	N/A
				Mineral Spirits (Commerical grade)					

Table 5-1 (continued). Experimental conditions and summary of results for Intermediate Volatility Organic Compounds (IVOCs) under different conditions

12	470	HONO	198(74)	0.12	0.06	>500	95	0.17	N/A
13	680	HONO +HONO	107(196)	0.12	0.06	>500	52(1^{st}) 100 (2^{nd})	0.17	N/A
14	146	H_2O_2	14(125)	0.09	0.05	N/A	10	N/A	N/A
				n-pentadecane					
15	192	HONO	174(48)	0.08	0.06	>500	>500	0.17	N/A
16	110	H_2O_2 + H_2O_2	65(202)	0.09	0.04	N/A	45	N/A	N/A
				2,6,10 - trimethyl dodecane (TMDD)					
17	253	H_2O_2	83(81)	0.13	0.06	N/A	N/A	N/A	N/A
18	192	HONO	122(70)	0.11	0.06	>500	100	0.18	N/A

Maximum SOA and ozone concentrations are reported
f_{43} and f_{44} at peak SOA concentrations are reported
Nitrate/Org and HCl/Org ratios are averaged over the duration of experiment
NO_x concentrations are reported from chemiluminescence NO_x monitor

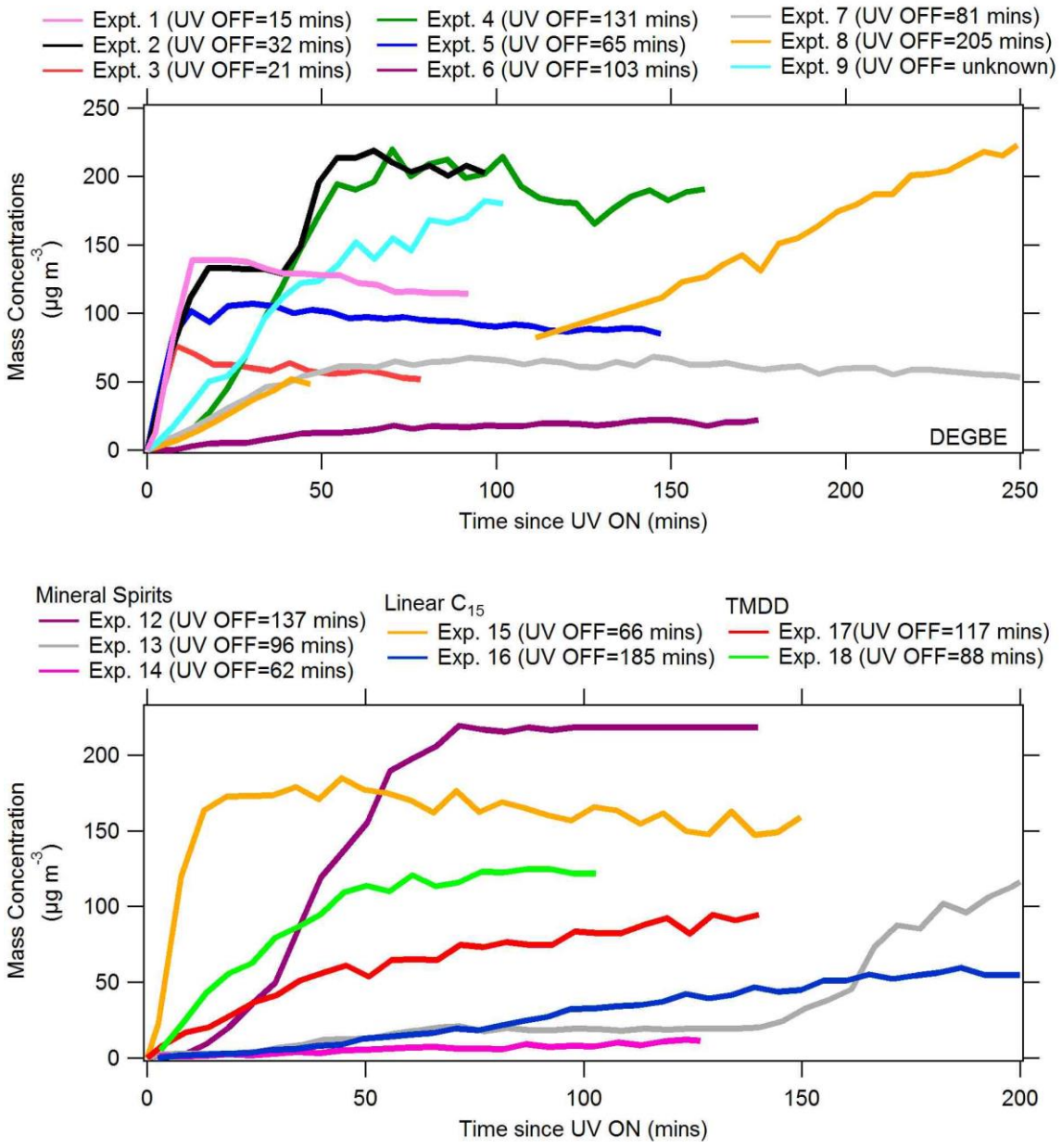

Figure 5-1. Summary of organic aerosol formation for all IVOC experiments from ACSM. Texanol® did not form significant aerosol. Top panel shows organic aerosol formation from DEGBE and bottom panel shows organic aerosol from other IVOCs.

5.3.1 Organic Aerosol bulk composition

Little is known about the chemical mechanism of glycol ether oxidation in the presence of chlorine. Chlorine chemistry usually proceeds either via H-abstraction or by Cl-addition on to an unsaturated carbon. DEGBE does not possess a C-C double bond, and hence, it is likely that the oxidation mechanism will be similar to that of OH radical chemistry. Low levels of organochlorides: 0.3%, 0.22% and 0.2% in experiments 1, 2 and 3 are observed (Table 5-1). These measurements are based on the tracer signal ratios from the ACSM (f_{HCl}+)(Wang and Hildebrandt Ruiz, 2017). f_{HCl}+ denotes the fraction of organics attributed to HCl in the ACSM and has been shown to be a proxy for measuring organochlorides. The low levels observed here indicate that organochlorides are not formed at significant concentrations, consistent with the lack of a double bond in DEGBE. Nitrate over organics ratio in experiments 4, 5, 6 and 7 were 16%, 11%, 15% and 12% respectively (Table 5-1). This, in turn, suggests a significant proportion of OA could be attributed to organic nitrates.

The bulk organic aerosol composition for mineral spirits has previously not been reported to our knowledge. Nitrate over organics ratio in experiments 12 and 13 were 17% (Table 5-1). This is similar to the other IVOCs reported in this study including linear pentadecane (expt. 15), 2,6,10 trimethyl dodecane (exp. 18) and DEGBE (experiments 4, 5, 6 and 7). This suggests that formation of organic nitrates represents an important pathway for oxidation of all of these IVOCs including combustion and non-combustion sources.

5.3.2 Ozone formation from different IVOCs

Ozone formation can occur during photo-oxidation experiments from IVOCs including those from non-combustion sources (Li et al., 2018). The ozone concentrations for all experiments conducted here (high NO_x-OH and low NO_x-OH) where instruments were available are reported in Table 1-1. In Figure 5-2 and Figure 5-3, ozone formation and decay from DEGBE and mineral spirits under high NO_x-OH conditions is shown. Ozone formation from linear pentadecane in Expt. 15 exceeded 500 ppb (outside of instrument range at the time) with initial level of NO_x also exceeding that value. For 2, 6, 10- trimethyl dodecane, an initial injection of 175 ppb NO and high level of NO_2 (outside calibration range) in Expt. 18, resulted in a maximum ozone concentration of 100 ppb within 20 minutes.

The gas-phase reactions (including ozone formation) from non-combustion sources (DEGBE, Texanol® and commercial grade mineral spirits) are not yet part of atmospheric photo-chemical models, though efforts are on-going in the research community, most notably the SAPRC-11 model, which includes coatings VOCs (Carter, 2011). The addition of the contribution of these sources has the potential to improve the predicted ozone concentrations in these models.

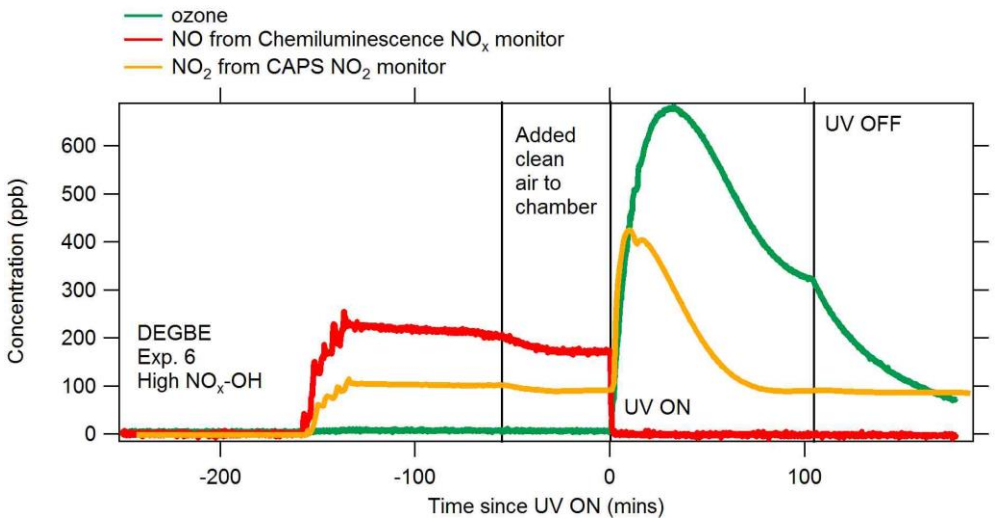

Figure 5-2. Ozone formation from DEGBE under high NO_x-OH conditions.

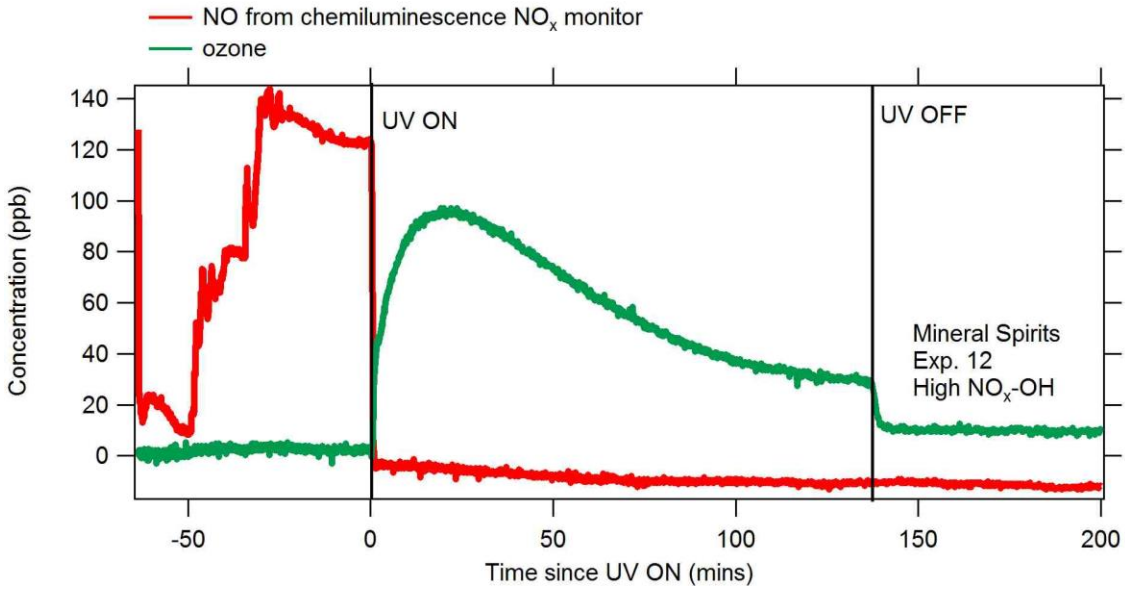

Figure 5-3. Ozone formation from mineral spirits under high NO_x-OH conditions.

5.3.3 Oxidative properties of SOA from different IVOCs

For DEGBE, the f_{44} and f_{43} values observed under low NO_x-chlorine conditions are similar to those seen under low NO_x-OH and high NO_x-OH conditions (Table 5-1, Figure 5-4). The observed f_{44} over f_{43} ratio in our set of experiments is greater than 2 (during experiments 3, 4, 6 and 7) and between 1.57-2 (during experiments 1, 2, 8 and 9). The lowest f_{44} over f_{43} ratio (1.19) was observed during Expt. 5 which had the highest NO_x concentrations (>1000 ppb). The absolute maximum f_{44} (averaged over experiment time-scale) was observed in experiment 6 (15%). We did not observe a decrease in the f_{44} over f_{43} ratio after 100 minutes of photo-oxidation, which has previously been hypothesized to be due to fragmentation pathway taking over from cyclisation pathway in glycol ether oxidation mechanism (Li and Cocker, 2018). Their hypothesis (Li and Cocker, 2018) for this trend was that fragmented products may have a high volatility (due to their smaller size) and evaporate from the OA, decreasing the OA oxidation state. In our set of experiments, after initial photo-oxidation and start of SOA formation, the oxidation states remain constant. The additional injection of Cl_2 in Expt. 2 resulted in a significant increase in OA but no noticeable change in f_{44} and f_{43} (Figure 5-4 and Figure 5-5). Figure 5-4 plots the f_{44} vs f_{43} parameterization (Ng et al., 2011b) and Figure 5-5 plots the organic aerosol formation and gas-phase products from DEGBE under low NO_x-Cl conditions. This indicates that extended oxidation of DEGBE under high chlorine concentrations does not change the oxidation state of SOA after initial oxidation process.

For mineral spirits, the f_{44} and f_{43} values are different under high NO_x-OH and low NO_x-OH conditions. In Expt. 12 (high NO_x-OH), a higher f_{44} (12%) and lower f_{43} (6%) is

observed compared to Expt. 14 (low NO_x-OH) where the f_{44} and f_{43} values are 8% and 11% respectively. This could imply that fragmentation (and less oxidized products) has more of an impact in the oxidation process under low NOx-OH conditions. We see a similar result for both linear pentadecane and 2,6,10 trimethyl dodecane (Table 5-1). For example, in Expt. 18 (high NO_x-OH), we see that a higher f_{44} (12%) and lower f_{43} (6%) than Expt. 17 (low NO_x-OH) where the corresponding f_{44} and lower f_{43} values are 5% and 13% respectively. It may suggest that the commercial grade mineral spirits has constituents which undergo oxidation with similar mechanisms to glycol ethers under high NO_x-OH conditions while under low NO_x-OH conditions, it follows the a mechanism similar to linear pentadecane and 2,6,10- trimethyl dodecane (Figure 5-4).

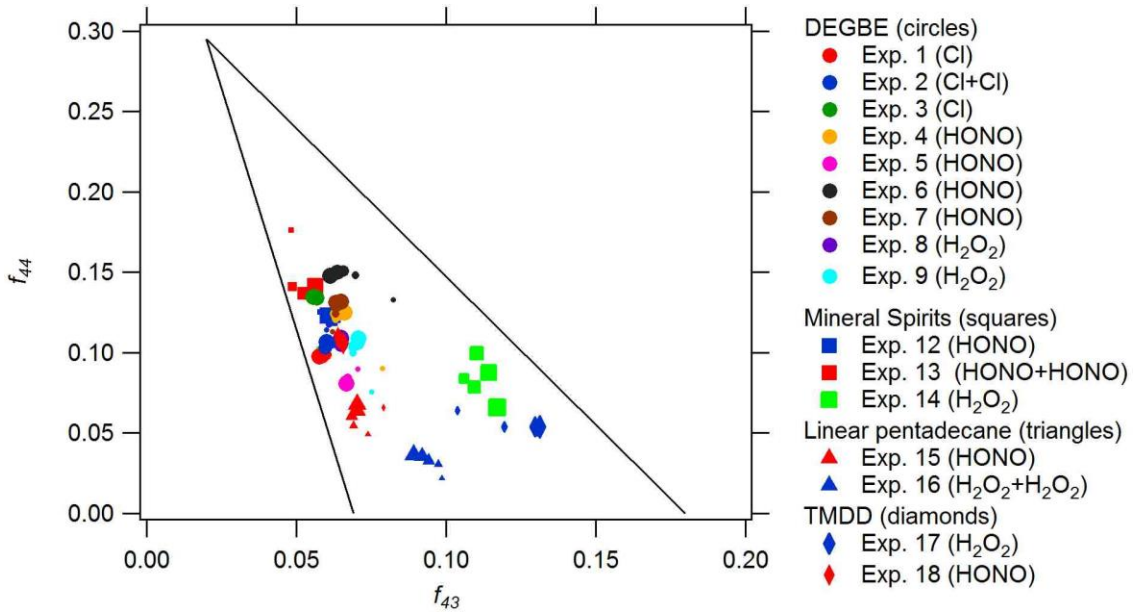

Figure 5-4. f_{43} and f_{44} signals from all experiments as measured by ACSM. f_{43} is used as a tracer for $C_2H_3O^+$ (or fragmentation) and f_{44} for CO_2^+ (or oxidation states) of organic aerosol respectively. The marker size is a function of experiment time (maximum size corresponds to 100 minutes after photo-oxidation is initiated). Black solid lines show typical ambient measurements (Ng et al., 2011b).

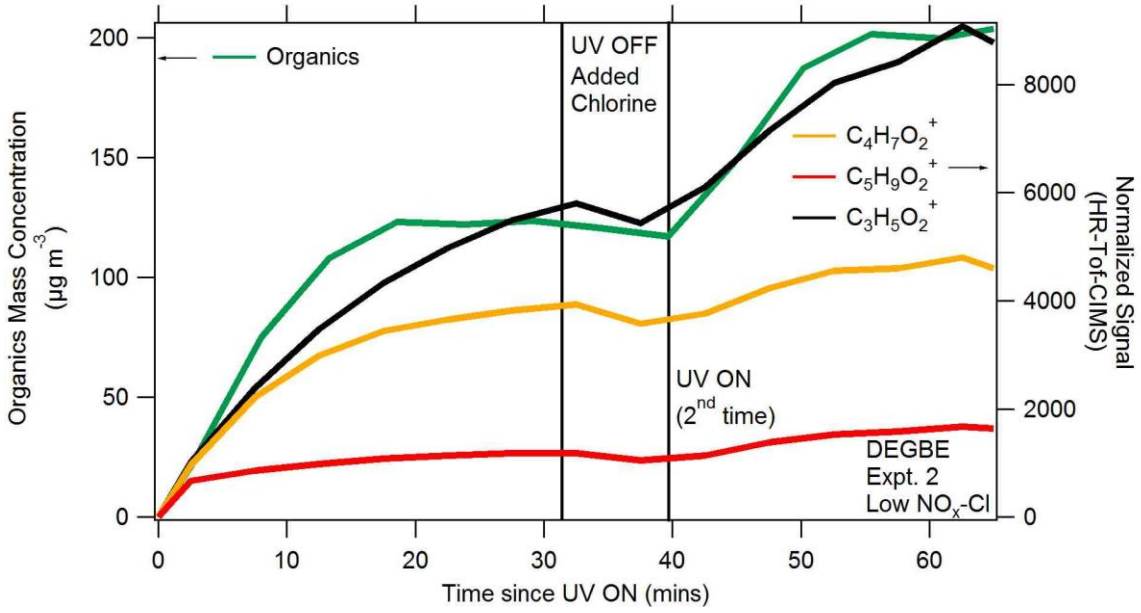

Figure 5-5. Organic aerosol formation (left) from ACSM and gas-phase products identified from the HR-Tof-CIMS under Low NO_x-Cl conditions for DEGBE (right). Gas-phase species shown were normalized against total water cluster reagent ion signal.

Using Equations 1-4, 2-3 and 2-4, elemental ratios (H:C and O:C) can be estimated from f_{43} and f_{44} signals. Figure 5-6 plots the "Van Krevelan" diagram (Van Krevelan, 1950) which shows the elemental ratios from all experiments conducted in this dissertation compared to Riverside, California and New York SV-OOA (semi-volatile oxidized organic aerosol) and branched C_{11} alkane (Tkacik et al., 2012). Linear pentadecane (low NO_x-OH and high NO_x-OH) and mineral spirits (low NO_x-OH) appears to be closest to ambient SV-OOA while all other IVOCs appear more oxidized under all conditions.

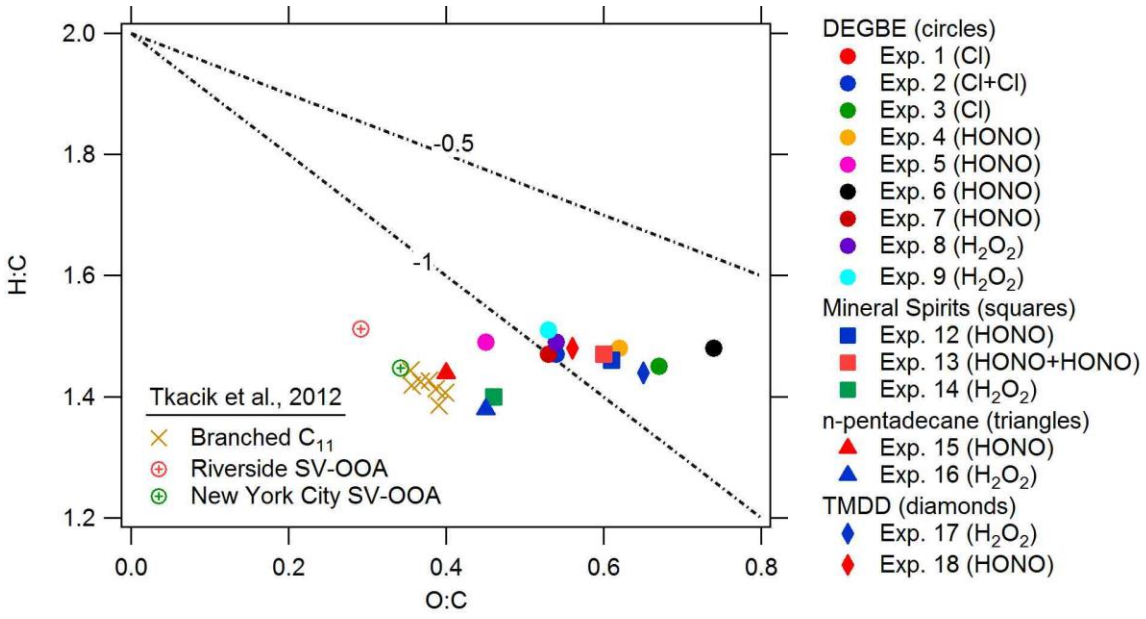

Figure 5-6. Elemental ratios (H:C and O:C) for all experiments derived from f_{43} and f_{44} correlations. SV-OOA represents semi-volatile oxidized organic aerosol in ambient environments. Dotted lines are drawn to represent slopes of -1 and -0.5.

5.3.4 Experimental volatility of Secondary Organic Aerosol from all IVOCs

The SOA formed from different IVOCs under different conditions evaporates at different temperatures. Figure 5-7 (top panel) shows the change in organic aerosol loading when step-wise temperature ramp is employed in the thermo-denuder in a single experiment. Figure 5-7 (bottom panel) shows the organic mass fraction remaining at different temperatures for all experiments where thermo-denuder was employed. Consistently, over half of the OA consistently evaporated around 70 º-90 º C. The T_{50} or the temperature at which half of the organic aerosol evaporates is dependent on the SOA mass. Hence, conclusions about volatility need an evaporation kinetic models to

estimate volatility distributions (Karnezi et al., 2014). Here, the SOA mass (pre-corrected organics) from the ACSM varied from 105-217 µg m^{-3}.

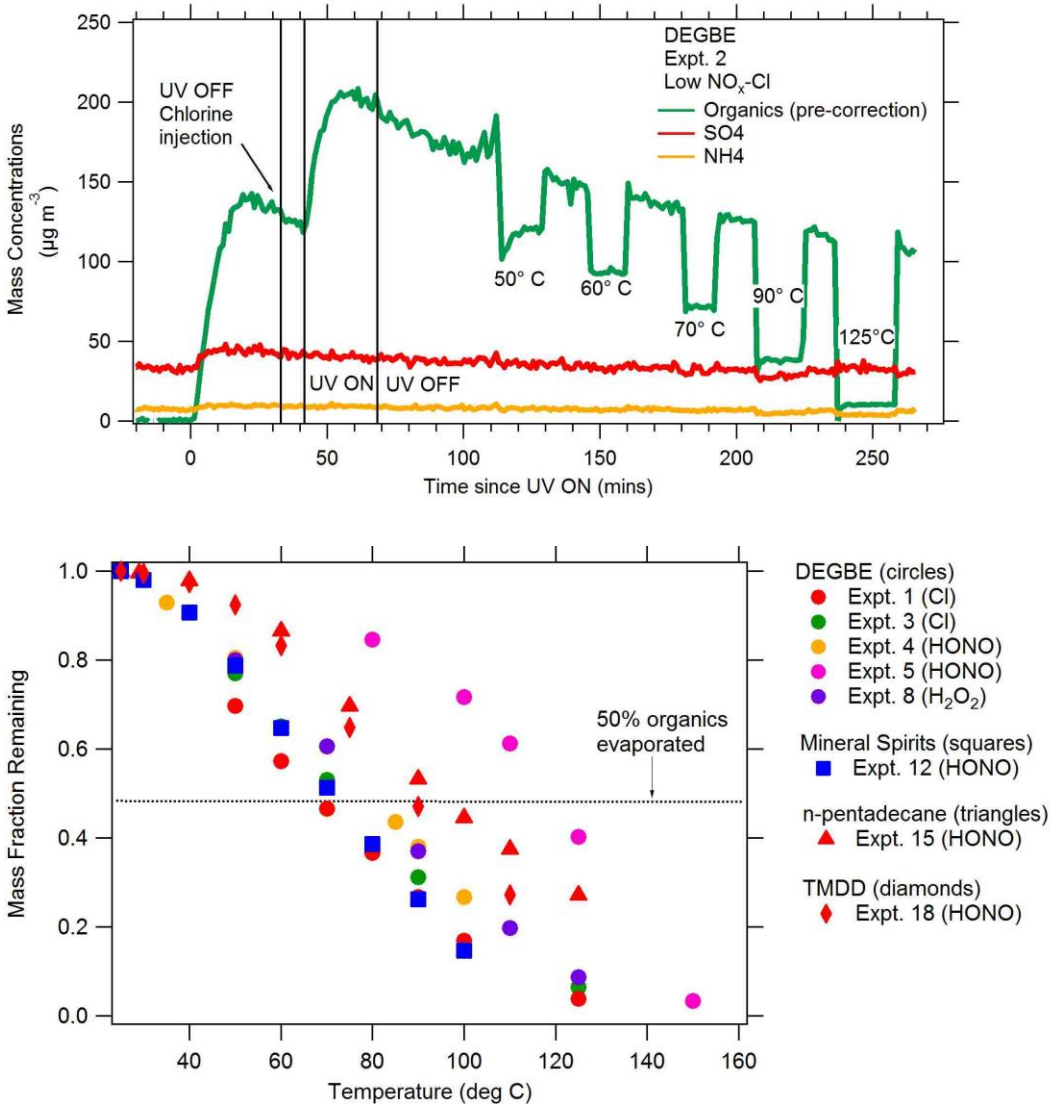

Figure 5-7. Top panel shows change in organic aerosol loading when step-wise temperature ramp is employed in Expt. 2 (DEGBE-low NO_x-Cl) and bottom panel shows organic mass fraction remaining as a function of temperature for all experiments where thermo- denuder data was available. Organic concentrations shown in top panel have not been corrected for particle-wall losses.

Aimanant and Ziemann (2013) reported that a majority of particle phase products desorb between 73 and 85 °C for 2, 6, 10-trimethyl dodecane and between 82-100 °C for linear pentadecane. This seems consistent with results reported in this dissertation. Overall, compared to other IVOCs, it appears that n-pentadecane has a lower volatility than other IVOCs including DEGBE and mineral spirits.

For DEGBE, Experiment 5 is a clear outlier where excess NO_x was added (>1000 ppb). This appears to change the T_{50} and form much lower volatile organic aerosol as compared to other experiments. In Figure 5-6, it is noted that among DEGBE experiments, Experiment 5 had the least O: C ratio implying that the oxidation states and the volatility are altered in the presence of excess NO_x.

5.3.5 Composition of SOA

5.3.5.1 Particle-phase composition

The particle-phase composition of DEGBE under low NO_x-Cl conditions is evaluated using the FIGAERO-CIMS. FIGAERO inlet was unavailable in other experiments. Under low NO_x-Cl conditions, the majority of C_1-C_8 and C_{16}-C_{18} oxidized particle-phase species (H_3O^+ reagent) volatilize around the temperature range 70-90 °C (Figure 5-8). Several species desorb at m/z >200, which are low-volatility products expected to form during initial stages of photo-oxidation. It has also been shown previously that under low NO_x-Cl conditions (Dhulipala et al., 2018 *(in review)*); higher degree of oxidation is possible at much shorter timescales. This suggests that chlorine can expedite the oxidation process for glycol ethers. Two competing pathways, namely, fragmentation and cyclisation for glycol ethers under low NO_x-OH and high NO_x

conditions have previously been reported , with fragmentation being the final step in glycol ether oxidation mechanism (Li and Cocker, 2018). Previous work by Stemmler et al. suggests that $C_3H_5O_2^+$ and the other fragments could be associated with a ring structure such as the dioxolane group. Other fragments include several aldehyde, ketone and ester fragments (Figure 5-8).

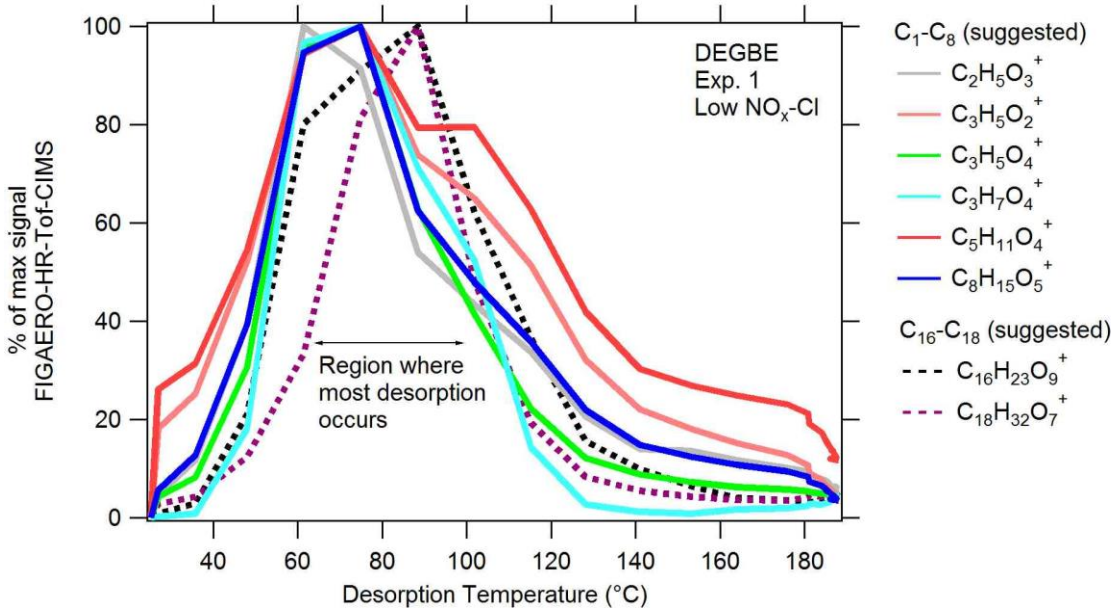

Figure 5-8. Particle-phase products from DEGBE under low NO_x-Cl conditions. Species shown were first normalized against total water cluster reagent ion signal and then normalized against their respective maxima.

5.3.5.2 Gas-phase composition of DEGBE oxidation products

Fragments associated with aldehyde and ketone formation are also observed during the Cl-initiated oxidation process of DEGBE from HR-Tof-CIMS data. Figure 5-9 plots the gas-phase products formed from DEGBE oxidation under different conditions. On the left y axis, high NO_x-OH condition is plotted and on the right y axis, low NO_x-OH

and low NO_x-Cl is plotted. High NO_x-OH condition forms products with intensities an order of magnitude higher than the other two cases. Some fragments reported here (for example, $C_5H_9O_2^+$) is possibly derived from furans. A difference in rate of formation of reaction products in three different conditions is also observed (Figure 5-9). Under low NO_x-OH conditions, the products are formed significantly slower than low NO_x-Cl and high NO_x-OH conditions. This makes sense as chlorine can accelerate the oxidation processes of VOCs in laboratory experiments (Dhulipala et al., 2018 *(in review)*) and the presence of NO_x aids glycol ether fragmentation (Li and Cocker, 2018). An addition of chlorine in Experiment 2 results in an increase in signal intensity of all gas-phase products along with increase in OA loading (Figure 5-5).

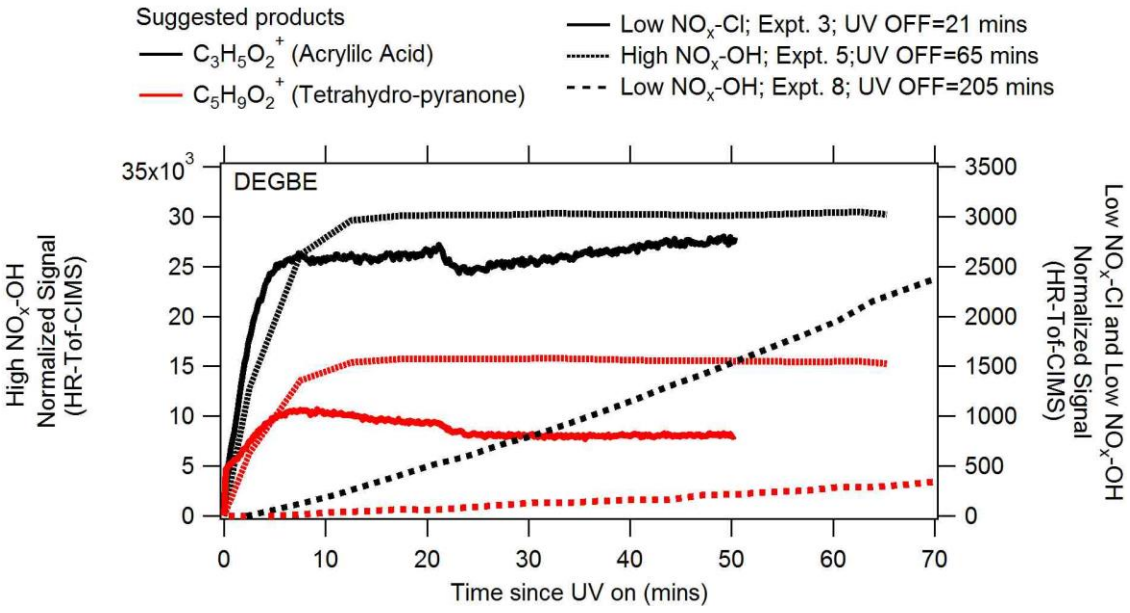

Figure 5-9. Gas-phase products identified from the HR-Tof-CIMS under different conditions for DEGBE. Species shown were normalized against total water cluster reagent ion signal.

5.3.5.3 Gas-phase composition of oxidation products - other IVOCs

Several fragments of oxidative products with aldehydes and ketone groups are again observed. Organic aerosol formation from mineral spirits has previously not been reported before, but it is expected that it will follow a chemical mechanism similar to that of its constituents (C_9-C_{11} alkanes). Another difference is that the signal intensities of other groups are orders of magnitude lower in low NO_x-OH conditions. This is consistent with the slower formation of organic aerosol observed with mineral spirits under low NO_x-OH conditions (Figure 5-1). Four identified peaks from high resolution analysis are shown in Figure 5-10. Here, different rates of formation of products are observed – some appear to form quicker than others under high NO_x-OH conditions. For example, $C_4H_9O_3^+$ forms and decays at a faster rate as compared to $C_4H_5O^+$, $C_6H_{11}O^+$ and $C_6H_{15}O_4^+$ under high NO_x-OH conditions. Intra-comparison between the two conditions shows a slower formation for all products under low NO_x-OH conditions. After a second injection of H_2O_2, it is seen that the gas-phase products again increase, indicating that not all of the mineral spirits had reacted. The products observed do not show a decay rate similar to high NO_x-OH conditions. Some alkyl nitrite species are also observed under high NO_x-OH conditions.

Under high NO_x-OH conditions, fragmented products for linear pentadecane in the gas-phase similar to mineral spirits are observed but the rate of formation of these gas-phase products is much slower.

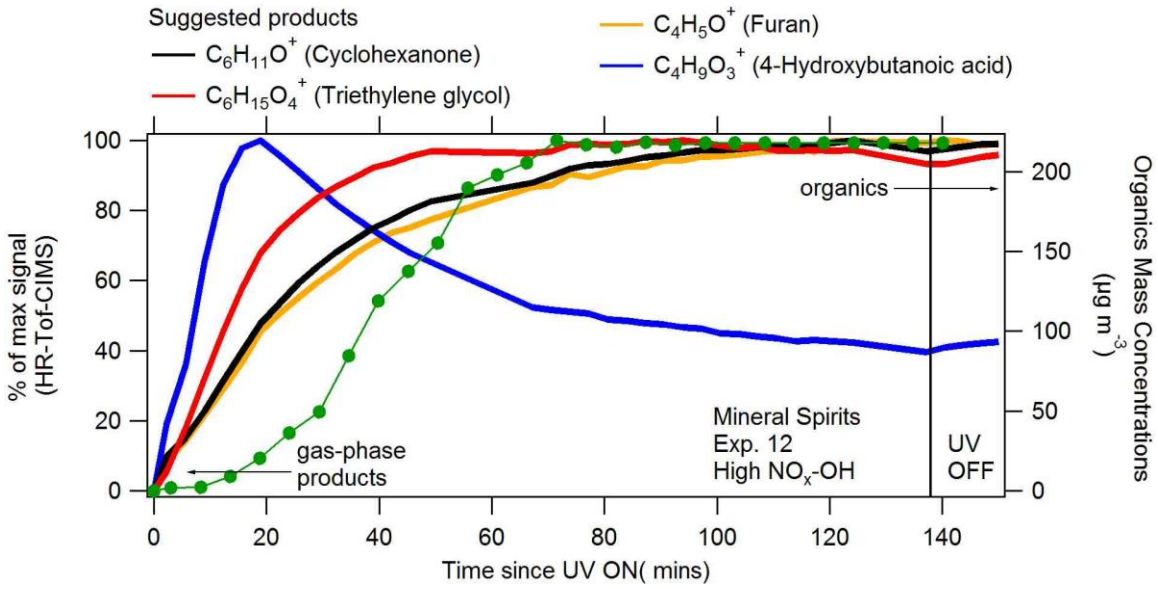

Figure 5-10. Gas-phase products identified from the HR-Tof-CIMS under high NO_x-OH conditions for mineral spirits (left) and organic aerosol formation from ACSM (right). Gas-phase species shown were first normalized against total water cluster reagent ion signal and then normalized against their respective maxima.

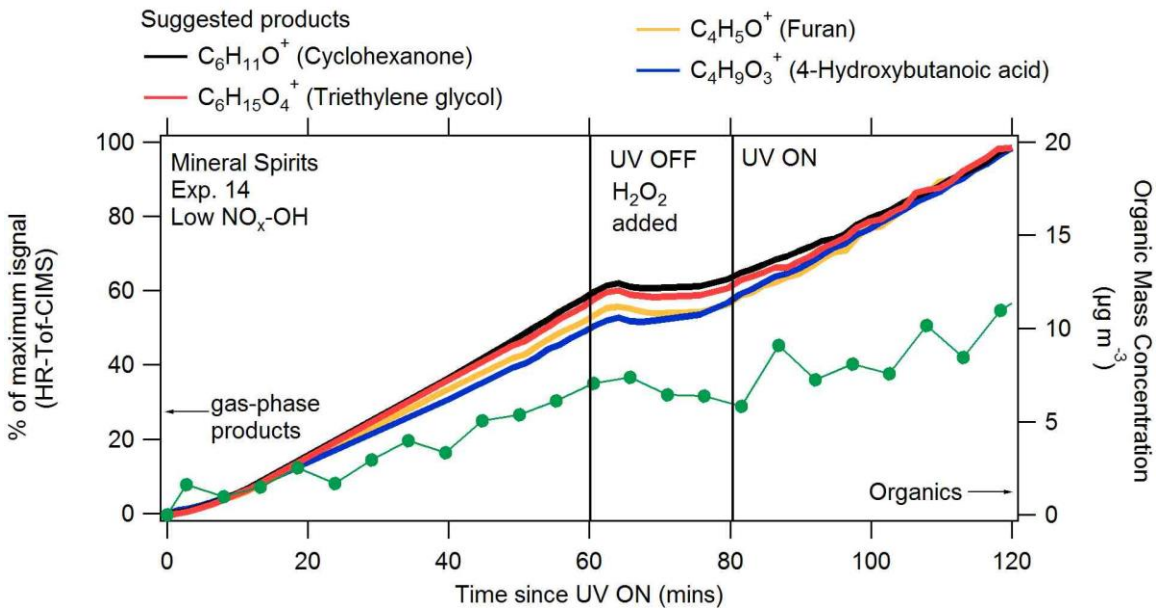

Figure 5-11. Gas-phase products identified from the HR-Tof-CIMS under low NO_x-OH conditions for mineral spirits (left) and organic aerosol formation from ACSM (right). Gas-phase species shown were first normalized against total water cluster reagent ion signal and then normalized against their respective maxima.

5.4 CONCLUSIONS

In this chapter, it is shown that IVOCs from both combustion and non-combustion sources are important sources of ozone formation and secondary organic aerosol formation. Specifically, it is shown that DEGBE can form SOA under low NO_x-Cl, low NO_x-OH and high NO_x-OH conditions. Other non-combustion related IVOCs such as Texanol® (no SOA formed) and mineral spirits (significant SOA formed). Then, gas-phase and particle-phase products under different conditions are reported. It was observed that high NO_x-OH and low NO_x-Cl conditions result in a faster generation of oxidized products in the gas-phase as compared to low NO_x-OH (for DEGBE). Next, volatility of the SOA using experimental thermo-denuder measurements was reported and it was

found to lie in the range between 70-90 °C. In all DEGBE experiments, fragmentation leads to higher volatility. This supports the hypothesis that presence of NO_x leads to fragmentation (Li and Cocker, 2018). Under extremely high NO_x-OH conditions, less fragmentation is observed. Among combustion-related IVOCs, linear pentadecane and 2, 6, 10- trimethyl dodecane were studied and their organic aerosol formation and ozone formation was reported. It is seen that they show similar experimental thermograms as other IVOCs under both low and high NO_x-OH conditions suggesting that they may have similar volatility, but that conclusion requires evaporation kinetic modeling (Karnezi et al., 2014).

Chapter 6: Summary and Future Work

6.1 SUMMARY

This work reports the particulate matter formation from three different categories of volatile organic compounds from combustion and non-combustion sources: 1 – aromatics (toluene) 2 –linear, branched and cyclic C_{10} alkanes 3 – selected volatile chemical products (VCPs) including diethylene glycol mono butyl ether (DEGBE), commercially available mineral spirits and Texanol®. Experimental methods included environmental chamber experiments with state-of-the-art instrumentation including an Aerosol Chemical Speciation Monitor (ACSM) and a High Resolution Time-of-Flight Chemical Ionization Mass Spectrometer (HR-ToF-CIMS) with a filter inlet for gases and aerosols (FIGAERO). Different experimental conditions – low NO_x-OH, high NO_x-OH, low NO_x-Cl and high NO_x-Cl were tested.

Secondary Organic Aerosol (SOA) formation from chlorine-initiated photo-oxidation of toluene was reported. Multi-generational gas-phase products were formed within minutes of oxidation, consistent with an order of difference in reaction rate constants of toluene-OH and toluene-Cl chemistry. Under high NO_x conditions, secondary OH radical generation was reported, which slowed down the gas-phase product formation. High oxidation states of organic aerosol were observed, which have previously been difficult to achieve in environmental chamber experiments with OH-radical initiated chemistry.

Then, the SOA formation from chlorine-initiated photo-oxidation under (low NO_x conditions) of C_{10} alkanes: n-decane, 2-methyl nonane and butyl cyclohexane was reported. Butyl cyclohexane formed the maximum SOA. Low levels (<2%) of organochlorides are observed in all experiments, suggesting Cl-chemistry of C_{10} alkanes proceeds via H-abstraction. Furan-containing groups are reported in both the gas-and-particle phase, consistent with this reaction pathway. Relative humidity (RH) was varied across experiments (0% and 33-55%) but no clear trend is observed in organic aerosol formation. Experimental volatility measurements are reported using a thermo-denuder and mass fraction remaining across different temperature ranges is reported. Under low RH conditions, a higher organic fraction remains in the particle-phase. The filter desorption temperature profiles of particle-phase products from the FIGAERO are also reported.

Finally, the SOA formation from selected VCPs of non-combustion origin including DEGBE, mineral spirits and Texanol® are reported and compared to combustion-related Intermediate Volatility Organic Compounds (IVOCs) such as n-pentadecane and 2, 6, 10 –trimethyl dodecane. Texanol® did not form SOA under low NO_x-OH, high NO_x-OH, and high NO_x-OH-Cl environments. All other VCPs and IVOCs listed above formed SOA. Ozone formation is also reported from all of these precursors. Gas- and particle-phase products from mineral spirits and DEGBE were reported for the first time. For DEGBE, it was observed that high NO_x-OH and low NO_x-Cl conditions result in a faster generation of oxidized products in the gas-phase as compared to low NO_x-OH conditions. Experimental volatility measurements are reported using a thermo-denuder

and mass fraction remaining across different temperature ranges is reported. It is observed that 50% of the organics evaporated at a temperature range of 80-100° C.

Overall, this dissertation improves knowledge of the reaction of VOCs (linear, branched, cyclic alkanes and aromatics) with chlorine radicals. Recent ambient measurements suggest that tropospheric concentrations of chlorine atoms (Cl) are higher than previously assumed, and that chlorine chemistry may be important in continental as well as coastal environments. The reactions of VOCs with chlorine can alter the SOA budget in the atmosphere and reduce discrepancy in modeling and experimental results. The contribution of selected non-combustion reactive volatile components, including those present in solvents and coatings is reported and compared to those from combustion sources. Recent evidence has shown that contribution of volatile chemical products (VCPs) from non-combustion sources has increased in the US and current emissions inventories for these VCPs are a work in progress.

6.2 FUTURE WORK

Chlorine-chemistry of VOCs remains a work in progress and needs more attention. Toluene contains a single aromatic ring and is used as a model compound for small aromatic VOCs. However, the Cl-chemistry of polycyclic aromatic hydrocarbons (PAHs) such as naphthalene has not been explored before and could result in highly oxidized organic aerosol. Reformulated gasoline (Odum et al., 1997) has high levels of aromatics and its reaction with chlorine should be explored next. The set of alkanes studied should be expanded to include C_8-C_{16} alkanes to cover a larger volatility range.

The experimental volatility from the thermo-denuder reported in this dissertation needs to be used in evaporation models (Karnezi et al., 2014) to predict the gas-particle partitioning behavior. This has not been reported before for C_{10} alkanes, DEGBE and mineral spirits. The procedures for filter desorption temperature profiles obtained from the FIGAERO are currently not standardized and valuable information on volatility and composition of oligomeric compounds in the particle-phase, can eventually be used in newer evaporation kinetic models, once they become available.

The set of IVOCs studied should be expanded to include volatile chemical products form the California Air Resources Board (CARB) database (CARB, 2015) which includes ingredients of personal care products, general purpose spray cleaners, paint strippers, caulk removers, laundry detergents, and hand lotions. More laboratory measurements, such as the ones described in this thesis, will be needed to quantify their potential to form PM.

References

Aiken, A. C., Decarlo, P. F., Kroll, J. H., Worsnop, D. R., J. Alex Huffman, Docherty, K. S., Ulbrich, I. M., Mohr, C., Kimmel, J. R., Sueper, D., Yele Sun, Zhang, Q., Trimborn, A., Northway, M., Ziemann, P. J., Canagaratna, M. R., Onasch, T. B., Alfarra, M. R., Prevot, A. S. H., Dommen, J., Duplissy, J., Metzger, A., Baltensperger, U. and Jimenez, J. L.: O / C and OM / OC Ratios of Primary , Secondary , and Ambient Organic Aerosols with High Resolution Time-of-Flight Aerosol Mass Spectrometry, Environ. Sci. Technol., 42(12), 4478–4485, doi:10.1021/es703009q, 2008.

Aimanant, S. and Ziemann, P. J.: Chemical Mechanisms of Aging of Aerosol Formed from the Reaction of n -Pentadecane with OH Radicals in the Presence of NO x, Aerosol Sci. Technol., 47(9), 979–990, doi:10.1080/02786826.2013.804621, 2013a.

Aimanant, S. and Ziemann, P. J.: Chemical Mechanisms of Aging of Aerosol Formed from the Reaction of n-Pentadecane with OH Radicals in the Presence of NOx, Aerosol Sci. Technol., 47(9), 979–990, doi:10.1080/02786826.2013.804621, 2013b.

Aljawhary, D., Lee, A. K. Y. and Abbatt, J. P. D.: High-resolution chemical ionization mass spectrometry (ToF-CIMS): Application to study SOA composition and processing, Atmos. Meas. Tech., 6(11), 3211–3224, doi:10.5194/amt-6-3211-2013, 2013.

Allan, J. D., Delia, A. E., Coe, H., Bower, K. N. and Worsnop, D. R.: A generalised method for the extraction of chemically resolved mass spectra from Aerodyne aerosol mass spectrometer data, J. Aerosol Sci., 35, 909–922, doi:10.1016/j.jaerosci.2004.02.007, 2004.

Alramadan, A. S., Sarathy, S. M., Khurshid, M. and Badra, J.: A blending rule for octane numbers of PRFs and TPRFs with ethanol, Fuel, 180(March 2007), 175–186, doi:10.1016/j.fuel.2016.04.032, 2016.

Alwe, H. D., Walawalkar, M., Sharma, A., Pushpa, K. K., Dhanya, S. and Naik, P. D.: Rate coefficients for the gas-phase reactions of chlorine atoms with cyclic ethers at 298 K, Int. J. Chem. Kinet., 45(5), 295–305, doi:10.1002/kin.20765, 2013.

Alwe, H. D., Walavalkar, M. P., Sharma, A., Dhanya, S. and Naik, P. D.: Tropospheric

oxidation of cyclic unsaturated ethers in the day-time: Comparison of the reactions with Cl, OH and O3based on the determination of their rate coefficients at 298K, Atmos. Environ., 82, 113–120, doi:10.1016/j.atmosenv.2013.10.009, 2014.

Angove, D., White, S., Keywood, M. and Azzi, M.: Studies of the Secondary Organic Aerosol Component of PM 2 . 5 Arising from the NEPM Air Toxic Precursors , Toluene and m-Xylene : Final Report, , (November), 2008.

Aschmann, S. M.: Products of the Gas-Phase Reactions of the OH Radical with 1-Methoxy-2-propanol and 2-Butoxyethanol, , 32(21), 3336–3345, doi:10.1021/es980455c, 1998.

Aschmann, S. M. and Atkinson, R.: Rate Constants for the Gas-Phase Reactions of Alkanes with Cl Atoms at 296 K, , 2662(1971), 1134–1138, 1976.

Aschmann, S. M. and Atkinson, R.: Rate constants for the gas-phase reactions of alkanes with Cl atoms at 296 ± 2 K, Int. J. Chem. Kinet., 27(6), 613–622, doi:10.1002/kin.550270611, 1995.

Aschmann, S. M., Chew, A. A., Arey, J. and Atkinson, R.: Products of the Gas-Phase Reaction of OH Radicals with Cyclohexane: Reactions of the Cyclohexoxy Radical, J. Phys. Chem. A, 101(43), 8042–8048, doi:10.1021/jp971869f, 1997.

Aschmann, S. M., Martin, P., Tuazon, E. C., Arey, J. and Atkinson, R.: Kinetic and product studies of the reactions of selected glycol ethers with OH radicals, Environ. Sci. Technol., 35(20), 4080–4088, doi:10.1021/es010831k, 2001.

Atkinson, R.: Atmospheric chemistry of VOCs and NO(x), Atmos. Environ., 34(12–14), 2063–2101, doi:10.1016/S1352-2310(99)00460-4, 2000.

Atkinson, R.: Rate constants for the atmospheric reactions of alkoxy radicals: An updated estimation method, Atmos. Environ., 41(38), 8468–8485, doi:10.1016/j.atmosenv.2007.07.002, 2007.

Atkinson, R. and Arey, J.: Atmospheric Degradation of Volatile Organic Compounds Atmospheric Degradation of Volatile Organic Compounds, Environ. Sci., 103(October), 4605–4638, doi:10.1021/cr0206420, 2003.

Atkinson, R., Arey, J., Aschmann, S. M. and Kwok, E. S. C.: Atmospheric Chemistry of Selected Linear, Branched and Cyclic C10 Alkane Components of Mineral Spirits., 2001.

Behnke, W., George, C., Scheer, V. and Zetzsch, C.: Production and decay of ClNO2 from the reaction of gaseous N2O 5 with NaCl solution: Bulk and aerosol experiments, J. Geophys. Res. Atmos., 102(D3), 3795–3804, doi:10.1029/96JD03057, 1997.

Birdsall, A. W. and Elrod, M. J.: Comprehensive NO-dependent study of the products of the oxidation of atmospherically relevant aromatic compounds., J. Phys. Chem. A, 115(21), 5397–407, doi:10.1021/jp2010327, 2011.

Birdsall, A. W., Andreoni, J. F. and Elrod, M. J.: Investigation of the role of bicyclic peroxy radicals in the oxidation mechanism of toluene, J. Phys. Chem. A, 114, 10655–10663, doi:10.1021/jp105467e, 2010.

Borbon, A., Sauvage, S., Gouw, J. A. De, Colomb, A., Gros, V., Freutel, F. and Crippa, M.: Volatile and intermediate volatility organic compounds in suburban Paris : variability , origin and importance for SOA formation, , 10439–10464, doi:10.5194/acp-14-10439-2014, 2014.

Bortoli, M. De, Knöppel, H., Pecchio, E., Peil, A., Rogora, L., Schauenburg, H., Schlitt, H. and Vissers, H.: Concentrations of selected organic pollutants in indoor and outdoor air in Northern Italy, Environ. Int., 12(1), 343–350, doi:https://doi.org/10.1016/0160-4120(86)90048-6, 1986.

Brook, R. D., Rajagopalan, S., Pope, C. A., Brook, J. R., Bhatnagar, A., Diez-Roux, A. V., Holguin, F., Hong, Y., Luepker, R. V., Mittleman, M. A., Peters, A., Siscovick, D., Smith, S. C., Whitsel, L. and Kaufman, J. D.: Particulate Matter Air pollution and Cardiovascular Disease: An Update to the Scientific Statement from the American Heart Association, Circulation, 121(21), 2331–2378, doi:10.1161/CIR.0b013e3181dbece1, 2010.

Brook, R. D., Rajagopalan, S., Iii, C. A. P., Brook, J. R., Bhatnagar, A., Diez-roux, A. V, Holguin, F., Hong, Y., Luepker, R. V, Mittleman, M. A., Peters, A., Siscovick, D., Smith, S. C., Whitsel, L. and Kaufman, J. D.: Particulate Matter Air Pollution and Cardiovascular Disease, , doi:10.1161/CIR.0b013e3181dbece1, 2016.

Cai, X., Ziemba, L. D. and Griffin, R. J.: Secondary aerosol formation from the oxidation of toluene by chlorine atoms., 2008.

Calvert, J. G., Atkinson, R., Becker, K. H., Kamens, R. M., Seinfeld, J. H., Wallington, T. H. and Yarwood, G.: The Mechanisms of Atmospheric Oxidation of the Aromatic Hydrocarbons, 1st ed., Oxford University Press, New York., 2002.

Canagaratna, M. R., Jimenez, J. L., Kroll, J. H., Chen, Q., Kessler, S. H., Massoli, P., Hildebrandt Ruiz, L., Fortner, E., Williams, L. R., Wilson, K. R., Surratt, J. D., Donahue, N. M., Jayne, J. T. and Worsnop, D. R.: Elemental ratio measurements of organic compounds using aerosol mass spectrometry: Characterization, improved calibration, and implications, Atmos. Chem. Phys., 15(1), 253–272, doi:10.5194/acp-15-253-2015, 2015.

CARB, C. A. R. B.: Regulation for Reducing Emissions from Consumer Products. [online] Available from: https://www.arb.ca.gov/consprod/regs/regs.htm, 2015a.

CARB, C. A. R. B.: The California Consumer Products Regulations., 2015b.

Carter, W. P. L.: Environmental chamber ttudies of ozone impacts of coatings VOCs., 2011.

Carter, W. P. L. and Heo, G.: Development of revised SAPRC aromatics mechanisms, Atmos. Environ., 77(October 2013), 404–414, doi:10.1016/j.atmosenv.2013.05.021, 2013.

Carter, W. P. L., Cocker, D. R., Fitz, D. R., Malkina, I. L., Bumiller, K., Sauer, C. G., Pisano, J. T., Bufalino, C. and Song, C.: A new environmental chamber for evaluation of gas-phase chemical mechanisms and secondary aerosol formation, Atmos. Environ., 39(40), 7768–7788, doi:10.1016/j.atmosenv.2005.08.040, 2005.

Chacon-Madrid, H. J. and Donahue, N. M.: Fragmentation vs. functionalization: Chemical aging and organic aerosol formation, Atmos. Chem. Phys., 11(20), 10553–10563, doi:10.5194/acp-11-10553-2011, 2011.

Chan, A. W. H., Kautzman, K. E., Chhabra, P. S., Surratt, J. D., Chan, M. N., Crounse, J. D., Wennberg, P. O., Flagan, R. C., Seinfeld, J. H. and Sciences, P.: and Physics Secondary organic aerosol formation from photooxidation of naphthalene and alkylnaphthalenes : implications for oxidation of intermediate volatility organic compounds (IVOCs), , (2007), 3049–3060, 2009.

Chang, S. and Allen, D. T.: Atmospheric chlorine chemistry in southeast Texas: Impacts on ozone formation and control, Environ. Sci. Technol., 40(1), 251–262, doi:10.1007/s10479-006-0033-8, 2006a.

Chang, S. and Allen, D. T.: Chlorine chemistry in urban atmospheres: Aerosol formation associated with anthropogenic chlorine emissions in southeast Texas, Atmos. Environ.,

40, 512–523, doi:10.1016/j.atmosenv.2006.04.070, 2006b.

Chang, S., Tanaka, P., Mcdonald-buller, E. and Allen, D. T.: Emission inventory for atomic chlorine precursors in Southeast Texas, Rep. Contract 9880077600-18 between Univ. Texas Texas Nat. Resour. Conserv. Comm., 1–27, 2001.

Chen, J. and Luo, D.: Ozone formation potentials of organic compounds from different emission sources in the South Coast Air Basin of California, Atmos. Environ., 55, 448–455, doi:10.1016/j.atmosenv.2012.02.082, 2012.

Chhabra, P. S., Ng, N. L., Canagaratna, M. R., Corrigan, a. L., Russell, L. M., Worsnop, D. R., Flagan, R. C. and Seinfeld, J. H.: Elemental composition and oxidation of chamber organic aerosol, Atmos. Chem. Phys., 11(17), 8827–8845, doi:10.5194/acp-11-8827-2011, 2011.

Chuang, W. K. and Donahue, N. M.: A two-dimensional volatility basis set-Part 3: Prognostic modeling and NOxdependence, Atmos. Chem. Phys., 16(1), 123–134, doi:10.5194/acp-16-123-2016, 2016.

Cohen, A. J., Brauer, M., Burnett, R., Anderson, H. R., Frostad, J., Estep, K., Balakrishnan, K., Brunekreef, B., Dandona, L., Dandona, R., Feigin, V., Freedman, G., Hubbell, B., Jobling, A., Kan, H., Knibbs, L., Liu, Y., Martin, R., Morawska, L., Pope, C. A., Shin, H., Straif, K., Shaddick, G., Thomas, M., van Dingenen, R., van Donkelaar, A., Vos, T., Murray, C. J. L. and Forouzanfar, M. H.: Estimates and 25-year trends of the global burden of disease attributable to ambient air pollution: an analysis of data from the Global Burden of Diseases Study 2015, Lancet, 389(10082), 1907–1918, doi:10.1016/S0140-6736(17)30505-6, 2017.

Colombo, A., Bortoli, M., Helmut, K., Schauenburg, H. and Vissers, H.: Small Chamber Tests and Headspace Analysis of Volatile Organic Compounds Emitted from Household Products, Indoor Air, 1(1), 13–21, doi:10.1111/j.1600-0668.1991.02-11.x, 1991.

Cubison, M. J. and Jimenez, J. L.: Statistical precision of the intensities retrieved from constrained fitting of overlapping peaks in high-resolution mass spectra, Atmos. Meas. Tech., 8(6), 2333–2345, doi:10.5194/amt-8-2333-2015, 2015.

Decarlo, P. F., Kimmel, J. R., Trimborn, A., Northway, M. J., Jayne, J. T., Aiken, A. C., Gonin, M., Fuhrer, K., Horvath, T., Docherty, K. S., Worsnop, D. R. and Jimenez, J. L.: Field-Deployable, High-Resolution, Time-of-Flight Aerosol Mass Spectrometer, Anal. Chem., 78(24), 8281–8289, doi:8410.1029/2001JD001213.Analytical, 2006.

Diehl, J. W. and Di Sanzo, F. P.: Determination of aromatic hydrocarbons in gasolines by flow modulated comprehensive two-dimensional gas chromatography, J. Chromatogr. A, 1080(2), 157–165, doi:10.1016/j.chroma.2004.11.054, 2005.

Donahue, N. M., Robinson, a L., Stanier, C. O. and Pandis, S. N.: Coupled partitioning, dilution, and chemical aging of semivolatile organics., Environ. Sci. Technol., 40(8), 2635–43 [online] Available from: http://www.ncbi.nlm.nih.gov/pubmed/16683603, 2006.

Donahue, N. M., Epstein, S. a., Pandis, S. N. and Robinson, a. L.: A two-dimensional volatility basis set: 1. organic-aerosol mixing thermodynamics, Atmos. Chem. Phys., 11(7), 3303–3318, doi:10.5194/acp-11-3303-2011, 2011.

Donahue, N. M., Kroll, J. H., Pandis, S. N. and Robinson, A. L.: A two-dimensional volatility basis set-Part 2: Diagnostics of organic-aerosol evolution, Atmos. Chem. Phys., 12(2), 615–634, doi:10.5194/acp-12-615-2012, 2012.

Dunmore, R. E., Hopkins, J. R., Lidster, R. T., Lee, J. D., Evans, M. J., Rickard, A. R. and Lewis, A. C.: Diesel-related hydrocarbons can dominate gas phase reactive carbon in megacities, , 9983–9996, doi:10.5194/acp-15-9983-2015, 2015.

Emanuelsson, E.: Formation , Ageing and Thermal Properties of Secondary Organic Aerosol. [online] Available from: https://gupea.ub.gu.se/handle/2077/31839\nhttp://hdl.handle.net/2077/31839, 2013.

EPA: Toxics Release Inventory-list of Toxic Chemicals within the Glycol Ethers Category., 2000.

EPA: Inventory of U . S . Greenhouse Gas Emissions and Sinks : 1990-2009, , 1990–2009, doi:EPA 430-R-13-001, 2016.

Fabri, J., Graeser, U. and Simo, T. A.: Toluene, in Ullmann's Encyclopedia of Industrial Chemistry, Wiley-VCH Verlag GmbH & Co. KGaA., 2000.

Fantechi, G., Jensen, N. R., Saastad, O. L. E., Hjorth, J. and Peeters, J.: Reactions of Cl Atoms with Selected VOCs : Kinetics , Products and Mechanisms, , 247–267, 1998.

Faxon, C. B. and Allen, D. T.: Chlorine chemistry in urban atmospheres: a review, Environ. Chem., 10(3), 221, doi:10.1071/EN13026, 2013.

Faxon, C. B., Dhulipala, S. V., Allen, D. T. and Hildebrandt Ruiz, L.: Heterogeneous Production of Cl2 from Particulate Chloride: Effects of Particle Composition and Relative Humidity, Am. Inst. Chem. Eng. J., 2018.

Finlayson-Pitts, B. J.: Chlorine atoms as a potential tropospheric oxidant in the marine boundary layer, Res. Chem. Intermed., 19(3), 235–249, doi:10.1163/156856793X00091, 1993.

Finlayson-Pitts, B. J. and Pitts, J. N.: Pollution : Tropospheric Air Airborne Toxics , Ozone , Aromatic Polycyclic and Particles Hydrocarbons , Science (80-.)., 276(5315), 1045–1052, doi:10.1126/science.276.5315.1045, 1997.

Finlayson-Pitts, B. J., Ezell, M. J. and Pitts, J. N.: Formation of chemically active chlorine compounds by reactions of atmospheric NaCl particles with gaseous N2O5 and ClONO2, Nature, 337(6204), 241–244, doi:10.1038/337241a0, 1989.

Fortner, E. C., Zheng, J., Zhang, R., Knighton, W. B., Volkamer, R. M., Sheehy, P., Molina, L. and Andŕe, M.: Measurements of volatile organic compounds using proton transfer reaction-mass spectrometry during the MILAGRO 2006 campaign, Atmos. Chem. Phys., 9(2), 467–481, doi:10.5194/acp-9-467-2009, 2009.

Fraser, M. P., Cass, G. R., Simoneit, B. R. T. and Rasmussen, R. A.: Air quality model evaluation data for organics. 4. C2-C36 non- aromatic hydrocarbons, Environ. Sci. Technol., 31(8), 2356–2367, doi:10.1021/es960980g, 1997.

Gligorovski, S. and Abbatt, J. P. D.: An indoor chemical cocktail., Science, 359(6376), 632–633, doi:10.1126/science.aar6837, 2018.

Graedel, T. E. and Keene, W. C.: Tropospheric budget of reactive chlorine, Global Biogeochem. Cycles, 9(1), 47–77, doi:10.1029/94GB03103, 1995.

Hallquist, M., Wenger, J. C., Baltensperger, U., Rudich, Y., Simpson, D., Claeys, M. and Dommen, J.: The formation , properties and impact of secondary organic aerosol : current and emerging issues, Atmos. Chem. Phys., (November 2008), 5155–5236, 2009.

Hayes, P. L., Carlton, A. G., Baker, K. R., Ahmadov, R., Washenfelder, R. A., Alvarez, S., Rappenglück, B., Gilman, J. B., Kuster, W. C., De Gouw, J. A., Zotter, P., Prévôt, A. S. H., Szidat, S., Kleindienst, T. E., Offenberg, J. H., Ma, P. K. and Jimenez, J. L.: Modeling the formation and aging of secondary organic aerosols in Los Angeles during CalNex 2010, Atmos. Chem. Phys., 15(10), 5773–5801, doi:10.5194/acp-15-5773-2015, 2015.

Heald, C. L., Kroll, J. H., Jimenez, J. L., Docherty, K. S., DeCarlo, P. F., Aiken, a. C., Chen, Q., Martin, S. T., Farmer, D. K. and Artaxo, P.: A simplified description of the evolution of organic aerosol composition in the atmosphere, Geophys. Res. Lett., 37(8), n/a-n/a, doi:10.1029/2010GL042737, 2010.

Hildebrandt, L., Donahue, N. M. and Pandis, S. N.: High formation of secondary organic aerosol from the photo-oxidation of toluene, Atmos. Chem. Phys., 9(9), 2973–2986, doi:10.5194/acp-9-2973-2009, 2009.

Hildebrandt Ruiz, L., Paciga, A. L., Cerully, K. M., Nenes, A., Donahue, N. M. and Pandis, S. N.: Formation and aging of secondary organic aerosol from toluene: Changes in chemical composition, volatility, and hygroscopicity, Atmos. Chem. Phys., 15(14), 8301–8313, doi:10.5194/acp-15-8301-2015, 2015.

Huang, M., Zhang, W., Gu, X., Hu, C., Zhao, W., Wang, Z. and Fang, L.: Size distribution and chemical composition of secondary organic aerosol formed from Cl-initiated oxidation of toluene, J. Environ. Sci., 24(5), 860–864, doi:10.1016/S1001-0742(11)60840-1, 2012.

Huang, M., Liu, X., Hu, C., Guo, X., Gu, X., Zhao, W., Wang, Z., Fang, L. and Zhang, W.: Aerosol laser time-of-flight mass spectrometer for the on-line measurement of secondary organic aerosol in smog chamber, Meas. J. Int. Meas. Confed., 55(3), 394–401, doi:10.1016/j.measurement.2014.05.038, 2014.

Huffman, J. A., Ziemann, P. J., Jayne, J. T., Worsnop, D. R. and Jimenez, J. L.: Development and characterization of a fast-stepping/scanning thermodenuder for chemically-resolved aerosol volatility measurements, Aerosol Sci. Technol., 42(5), 395–407, doi:10.1080/02786820802104981, 2008.

Jang, M. and Kamens, R. M.: Characterization of secondary aerosol from the photooxidation of toluene in the presence of NOx and 1-propene, Environ. Sci. Technol., 35(18), 3626–3639, doi:10.1021/es010676+, 2001.

Jathar, S. H., Miracolo, M. a., Presto, a. a., Donahue, N. M., Adams, P. J. and Robinson, a. L.: Modeling the formation and properties of traditional and non-traditional secondary organic aerosol: problem formulation and application to aircraft exhaust, Atmos. Chem. Phys., 12(19), 9025–9040, doi:10.5194/acp-12-9025-2012, 2012.

Jathar, S. H., Gordon, T. D., Hennigan, C. J., Pye, H. O. T., Pouliot, G., Adams, P. J., Donahue, N. M. and Robinson, A. L.: Unspeciated organic emissions from combustion

sources and their influence on the secondary organic aerosol budget in the United States, Proc. Natl. Acad. Sci., 111(29), 10473–10478, doi:10.1073/pnas.1323740111, 2014.

Jimenez, J. ., Canagaratna, M. R., Donahue, N. M., Prevot, A. S. H., Zhang, Q., Kroll, J. H., DeCarlo, P. F., Allan, J. D., Coe, H., Ng, N. L., Aiken, A. C., Docherty, K. D., Ulbrich, I. M., Grieshop, A. P., Robinson, A. L., Duplissy, J., Smith, J. D., Wilson, K. R., Lanz, V. A., Hueglin, C., Sun, Y. L., Tian, J., Laaksonen, A., Raatikainen, T., Rautiainen, J., Vaattovaara, P., Ehn, M., Kulmala, M., Tomlinson, J. M., Collins, D. R., Cubison, M. J., Dunlea, E. J., Huffman, J. A., Onasch, T. B., Alfarra, M. R., Williams, P. I., Bower, K., Kondo, Y., Schneider, J., Drewnick, F., Borrmann, S., Weimer, S., Demerjian, K., Salcedo, D., Cottrell, L., Griffin, R., Takami, A., Miyoshi, T., Hatakeyama, S., Shimono, A., Sun, J. Y., Zhang, Y. M., Dzepina, K., Kimmel, J. R., Sueper, D., Jayne, J. T., Herndon, S. C., Trimborn, A. M., Williams, L. R., Wood, E. C., Middlebrook, A. M., Kolb, C. E., Baltensperger, U. and Worsnop, D. R.: Evolution of Organic Aerosols in the Atmosphere, Science (80-.)., 326, 1525–1529, doi:10.1126/science.1180353, 2009.

Jordan, C. E., Ziemann, P. J., Griffin, R. J., Lim, Y. B., Atkinson, R. and Arey, J.: Modeling SOA formation from OH reactions with C8–C17 n-alkanes, Atmos. Environ., 42(34), 8015–8026, doi:10.1016/j.atmosenv.2008.06.017, 2008.

Kampa, M. and Castanas, E.: Human health effects of air pollution, Environ. Pollut., 151(2), 362–367, doi:10.1016/j.envpol.2007.06.012, 2008.

Karlsson, R. S., Szente, J. J., Ball, J. C. and Maricq, M. M.: Homogeneous Aerosol Formation by the Chlorine Atom Initiated Oxidation of Toluene, J. Phys. Chem. A, 105(1), 82–96, doi:10.1021/jp001831u, 2001a.

Karlsson, R. S., Szente, J. J., Ball, J. C. and Maricq, M. M.: Homogeneous aerosol formation by the chlorine atom initiated oxidation of toluene, J. Phys. Chem. A, 105(1), 82–96, doi:10.1021/jp001831u, 2001b.

Karnezi, E., Riipinen, I. and Pandis, S. N.: Measuring the atmospheric organic aerosol volatility distribution: A theoretical analysis, Atmos. Meas. Tech., 7(9), 2953–2965, doi:10.5194/amt-7-2953-2014, 2014.

Kebabian, P. L., Herndon, S. C. and Freedman, A.: Attenuated Phase Shift Spectroscopy, Anal. Chem., 77(2), 724–728, doi:10.1029/2003JD004091.(9), 2005.

Kebabian, P. L., Wood, E. C., Herndon, S. C. and Freedman, A.: A practical alternative to

chemiluminescence-based detection of nitrogen dioxide: Cavity attenuated phase shift spectroscopy, Environ. Sci. Technol., 42(16), 6040–6045, doi:10.1021/es703204j, 2008.

Kettle, A. J. and Andreae, M. O.: Flux of dimethylsulfide from the oceans: A comparison of updated data sets and flux models, J. Geophys. Res. Atmos., 105(D22), 26793–26808, doi:10.1029/2000JD900252, 2000.

Khalil, M. A. K., Moore, R. M., Harper, D. B., Lobert, J. M., Erickson, D. J., Koropalov, V., Sturges, W. T. and Keene, W. C.: Natural emissions of chlorine-containting gases: Reactive Chlorine Emisssions Inventory, J. Geophys. Res., 104, 8333–8346, 1999.

Knöppel, H. and Schauenburg, H.: Screening of household products for the emission of volatile organic compounds, Environ. Int., 15(1), 413–418, doi:https://doi.org/10.1016/0160-4120(89)90056-1, 1989.

Van Krevelan, D. W.: Graphical statistical method for the study of structure and reaction processes of coal, Fuel, 29(4), 269–284, 1950.

Kroll, J. H., Donahue, N. M., Jimenez, J. L., Kessler, S. H., Canagaratna, M. R., Wilson, K. R., Altieri, K. E., Mazzoleni, L. R., Wozniak, A. S., Bluhm, H., Mysak, E. R., Smith, J. D., Kolb, C. E. and Worsnop, D. R.: Carbon oxidation state as a metric for describing the chemistry of atmospheric organic aerosol, Nat. Chem., 3(2), 133–139, doi:10.1038/nchem.948, 2011.

Lelieveld, J., Evans, J. S., Fnais, M., Giannadaki, D. and Pozzer, A.: The contribution of outdoor air pollution sources to premature mortality on a global scale., Nature, 525(7569), 367–71, doi:10.1038/nature15371, 2015.

Li, L. and Cocker, D. R.: Molecular structure impacts on secondary organic aerosol formation from glycol ethers, Atmos. Environ., 180(February), 206–215, doi:10.1016/j.atmosenv.2017.12.025, 2018.

Li, L., Tang, P., Nakao, S., Chen, C. and Iii, D. R. C.: Role of methyl group number on SOA formation from monocyclic aromatic hydrocarbons photooxidation under low-NO x conditions, , 2255–2272, doi:10.5194/acp-16-2255-2016, 2016.

Li, W., Li, L., Chen, C., Kacarab, M., Peng, W., Price, D., Xu, J. and Cocker, D. R.: Potential of select intermediate-volatility organic compounds and consumer products for secondary organic aerosol and ozone formation under relevant urban conditions, Atmos. Environ., 178(August 2017), 109–117, doi:10.1016/j.atmosenv.2017.12.019,

2018.

Lim, Y. B. and Ziemann, P. J.: Effects of molecular structure on aerosol yields from OH radical-initiated reactions of linear, branched, and cyclic alkanes in the presence of NO x, Environ. Sci. Technol., 43(7), 2328–2334, doi:10.1021/es803389s, 2009a.

Lim, Y. B. and Ziemann, P. J.: Effects of molecular structure on aerosol yields from OH radical-initiated reactions of linear, branched, and cyclic alkanes in the presence of NOx., Environ. Sci. Technol., 43(7), 2328–34 [online] Available from: http://www.ncbi.nlm.nih.gov/pubmed/19452882, 2009b.

Lim, Y. Bin and Ziemann, P. J.: Chemistry of secondary organic aerosol formation from OH radical-initiated reactions of linear, branched, and cyclic alkanes in the presence of NOx, Aerosol Sci. Technol., 43(6), 604–619, doi:10.1080/02786820902802567, 2009c.

Linstrom, P. J. and Mallard, W. G.: NIST Chemistry WebBook, Natl. Inst. Stand. Technol., Database 6, doi:10.5860/CHOICE.35-2709, 2001.

Liu, P., Ziemann, P. J., Kittelson, D. B., Mcmurry, P. H., Liu, P., Ziemann, P. J., Kittelson, D. B., Mcmurry, P. H., Liu, P., Ziemann, P. J., Kittelson, D. B. and Mcmurry, P. H.: Generating Particle Beams of Controlled Dimensions and Divergence : II . Experimental Evaluation of Particle Motion in Aerodynamic Lenses and Nozzle Expansions Generating Particle Beams of Controlled Dimensions and Divergence : 11 . Experimental Evaluatio, Aerosol Sci. Technol., 22(3), 314–324, doi:10.1080/02786829408959749, 1995a.

Liu, P., Ziemann, P. J., Kittelson, D. B. and McMurry, P. H.: Generating particle beams of controlled dimensions and divergence: I. Theory of particle motion in aerodynamic lenses and nozzle expansions, Aerosol Sci. Technol., 22(3), 293–313, doi:10.1080/02786829408959748, 1995b.

Lopez-Hilfiker, F. D., Mohr, C., Ehn, M., Rubach, F., Kleist, E., Wildt, J., Mentel, T. F., Lutz, a., Hallquist, M., Worsnop, D. and Thornton, J. a.: A novel method for online analysis of gas and particle composition: Description and evaluation of a filter inlet for gases and AEROsols (FIGAERO), Atmos. Meas. Tech., 7, 983–1001, doi:10.5194/amt-7-983-2014, 2014.

Ma, P. K., Zhao, Y., Robinson, A. L., Worton, D. R., Goldstein, A. H., Ortega, A. M., Jimenez, J. L., Zotter, P., Prévôt, A. S. H., Szidat, S. and Hayes, P. L.: Evaluating the impact of new observational constraints on P-S/IVOC emissions, multi-generation oxidation, and chamber wall losses on SOA modeling for Los Angeles, CA, Atmos. Chem. Phys.,

17(15), 9237–9259, doi:10.5194/acp-17-9237-2017, 2017.

McDonald, B. C., Gentner, D. R., Goldstein, A. H. and Harley, R. A.: Long-term trends in motor vehicle emissions in U.S. urban areas, Environ. Sci. Technol., 47(17), 10022–10031, doi:10.1021/es401034z, 2013.

McDonald, B. C., de Gouw, J. A., Gilman, J. B., Jathar, S. H., Akherati, A., Cappa, C. D., Jimenez, J. L., Lee-Taylor, J., Hayes, P. L., McKeen, S. A., Cui, Y. Y., Kim, S.-W., Gentner, D. R., Isaacman-VanWertz, G., Goldstein, A. H., Harley, R. A., Frost, G. J., Roberts, J. M., Ryerson, T. B. and Trainer, M.: Volatile chemical products emerging as largest petrochemical source of urban organic emissions, Science (80-.)., 359(6377), 760–764, doi:10.1126/science.aaq0524, 2018.

McMurry, P. H.: A review of atmospheric aerosol measurements, Dev. Environ. Sci., 1(C), 443–517, doi:10.1016/S1474-8177(02)80020-1, 2002.

Miracolo, M. a, Presto, A. a, Lambe, A. T., Hennigan, C. J., Donahue, N. M., Kroll, J. H., Worsnop, D. R. and Robinson, A. L.: Photo-oxidation of low-volatility organics found in motor vehicle emissions: production and chemical evolution of organic aerosol mass., Environ. Sci. Technol., 44(5), 1638–43, doi:10.1021/es902635c, 2010.

Molina, M. J., Zhang, R., Broekhuizen, K., Lei, W., Navarro, R. and Molina, L. T.: Experimental study of intermediates from OH-initiated reactions of toluene [8], J. Am. Chem. Soc., 121(10), 10225–10226, doi:10.1021/ja992461u, 1999.

Morakinyo, O. M., Mokgobu, M. I., Mukhola, M. S. and Hunter, R. P.: Health Outcomes of Exposure to Biological and Chemical Components of Inhalable and Respirable Particulate Matter., Int. J. Environ. Res. Public Health, 13(6), 1–22, doi:10.3390/ijerph13060592, 2016.

Nazaroff, W. W. and Weschler, C. J.: Cleaning products and air fresheners: Exposure to primary and secondary air pollutants, Atmos. Environ., 38(18), 2841–2865, doi:10.1016/j.atmosenv.2004.02.040, 2004.

Nelson, L., Rattigan, O., Neavyn, R., Sidebottom, H., Treacy, J. and Nielsen Ole, J.: Absolute and relative rate constants for the reactions of hydroxyl radicals and chlorine atoms with a series of aliphatic alcohols and ethers at 298 K, Int. J. Chem. Kinet., 22(11), 1111–1126, doi:10.1002/kin.550221102, 1990.

Ng, N. L., Kroll, J. H., Chan, A. W. H., Chhabra, P. S., Flagan, R. C. and Seinfeld, J. H.: and

Physics Secondary organic aerosol formation from m -xylene , toluene , and benzene, , (3), 3909–3922, 2007.

Ng, N. L., Canagaratna, M. R., Zhang, Q., Jimenez, J. L., Tian, J., Ulbrich, I. M., Kroll, J. H., Docherty, K. S., Chhabra, P. S., Bahreini, R., Murphy, S. M., Seinfeld, J. H., Hildebrandt, L., Donahue, N. M., Decarlo, P. F., Lanz, V. a., Prévôt, a. S. H., Dinar, E., Rudich, Y. and Worsnop, D. R.: Organic aerosol components observed in Northern Hemispheric datasets from Aerosol Mass Spectrometry, Atmos. Chem. Phys., 10(10), 4625–4641, doi:10.5194/acp-10-4625-2010, 2010.

Ng, N. L., Herndon, S. C., Trimborn, A., Canagaratna, M. R., Croteau, P. L., Onasch, T. B., Sueper, D., Worsnop, D. R., Zhang, Q., Sun, Y. L. and Jayne, J. T.: An Aerosol Chemical Speciation Monitor (ACSM) for routine monitoring of the composition and mass concentrations of ambient aerosol, Aerosol Sci. Technol., 45(7), 770–784, doi:10.1080/02786826.2011.560211, 2011a.

Ng, N. L., Canagaratna, M. R., Jimenez, J. L., Chhabra, P. S., Seinfeld, J. H. and Worsnop, D. R.: Changes in organic aerosol composition with aging inferred from aerosol mass spectra, Atmos. Chem. Phys., 11(13), 6465–6474, doi:10.5194/acp-11-6465-2011, 2011b.

Nielsen, J.: The health of cleaners., 1995.

Noda, J., Volkamer, R. and Molina, M. J.: Dealkylation of alkylbenzenes: a significant pathway in the toluene, o-, m-, p-xylene + OH reaction., J. Phys. Chem. A, 113(35), 9658–66, doi:10.1021/jp901529k, 2009.

Odum, J. R., Jungkamp, T. P. W., Griffin, R. J., Forstner, H. J. L., Flagan, R. C. and Seinfeld, J. H.: Aromatics, reformulated rasoline, and atmospheric organic aerosol, Environ. Sci. Technol., 31(7), 1890–1897, 1997.

Ofner, J., Balzer, N., Buxmann, J., Grothe, H., Schmitt-Kopplin, P., Platt, U. and Zetzsch, C.: Halogenation processes of secondary organic aerosol and implications on halogen release mechanisms, Atmos. Chem. Phys., 12(13), 5787–5806, doi:10.5194/acp-12-5787-2012, 2012.

Pathak, R. K., Presto, A. A., Lane, T. E., Stanier, C. O., Donahue, N. M. and Pandis, S. N.: Ozonolysis of α-pinene: Parameterization of secondary organic aerosol mass fraction, Atmos. Chem. Phys., 7(14), 3811–3821, doi:10.5194/acp-7-3811-2007, 2007.

Person, A., Laurent, A.-M., Festy, B., Anguenot, F., Aigueperse, J. and Hardy, S.: Impact atmospherique des composes organiques volatils COV generes dans l'habitat par les produits usage domestique: characteristation des emissions et modelisation de l'exposition, Atmos. Pollut. Res., 159–176, 1991.

Presto, A. a, Miracolo, M. a, Kroll, J. H., Worsnop, D. R., Robinson, A. L. and Donahue, N. M.: Intermediate-volatility organic compounds: a potential source of ambient oxidized organic aerosol., Environ. Sci. Technol., 43(13), 4744–9 [online] Available from: http://www.ncbi.nlm.nih.gov/pubmed/19673260, 2009.

Presto, A. A., Miracolo, M. A., Donahue, N. M. and Robinson, A. L.: Secondary Organic Aerosol Formation from High-NO x Photo-Oxidation of Low Volatility Precursors : n - Alkanes, Atmos. Chem. Phys., 44(6), 2029–2034, 2010.

Qiu, C., Khalizov, A. F. and Zhang, R.: Soot aging from OH-initiated oxidation of toluene., Environ. Sci. Technol., 46(17), 9464–72, doi:10.1021/es301883y, 2012.

Robinson, A. L., Donahue, N. M., Shrivastava, M. K., Weitkamp, E. a, Sage, A. M., Grieshop, A. P., Lane, T. E., Pierce, J. R. and Pandis, S. N.: Rethinking organic aerosols: semivolatile emissions and photochemical aging., Science, 315(5816), 1259–1262, doi:10.1126/science.1133061, 2007.

Rogge, W. F., Hildemann, L. M., Mazurek, M. A., Cass, G. R. and Simoneit, B. R. T.: Sources of Fine Organic Aerosol. 3. Road Dust, Tire Debris, and Organometallic Brake Lining Dust: Roads as Sources and Sinks, Environ. Sci. Technol., 27(9), 1892–1904, doi:10.1021/es00046a019, 1993.

Sack, T. M., Steele, D. H., Hammerstrom, K. and Remmers, J.: A survey of household products for volatile organic compounds, Atmos. Environ. Part A, Gen. Top., 26(6), 1063–1070, doi:10.1016/0960-1686(92)90038-M, 1992.

Sarwar, G., Simon, H., Bhave, P. and Yarwood, G.: Examining the impact of heterogeneous nitryl chloride production on air quality across the United States, Atmos. Chem. Phys., 12(14), 6455–6473, doi:10.5194/acp-12-6455-2012, 2012.

Schauer, J. J., Kleeman, M. J., Cass, G. R. and Simoneit, B. R. T.: Measurement of emissions from air pollution sources. 2. C1 through C30 organic compounds from medium duty diesel trucks, Environ. Sci. Technol., 33(10), 1578–1587, doi:10.1021/es980081n, 1999.

Schauer, J. J., Kleeman, M. J., Cass, G. R. and Simoneit, B. R. T.: Measurement of emissions from air pollution sources. 3. C1-C29 organic compounds from fireplace combustion of wood, Environ. Sci. Technol., 35(9), 1716–1728, doi:10.1021/es001331e, 2001.

Schauer, J. J., Kleeman, M. J., Cass, G. R. and Simoneit, B. R. T.: Measurement of emissions from air pollution sources. 5. C1 - C32 organic compounds from gasoline-powered motor vehicles, Environ. Sci. Technol., 36(6), 1169–1180, doi:10.1021/es0108077, 2002.

Seinfeld, J. H. and Pandis, S. N.: Atmospheric Chemistry and Physics : From Air Pollution to Climate Change, 2nd ed., John Wiley and Sons,Inc., 2006.

Shin, H. M., McKone, T. E. and Bennett, D. H.: Contribution of low vapor pressure-volatile organic compounds (LVP-VOCs) from consumer products to ozone formation in urban atmospheres, Atmos. Environ., 108, 98–106, doi:10.1016/j.atmosenv.2015.02.067, 2015.

Singh, H. B. and Kasting, J. F.: Chlorine-hydrocarbon photochemistry in the marine troposphere and lower stratosphere, J. Atmos. Chem., 7(3), 261–285, doi:10.1007/BF00130933, 1988.

Spicer, C. W., Chapman, E. G., Finlayson-Pitts, B. J., Plastridge, R. A., Hubbe, J. M., Fast, J. D. and Berkowitz, C. M.: Unexpectedly high concentrations of molecular chlorine in coastal air, Nature, 394(6691), 353–356, doi:10.1038/28584, 1998.

Steinemann, A.: Volatile emissions from common consumer products, Air Qual. Atmos. Heal., 8(3), 273–281, doi:10.1007/s11869-015-0327-6, 2015.

Stemmler, K., Kinnison, D. J. and Alistair Kerr, J.: Room temperature rate coefficients for the reactions of oh radicals with some monoethylene glycol monoalkyl ethers, J. Phys. Chem., 100(6), 2114–2116, doi:10.1021/jp9520355, 1996.

Suh, I., Zhang, D., Zhang, R., Molina, L. T. and Molina, M. J.: Theoretical study of OH addition reaction to toluene, Chem. Phys. Lett., 364(5–6), 454–462, doi:10.1016/S0009-2614(02)01364-7, 2002.

Suh, I., Zhang, R., Molina, L. T. and Molina, M. J.: Oxidation mechanism of aromatic peroxy and bicyclic radicals from OH-toluene reactions, J. Am. Chem. Soc., 125(41), 12655–12665, doi:10.1021/ja0350280, 2003.

Tanaka, P. L., Oldfield, S., Neece, J. D. and Mullins, C. B.: Anthropogenic Sources of Chlorine and Ozone Formation in Urban Atmospheres, , 34(21), 4470–4473, 2000.

Tichenor, B. A. and Mason, M. A.: Organic emissions from consumer products and building materials to the indoor environment, J. Air Pollut. Control Assoc., 38(3), 264–268, doi:10.1080/08940630.1988.10466376, 1988.

Tkacik, D. S., Presto, A. a, Donahue, N. M. and Robinson, A. L.: Secondary organic aerosol formation from intermediate-volatility organic compounds: cyclic, linear, and branched alkanes., Environ. Sci. Technol., 46(16), 8773–81 [online] Available from: http://lib.bioinfo.pl/paper:22823284\nhttp://adsabs.harvard.edu/abs/2012EnST...46.8773T, 2012.

Toxic Substances Control Act: TSCA Chemical Substance Inventory, [online] Available from: https://www.epa.gov/tsca-inventory (Accessed 26 October 2016), 2016.

Vejrup, K.: The importance of chemical components in cleaning agents for the indoor environment., 1996.

Wallace, L. A.: Comparison of risks from outdoor and indoor exposure to toxic chemicals, Environ. Health Perspect., 95(7), 7–13, doi:10.1289/ehp.91957, 1991.

Wang, D. S. and Hildebrandt Ruiz, L.: Secondary organic aerosol from chlorine-initiated oxidation of isoprene, Atmos. Chem. Phys., 17(22), 13491–13508, doi:10.5194/acp-17-13491-2017, 2017.

Wang, D. S. and Hildebrandt Ruiz, L.: Chlorine-initiated oxidation of n-alkanes under high NOx conditions: Insights into secondary organic aerosol composition and volatility using a FIGAERO-CIMS, Atmos. Chem. Phys. Discuss., (3), 1–26, doi:10.5194/acp-2018-443, 2018.

Wang, L., Arey, J. and Atkinson, R.: Reactions of chlorine atoms with a series of aromatic hydrocarbons, Environ. Sci. Technol., 39(14), 5302–5310, doi:10.1021/es0479437, 2005.

Wang, M., Zhu, T., Zheng, J., Zhang, R. Y., Zhang, S. Q., Xie, X. X., Han, Y. Q. and Li, Y.: Use of a mobile laboratory to evaluate changes in on-road air pollutants during the Beijing 2008 summer olympics, Atmos. Chem. Phys., 9(21), 8247–8263, doi:10.5194/acp-9-8247-2009, 2009.

Wang, S. C. and Flagan, R. C.: Scanning electrical mobility spectrometer, Aerosol Sci.

Technol., 13(2), 230–240, doi:10.1080/02786829008959441, 1990.

Warneke, C., De Gouw, J. A., Holloway, J. S., Peischl, J., Ryerson, T. B., Atlas, E., Blake, D., Trainer, M. and Parrish, D. D.: Multiyear trends in volatile organic compounds in Los Angeles, California: Five decades of decreasing emissions, J. Geophys. Res. Atmos., 117(17), 1–10, doi:10.1029/2012JD017899, 2012.

Weschler, C. J. and Carslaw, N.: Indoor Chemistry, Environ. Sci. Technol., acs.est.7b06387, doi:10.1021/acs.est.7b06387, 2018.

Winer, A. M.: LONG PATHLENGTH DIFFERENTIAL OPTICAL ABSORPTION (DOAS) MEASUREMENTS OF GASEOUS HONO , NO2 AND HCHO IN THE CALIFORNIA SOUTH COAST AIR BASIN, , 20(3), 423–445, 1994.

Winer, A. M., Peters, J. W., Smith, J. P. and Pitts, J. N.: Response of commercial chemiluminescent NO-NO2analyzers to other nitrogen-containing compounds, Environ. Sci. Technol., 8(13), 1118–1121, doi:10.1021/es60098a004, 1974.

Wolkoff, P.: Volatile Organic Compounds Sources, Measurements, Emissions, and the Impact on Indoor Air Quality, Indoor Air, 5(S3), 5–73, doi:10.1111/j.1600-0668.1995.tb00017.x, 1995.

Wolkoff, P., Schneider, T., Kildesø, J., Degerth, R., Jaroszewski, M. and Schunk, H.: Risk in cleaning: Chemical and physical exposure, Sci. Total Environ., 215(1–2), 135–156, doi:10.1016/S0048-9697(98)00110-7, 1998.

Wooley, J., Nazaroff, W. W. and Hodgson, A. T.: Release of ethanol to the atmosphere during use of consumer cleaning products, J. Air Waste Manag. Assoc., 40(8), 1114–1120, doi:10.1080/10473289.1990.10466756, 1990.

Yarwood, G., Whitten, G. Z., Jung, J., Heo, G. and Allen, D. T.: Development, Evaluation and Testing of Version 6 of the Carbon Bond Chemical Mechanism (CB6), , (582), 2010.

Ye, P., Ding, X., Hakala, J., Hofbauer, V., Robinson, E. S. and Donahue, N. M.: Aerosol Science and Technology Vapor wall loss of semi-volatile organic compounds in a Teflon chamber Vapor wall loss of semi-volatile organic compounds in a Teflon chamber, , doi:10.1080/02786826.2016.1195905, 2016.

Young, C. J., Washenfelder, R. A., Edwards, P. M., Parrish, D. D., Gilman, J. B., Kuster, W. C., Mielke, L. H., Osthoff, H. D., Tsai, C., Pikelnaya, O., Stutz, J., Veres, P. R., Roberts, J.

M., Griffith, S., Dusanter, S., Stevens, P. S., Flynn, J., Grossberg, N., Lefer, B., Holloway, J. S., Peischl, J., Ryerson, T. B., Atlas, E. L., Blake, D. R. and Brown, S. S.: Chlorine as a primary radical: Evaluation of methods to understand its role in initiation of oxidative cycles, Atmos. Chem. Phys., 14(7), 3427–3440, doi:10.5194/acp-14-3427-2014, 2014.

Zhang, X., Cappa, C. D., Jathar, S. H., McVay, R. C., Ensberg, J. J., Kleeman, M. J. and Seinfeld, J. H.: Influence of vapor wall loss in laboratory chambers on yields of secondary organic aerosol, Proc. Natl. Acad. Sci., 111(16), 5802–5807, doi:10.1073/pnas.1404727111, 2014.

Zhang, Z., Lin, L. and Wang, L.: Atmospheric oxidation mechanism of naphthalene initiated by OH radical. A theoretical study., Phys. Chem. Chem. Phys., 14(8), 2645–50, doi:10.1039/c2cp23271e, 2012.

Zhao, Y., Hennigan, C. J., May, A. A., Tkacik, D. S., Gouw, J. A. De, Gilman, J. B., Kuster, W. C., Borbon, A. and Robinson, A. L.: Intermediate-Volatility Organic Compounds: A Large Source of Secondary Organic Aerosol, 2014.

Ziemann, P. J. and Atkinson, R.: Kinetics, products, and mechanisms of secondary organic aerosol formation, Chem. Soc. Rev., 41(19), 6582, doi:10.1039/c2cs35122f, 2012.